
HOST UNIVERSITY: Ghent University

FACULTY: Faculty of Engineering

DEPARTMENT: Department of Flows, Heat and Combustion

Academic Year 2012-2013

# Characterisation of the far field temperature under the ceiling in the Travelling Fires framework

Hélène SIRVAIN

Promoter(s): Prof. dr. ir. Bart Merci

Master thesis submitted in the Erasmus Mundus Study Programme

**International Master of Science in Fire Safety Engineering**

# Disclaimer

This thesis is submitted in partial fulfilment of the requirements for the degree of *The International Master of Science in Fire Safety Engineering (IMFSE)*. This thesis has never been submitted for any degree or examination to any other University/programme. The author(s) declare(s) that this thesis is original work except where stated. This declaration constitutes an assertion that full and accurate references and citations have been included for all material, directly included and indirectly contributing to the thesis. The author(s) gives (give) permission to make this master thesis available for consultation and to copy parts of this master thesis for personal use. In the case of any other use, the limitations of the copyright have to be respected, in particular with regard to the obligation to state expressly the source when quoting results from this master thesis. The thesis supervisor must be informed when data or results are used.

The 29th of April 2013,

# Abstract

Nowadays, the structural stability of a building subjected to a fire is assessed by traditional fire design methods that consider the burning of the entire floor plate with uniform thermal atmospheres within the enclosure, for all types of compartments. For large compartments, it has been proved by experiments that the burning area tends to move across the floor plate, resulting in non-uniform temperature distribution inside the compartment. A new methodology of fire design called the Travelling Fires methodology has been created to take into account the travelling characteristic of the fire for structural analysis.

In this new methodology, the temperature field of the gases under the ceiling above the burning area is at a constant value of 1200 °C, and is defined by Alpert unconfined ceiling jet expression for the rest of the compartment. An investigation on the definition of this far field temperature will be carried out in this master thesis. Numerical simulations with the Fire Dynamics Simulator (NIST) have been performed in order to study the temperature distribution under the ceiling in large compartments and to determine the limitations of Alpert equation in this context. Finally, a new analytical method to characterise the temperature distribution within the studied compartment will be extracted from the simulations results and its limitations presented.

# Abstract (French) - Résumé

Aujourd'hui, la stabilité structurelle d'un bâtiment soumis à un incendie est déterminée par les méthodes de dimensionnement traditionnelles qui considèrent que la totalité de la surface au sol brûle simultanément, générant un champ de températures uniforme dans le milieu confiné, et cela pour tous les types de compartiments. Pour ce qui est des compartiments de grande échelle, il a été prouvé suite à des expériences que le foyer tend à se déplacer, générant un champ de températures non-uniforme au sein du milieu confiné. Une nouvelle méthode de dimensionnement appelé la méthode des « Travelling Fires » a été crée pour prendre en compte ce déplacement du foyer dans le cadre de l'analyse structurelle des bâtiments.

Dans cette nouvelle méthode de dimensionnement, le champs de température des gas sous le plafond à la verticale du foyer prend un valeur constante de 1200°C, et est définie par l'équation pour les panaches de fumée non confinés d'Alpert pour le reste du compartiment. Des recherches sur la définition de ce champs de températures loin des flammes va être réalisée dans le cadre de cette master thesis. Des simulations numériques à l'aide du logiciel Fire Dynamics Simulator (NIST) ont été réalisées pour déterminer ce champ de température dans les compartiments de grande dimension, et déterminer les restrictions liées à l'équation d'Alpert. Enfin, un nouvel outil permettant de caractériser le champ de températures dans le compartiment étudié sera extrait des résultats des simulations numériques et les limites du modèle seront explicitées.

# Table of contents

# List of abbreviations

| | |
|---|---|
| $c_p$ | Heat capacity |
| $\nabla(r)$ | Characteristic density defect parameter |
| E | Entrainment rate |
| F | Friction factor |
| FDS | Fire Dynamics Simulator |
| g | Gravitational acceleration |
| h | Convective heat transfer coefficient |
| $h^*$ | Ceiling jet thickness |
| H | Ceiling height |
| HRR | Heat Release Rate |
| K | Thermal boundary condition parameter |
| MTR | Measure of Turbulence Resolution |
| $\dot{Q}$ | Heat Release Rate of the fire |
| $\dot{Q}^*$ | Non – dimensional heat release rate |
| $Q''$ | Heat transfer parameter |
| $\rho$ | Density |
| r | Radial distance from the fire axis |
| $r^*$ | Radial distance from the temperature peak |
| Ri | Richardson number |
| S | Pressure gradient parameter |
| t | Time |
| T | Temperature [°C] |
| $T^*$ | Non – dimensional temperature |
| v | r-coordinate mean-time gas velocity |
| V(r) | Characteristic velocity jet velocity |
| u | z-coordinate mean-time gas velocity |

# List of tables and figures

# CHAPTER 1

# Introduction and objectives

Nowadays and for the last past years, buildings have been designed to resist to a fire with traditional methods where single structural elements are subjected to the ISO-834 T-time gas temperature curve or the parametric T-time gas temperature curves. Those fire design methods are very suitable for common size enclosures (dwellings, offices…), since one of the main assumptions of these models is the uniformity of the gas properties in space. This assumption is applicable for certain a range of geometries and fire powers. However, new constructions techniques and construction materials made it possible to create new types of compartments such as atriums, big open spaces, big warehouses... that have large floor areas and more complex geometries, implying that the traditional fire design methods cannot be applied because of the non-homogeneity of the gas field. For instance, the parametric fire design method used in the EUROCODES only apply for compartments surfaces up to 500 $m^2$ and ceiling height up to 4 meters (1).

To account for these problems on how to characterise the fire environment in large and complex buildings, a new fire design methodology has been developed by Rein (2) in 2007 and refined in 2011 by Stern Gottfried (3).

## 1) The Travelling Fires Methodology

This fire design method diverges from the traditional methods in the sense that the whole floor plate is not burning at the same time, but only a percentage of the total area is burning and the fire travels along the entire floor surface and dies out when all the fuel is burnt. The fire design is not a single fire anymore but a whole family of fires ranging from 1% of the floor plate burning at the same time to the whole compartment burning (100%).

This movement results in a non-uniform temperature distribution, characterised by two geographical zones: the near field zone and the far field zone that have a location relative to the burning area.

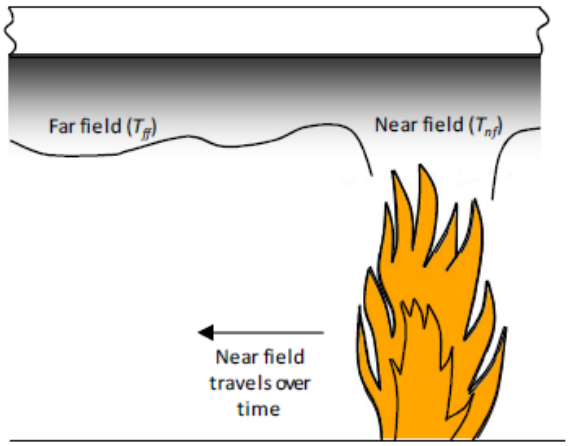


*Figure 1: Near field and far field of the Travelling Fires*

If a structural element is within the near field zone, it means that it is located close to the flames (or within the flames, in case of flame impingement), so it will be subjected to high temperatures, but for short time duration. On the contrary, if the element is in the far field zone, it means that it is far from the flames, resulting in lower temperatures but for a longer time.

The near field temperatures are represented by a constant value equal to 1200°C, the near field zone width corresponds to the burning area width. The 1200°C account for the worst case scenario of

the temperature within the flaming region, given that the values for experiments are between 800°C and 1000°C (4) .

The far field temperatures are expressed using Alpert's ceiling jet correlation (5) for discretized radial positions:

$$\Delta T = \frac{5{,}38\ (\dot{Q}/r)^{2/3}}{H} \quad [eq.\ 1]$$

, where $\Delta T$ represents the temperature difference between the hot gases and ambient conditions $\Delta T = T_{gas} - T_{\infty}$ .

From the hot gases temperatures distribution input, simple 1-D heat transfer calculations (3) are implemented in order to determine the temperature of the reinforcement bars within the concrete or the steal temperatures for steel members. Then a structural analysis is carried on and depending on the failure criteria (3) , the building will withstand or not the family of Travelling Fires.

## 2) Problem definition

The main focus of this master thesis is the characterisation of the far field temperature of the hot gases. As mentioned earlier, the temperature of the gases under the ceiling far away from the flames is represented by Alpert ceiling jet equation that was developed in the 1970's for the calculation of detection times. This correlation applies for an axis-symmetric, weak plume driven flow field under an unconfined ceiling that does not seem to represent properly the characteristics of a fire lasting several hours within a compartment.

In an effort to refine the far field temperature definition used in the methodology, a study will be carried out in order to determine if Alpert correlation represent the temperature field accurately and if not, find another more suitable tool to characterise it.

Given the enormous costs of carrying out experiments for large scale compartments, Fire Dynamics Simulator (FDS) version 5 will be used to perform numerical simulations. For more simplicity a studied compartment has been fixed by CERIB with the given dimensions of 30,25 m * 14,25 m * 4m. This implies that the compartment's general geometry influence will not be studied in this master thesis and the results will be only applicable to compartment geometries that are similar to the chosen compartment. However, such a compartment, with a 4m ceiling height is quite representative of nowadays office geometry.

## 3) Outline of the master thesis

This master thesis has been divided in five different chapters for more clearance. Chapter 2 is a short literature review of the already existing tools that characterises ceiling jet properties (unconfined and confined) and a more in depth analysis of Alpert equations that are used in the Travelling Fires methodology. Some of the limitations due to the use of Computational Fluid Dynamics (CFD) are mentioned as well in this literature review.

In the following chapter, simulations representing a single ceiling have been carried out in order to determine the parameters of the fire source that affect the temperature field of an unconfined ceiling jet, and check if whether or not FDS can represent the gas field properties of this ceiling jet quite fairly. A grid sensitivity analysis is included in this chapter.

In chapter 4, the same configuration is kept regarding the simulations, but screens are added on four sides of the ceiling in an effort to study the impact of smoke accumulation on the temperature and heat flux fields. The results from these simulations and some analytical calculations will allow the determination of the simulations set-up for the compartment, addressed in Chapter 5.

Chapter 5, and probably the most important chapter of this study, focuses on the final set of simulations within the compartment. From the numerical results, a correlation has been created representing quite fairly the temperature field under the ceiling as a function of simple input parameters such as the fire power $\dot{Q}$ and the radial position to the fire axis r. This makes possible a better characterisation of the temperature field for this type of compartment. However, more studies will be required to obtain a more general equation applicable in a whole range of more complex large enclosures.

Eventually, the general conclusions of this work are addressed in Chapter 6.

# CHAPTER 2: Literature Review

In this chapter, the analytical existing tools characterising the ceiling jet properties have been reviewed, and will be used to compare (if applicable for the given situation) to CFD simulations later on.

## 1) Ceiling jet formulas

When the smoke impinges on the ceiling, it will spread radially and not vertically anymore and create a so-called ceiling jet. The characteristics of the ceiling-jets have been studied for years, and couples of correlations were developed to approximate different quantities such as the temperature, velocity and heat flux fields.

### A) Unconfined ceiling jets

#### *a) Alpert: a review of the derivation*

Alpert's formulas that express the maximum temperature and velocity increase for an axis-symmetric unconfined ceiling jet have been derived in 1975. The Travelling Fires methodology is using Alpert unconfined ceiling jet to characterise the far field gas temperatures under the ceiling. To understand more deeply the physics behind these equations a short review has been carried out based on Alpert's 1975 article (6), where he describes the theoretical aspects of the ceiling-jet formulas

First of all, the fire phenomenon is divided in three different geographical regions: the first zone considers the flow close to the fire source, and is called the fire plume. As this plume rises, it interacts with the ceiling, in two different regions: close to the stagnation point (point on the ceiling surface where the smoke impinges before spreading radially) is the turning region with increased mixing and complex phenomena, and far away is the ceiling jet zone. The limit between the turning region and the ceiling jet is defined as the radial position where the vertical velocity of the gases $u$ in the plume is down to 5% of the maximum vertical gas velocity $u_{max}$. In this derivation, the properties of the edge of one region will be the boundary conditions for the following region, making possible to relate the ceiling jet characteristics with the fire and geometry features.

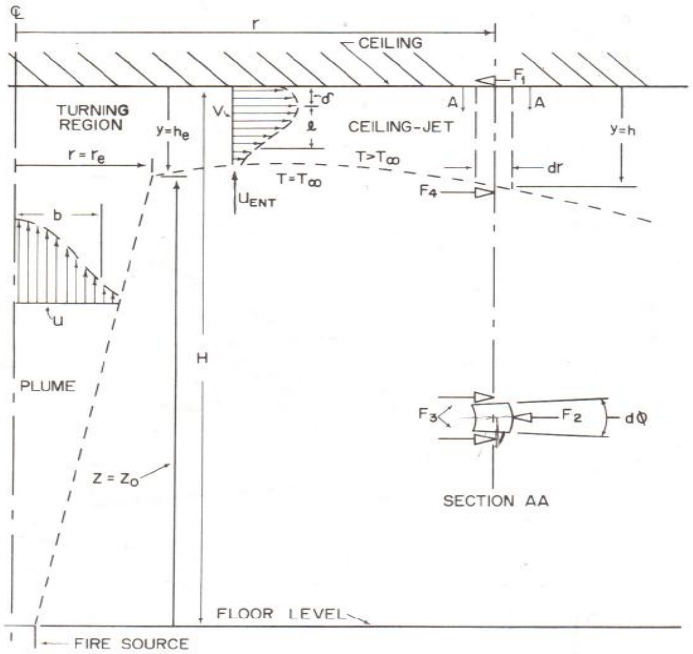


*Figure 2: Alpert ceiling jet configuration*

This derivation is presented in different steps for more clearance:

**Step 1**

The Mass, Momentum and Energy conservation equations and the Equation of State are written based on a cylindrical control volume (r, y, z) , considering the following assumptions :

- the flow is fully turbulent, and in a steady state
- the smoke is considered as an ideal gas
- the flow has a low velocity (Mach n° << 1)
- the Boussinesq approximation applies here (at heights far away from the fire source the entrainment is such that the density difference between the plume and the air outside is very small)
- there is an hydrostatic pressure distribution along the ceiling jet thickness
- the fire is treated as a point energy source (the chemical reaction zone has a negligible size compared to the ceiling height)
- the vertical mean velocity in the ceiling jet is negligible

**Step 2**

The governing equations are simplified using Ellison and Turner averaging method, relevant to turbulent entrainment for stratified cases (7) that defines the following parameters:

- V(r) : characteristic ceiling jet velocity; $Vh = \int_0^\infty vdy$where h is the ceiling jet thickness, v the r-coordinate mean time gas velocity

- $\nabla(r)$: characteristic density defect $\nabla = g\frac{(\rho_\infty - \rho)}{\rho_\infty}$

- S : pressure gradient parameter, that depends of the profile shape (S is constant if the density and velocity profiles are similar)

Moreover, the friction factor $F = \frac{\tau_w}{\rho_\infty \cdot V^2}$ and the ceiling height heat transfer parameter $Q'' = \frac{-q'' \cdot g}{\rho_\infty \cdot c_p \cdot T_\infty}$ are introduced by the author.

**Step 3**

In order to combine the governing equations, the Richardson number and the pressure gradient parameter S are used. The Richardson number, dimensionless number that represents the natural convection relative to the forced convection, is defined as follows $Ri = \frac{h^* \cdot \nabla}{V^2}$

The SRi factor is introduced in the momentum and energy equations, and both equations are combined. The same process is repeated for the mass and energy equations, but only the Richardson number is used instead of the SRi factor. These combinations are reorganised and turned into two expressions: one representative of the gradient of the thickness of the ceiling jet:

$$\frac{dh^*}{dr}(1 - 2\mathrm{SRi}) = F + (2 - SRi)E - \frac{h^*}{r} + \frac{Q''}{V \cdot \nabla} \cdot SRi \quad \text{[eq.2]}$$

and the other representing the gradient of the Richardson number:

$$\frac{dRi}{dr}(1 - 2\mathrm{SRi})\frac{h^*}{3\mathrm{Ri}} = F + (1 + SRi) \cdot (E + \frac{Q''}{3V\nabla}) - \frac{h}{3\mathrm{r}} \cdot (1 + ASRi) \quad \text{[eq.3]}$$

**Step 4**

The heat transfer at the ceiling is related to the fluid friction using Reynolds analogy (the heat flux in a turbulent system is analogous to fluid friction, so that the ratio of the momentum flux over the heat flux should be constant for all positions on the radial axis).This make possible to determine the ceiling heat transfer parameter $Q''$.

The thermal boundary condition parameter K is introduced: it varies as a function of the ceiling material properties. For an isothermal ceiling ($T_{wall} = T_\infty$), K is equal to $Pr^{-2/3}$and is equal to 0 for a

perfectly insulated ceiling (no heat losses to the compartment boundaries). If the velocity and density profiles are identical$Q''$is reduced to $Q'' = -F \cdot K$.

**Step 5**

The boundary conditions obtained by first determining the plume properties, coupling it with the turning region, and then coupling the turning region properties with the ceiling jet ones.

Plume properties from Morton and al. (1956) (8) are used, assuming a Gaussian profile for time-mean velocity, density defect and half-width. The assumptions made for coupling the fire plume and the turning region state that there is no heat lost to the ceiling in the turning region (since the turning region is a small area compared to the total ceiling area, so the energy lost by convection will not be important), that the exit maximum velocity (it is assumed that the velocity has a half Gaussian profile) is the same as the one in the plume that is entering the turning region.

The coupling between the turning region and the ceiling jet is straightforward: the conditions at the exit of the turning region are the upstream boundary conditions for the ceiling jet.

**Step 6**

With the boundary conditions determined, equations 2 and 3 can now be solved by using some simplifying assumptions (the entrainment rate E, is considered constant, so that the entrainment of air into the ceiling jet will be only influenced by the gravitational forces and F is constant as well implying that the Reynolds number is constant on the radial axis). First of all, equations 2 and 3 are put in a non-dimensional form by dividing all the distances by H.

It is hence possible to express non-dimensional velocity and density defect parameter from these equations that will allow the determination of the velocity and temperature profiles. The velocity is already defined and the density is linked to the temperature by the equation of State ($\rho \cdot T = \rho_\infty \cdot T_\infty$), that yields to $\frac{\Delta T_{max}}{T_\infty} = \frac{\nabla}{g}$(equation 57 from (6)).

This leads to the following formulas:

$$\bar{V} = (2\pi \cdot \bar{r} \cdot Ri)^{-1/3} \cdot \exp\left[\frac{-K}{3}\int_{\bar{r}_e}^{\bar{r}} (F/h^*)\, d\bar{r}\right] \quad \text{[eq.4]}$$

$$\bar{\nabla} = \left(1/\bar{h^*}\right)\left(\frac{Ri}{(2\pi\cdot\bar{r})^2}\right)^{1/3} \cdot \exp\left[\frac{-2\mathrm{K}}{3}\int_{\bar{r}_e}^{\bar{r}} (F/h^*)\, d\bar{r}\right] \quad \text{[eq.5]}$$

where $\bar{V}$and $\bar{\nabla}$are the non dimensional characteristic ceiling jet velocity and density deflect defined as follows :

$$\bar{V} = \frac{V}{(\frac{\dot{Q}\cdot g}{\rho_\infty \cdot c_p \cdot T_\infty})^{1/3} \cdot H^{-1/3}} \quad \text{[eq.6]}$$

$$\bar{\nabla} = \frac{\nabla}{(\frac{\dot{Q}\cdot g}{\rho_\infty \cdot c_p \cdot T_\infty})^{2/3} \cdot H^{-5/3}} \quad \text{[eq.7]}$$

**Step 7**

However, equations 4 and 5 do not depend on measurable quantities that can be determined by experiments. This is why equations 6 and 7 will be used to determine experimentally the velocity and temperature profiles underneath the ceiling.

Let's take the example of the temperature field: during the experiments, the maximum temperatures of the ceiling-jet are measured for different radial positions r. Then, the non-dimensional temperature difference $\bar{\Delta T_{max}} = \frac{\frac{g\cdot\Delta T_{max}}{T_\infty}}{(\frac{\dot{Q}\cdot g}{\rho_\infty \cdot c_p \cdot T_\infty})^{2/3} \cdot H^{-5/3}}$ is plotted in a natural log-log graph as a function of the non-dimensional radial position $\frac{r}{H}$. The results fit on a straight line, allowing a relation

between the non-dimensional data and $\frac{r}{H}$as follows:

$$\ln\left(\frac{\frac{g\cdot\Delta T_{max}}{T_\infty}}{H^{-5/3}.\left(\frac{Q\cdot g}{\rho_\infty\cdot c_p\cdot T_\infty}\right)^{2/3}}\right)=\alpha_T\ln\left(\frac{r}{H}\right)+\ln(\beta)[eq.8]$$

where $\alpha_T$is the slope given by the graphs.

This can be transformed with the use of the properties of the natural logarithm: $\alpha_T\ln(b)+\ln(\beta)=\ln(b^{\alpha_T}\cdot\beta)$ as follows

$$\frac{\frac{g\cdot\Delta T_{max}}{T_\infty}}{H^{-5/3}\cdot\left(\frac{Q\cdot g}{\rho_\infty\cdot c_p\cdot T_\infty}\right)^{2/3}}=\left(\frac{r}{H}\right)^{\alpha_T}\cdot\beta\ [eq.9]$$

and rearranged to obtain :

$$\Delta T_{max}=\frac{\frac{\dot{Q^{2/3}}}{H^{5/3}}}{\left(\frac{r}{H}\right)^{-\alpha_T}}\cdot A[eq.10]$$

where A is a constant term corresponding to $A=\frac{T_\infty\cdot\beta}{g^{1/3}\cdot(\rho_\infty\cdot c_p\cdot T_\infty)^{2/3}}$ .

From Alpert experiments, it is known that $\alpha_T\simeq-2/3$ that yields in $\Delta T_{max}=\frac{\left(\frac{\dot{Q}}{r}\right)^{2/3}}{H}\cdot A$ corresponding to the famous Alpert's expression for the far field of :

$$\Delta T_{max}=5{,}38\frac{\left(\frac{\dot{Q}}{r}\right)^{2/3}}{H}[eq.11]$$

The same process is repeated for the velocity field, where a slope of $\alpha_V\simeq-5/6$ is found, leading to the following expression:

$$V_{max}=\frac{0{,}197\cdot\dot{Q^{1/3}}H^{1/2}}{r^{5/6}}[\text{eq.12}]$$

Alpert's experiments were carried out for fires which range from 600kW to 98 MW, and for ceiling heights ranging from 4,6m to 18m. The excess temperature and velocities were measured for radial positions up to twice the ceiling height H.

Alpert's formulas have been reviewed in 2011 (9),considering only the convective part of the HRR, only taking into account in the regression fit data for well documented fire sources and considering the virtual plume origin. The new correlations are quite similar to the previous ones, noting that the coefficients are changed due to the different regression.

### *b) Heskestad : non dimensional ceiling jet*

Another set of correlations using non-dimensional variables was developed by Heskestad (10) : these formulas are quite comparable to Alpert ones, with slightly higher excess temperatures and substantial greater gas velocities when plotted both in non-dimensional forms.

Excess temperature:

$$\Delta T_0^{¤}=(0{,}225+\frac{0{,}27\cdot r}{H})^{-4/3}\text{for}\ 0{,}2\leqslant r/H<4{,}0$$
$$\text{and}\ \Delta T_0^{¤}=6{,}3\text{for}\ r/H\leqslant 0{,}2\ [\text{eq.13}]$$

Velocity :

$$U_0^{¤}=1{,}06\cdot(r/H)^{-0{,}69}\text{for}\ 0{,}17\leqslant r/H<4{,}0$$
$$\text{and}\ U_0^{¤}=3{,}61\text{for}\ r/H\leqslant 0{,}17\ [\text{eq.14}]$$

where $\Delta T_0^{¤} = \frac{\Delta T / T_\infty}{(\dot{Q}_0^{¤})^{1/3}}$ is the non-dimensional temperature and $\dot{Q}_0^{¤} = \frac{\dot{Q}}{\rho_\infty \cdot c_p \cdot g^{1/2} \cdot H^{5/2}}$ the non-dimensional HRR. The experiments to validate the correlations were based on alcohol pool fires.

Then, Heskestad and Delichatsios (11) found a relation between the non-dimensional excess temperature and the non-dimensional velocity:

$$\frac{\bar{U}_0}{\sqrt{\Delta \bar{T}_0}} = 0{,}68 \cdot \left(\frac{r}{H}\right)^{-0{,}63} for\ r/H \geqslant 0{,}3 \text{ [eq. 15]}$$

This relation is applicable for steady-state weakly plume fires but for time-dependant strong plumes as well. The experiments to determine the relation between the non-dimensional velocity and excess temperature were carried out in a 61m * 76m * 9,14m/18,28m (two floor to ceiling heights) room, where all the openings were closed during the experiments. The fuel was composed of wood cribs, with a HRR varying as a function of $\alpha t^2$. The magnitude of $\dot{Q}_{max}$ varied between 0,5 W and 4 MW, and the measurements were done at a maximum distance from plume axis of 12,19m.

Alpert and Heskestad maximum excess ceiling jet temperature have been plotted for a 1000kW fire under a 4m ceiling. The difference, as said earlier, is that Heskestad formula gives slightly higher temperatures than Alpert.

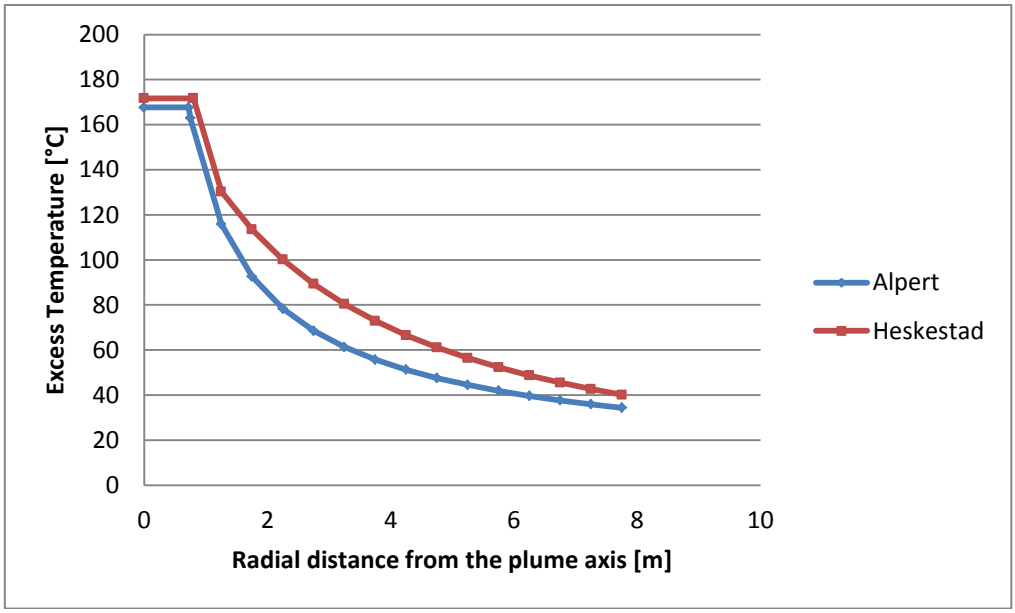


*Figure 3: Comparison between Alpert and Heskestad ceiling jet equations*

## B) Confined ceiling jets

### *a) Delichatsios : channel configuration*

The presence of ceiling beams or corridor walls can confine the ceiling jet partially, creating a consequent accumulation of smoke under the ceiling. Delichatsios (12) developed a formula to describe the averaged ceiling jet temperature and velocity within a smoke channel.

The channel configuration expressions can be applied in the following ranges:

- the corridor half-width should be greater than $0{,}2 * H$ (0,2*H corresponds more or less to the outer radius of the ceiling jet turning region)
- the flow must be contained fully : the beam depth $h_b$ should be greater than the quantity $(H/10) \cdot (l_b/H)^{-1/3}$

The ratio of the average excess ceiling temperature in the channel $\Delta T$ over the unconfined

maximum ceiling jet excess temperature $\Delta T_p$ is expressed as follows:

$$\frac{\Delta T}{\Delta T_p} = a \cdot (\frac{H}{l_b})^{1/3} \cdot \exp[-6{,}67 \cdot St \cdot \frac{Y}{H} \cdot (\frac{l_b}{H})^{1/3}] \text{ [eq.16]}$$

where a is a constant in the range of 0,24 to 0,29 ,Y is the distance along the channel measured from the impingement point and St is the Stanton number taken as 0,03.
Those equations are valid given that the following conditions apply :

1) $Y > l_b$
2) $\frac{h_b}{H} > 0{,}1(\frac{l_b}{H})^{-1/3}$
3) $\frac{l_b}{H} > 0{,}2$
4) $0{,}5 < \frac{Y}{H} \cdot (\frac{l_b}{H})^{1/3} < 3{,}0$

The experiments to validate the formulas were carried out in facilities where the height between the ceiling and the top of the fuel bed was varying between 2,74 m and 3,05m. The beam height varied between 0,305 and 0,61m and the fire power is not expressed.

Koslowski and Motevalli (13) carried out experiments that confirmed Delichatsios correlations, and that generalised it given the important number of experiments. Those experiments were taking place in a 3,5m ceiling height configuration, for fire powers ranging from 450 to 1160 kW. The only difference is that the average excess temperature in the channel is now expressed as a function of the non-dimensional HRR (defined in Heskestad non dimensional formulas for unconfined ceiling-jet) instead of the unconfined maximum ceiling jet excess temperature.

This set of correlations cannot be used in the analysis carried out, because of the dimensions of the studied compartment that are out of the range of applicability of the method, given the limitations of the model.

### *b) Two layer model: Evans / Cooper*

When the smoke reaches the walls of the compartment, it starts to accumulate and form a smoke layer under the ceiling. This accumulation of smoke will result in greater maximum temperatures of the gases under the ceiling, since the ceiling jet is no more diluted by entraining cold air. Moreover, studies by Yu and Feath (14) proved that the convective heat transfer rate is increased by around 35% when a smoke layer is formed compared to the situation where the ceiling jet is unconfined.

An engineering tool has been set up in order to determine the effect of the accumulation of a smoke layer in a compartment. Evans (15) and Cooper (16) have derived formulas that allow the determination of a substitute fire that would account for the greater temperatures and velocities caused by the presence of the smoke layer. The model considers that the environment is divided in two regions: the upper-layer that is hot and contains the smoke and a lower layer that is quiescent and at ambient conditions. Both layers have uniform properties, and a single temperature is considered to describe each of them. The fire in the compartment will be turned into a substitute fire with an unconfined ceiling jet that will account for smoke accumulation.

The studied fire has a HRR of $Q_1$ and the compartment height is $H_1$. The HRR is put in the non-dimensional form, that yields in :

$$Q^{\text{¤}}_{l,1} = \frac{Q_1}{\rho_\infty \cdot c_{p\infty} \cdot g^{1/2} Z^{5/2}_{l,1}} \text{ [eq. 17]}$$

where $Z_{I,1}$ is the distance between the fire source and the smoke layer.

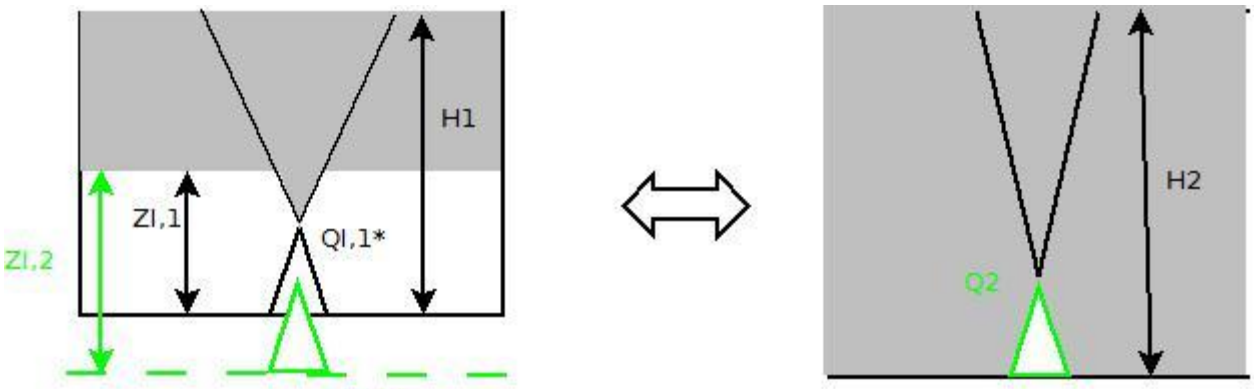


*Figure 4: Two-layers model configuration*

Then, $Q_{I,1}^{¤}$ is converted to obtain the substitute non-dimensional fire power $Q_{I,2}^{¤}$ with the following formula:

$$Q_{I,2}^{¤} = \left(\frac{1 + C_T \cdot (Q_{I,2}^{¤})^{2/3}}{\epsilon \cdot C_T} - \frac{1}{C_T}\right)^{3/2} \text{ [eq. 18]}$$

where $\epsilon$ is the temperature of the upper-layer divided by the lower-layer temperature and $C_T$ is a constant term related to the plume flow and equal to 9,115.

The position of the substitute fire source relative to the two layers interface becomes

$$Z_{I,2} = \left(\frac{\epsilon \cdot Q_{I,1}^{¤} \cdot C_T}{(Q_{I,2}^{¤})^{1/3} \cdot ((\epsilon - 1) \cdot (\beta^2 + 1) + \epsilon \cdot C_T \cdot (Q_{I,1}^{¤})^{2/3})}\right)^{2/5} \cdot Z_{I,1} \text{ [eq. 19]}$$

The substitute fire power is turned back to a dimensional property

$$Q_{c,2} = Q_{I,2}^{¤} \cdot \rho_{\infty,2} \cdot c_{p\infty} \cdot T_{\infty,2} \cdot g^{1/2} \cdot Z_{I,2}^{5/2} \text{[eq. 20]}$$

and the position relative to the ceiling is determined as follows: $H_2 = H_1 - Z_{I,1} + Z_{I,2}1$

Then, the temperature difference between the upper-layer and the lower-layer can be calculated using Heskestad dimensionless maximum temperature formula for unconfined ceiling jet flow (equation 13).

This calculation method was validated with a single set of small scale experiments, in a cylindrical enclosure (diameter 1,22m), with a 0,62 kW methane fire. The extrapolation of this method for real-scale cases may not be applicable.

An alternative way of calculating the substitute power and distance below the ceiling has been proposed by Cooper (16). The results of both methods are quite similar, giving more strength to this method. However, Cooper's method was not validated by carrying out some experiments.

An important drawback of this method is that the temperature of the uniform smoke layer is needed for the calculations, temperature that is in general not known a priori and quite hard to measure in case of an experiment. This method could have been used after calculating this uniform temperature from analytical methods such as Mc Caffrey, Quintiere and Harklerood method from the SFPE handbook (17). However, the previous correlation applies to small compartments, and was validated on floors area ranging from 0,14m² to 12m², that is non-representative of the studied compartment. Because of the previous reasons, this method will not be compared to the results of the simulations.

## 2) FDS limitations

As all the modelling tools, CFD softwares have limitations that should be kept in mind when carrying out analyses based on numerical simulations. Fire Dynamics Simulator solves numerically an approximation of Navier & Stockes equations for low-speed, thermally-driven flows. Here are some issues linked with the chosen thesis topic.

### A) Grid sensitivity

The most important parameter in a CFD calculation is the resolution of the mesh, since an approximation of the conservation equations (mass, momentum and energy) for the fluid are going to be solved for each cell that has discretized properties. The errors due to the discretization scheme are directly linked to the cell size since FDS uses a second order accurate approximation of temporal and spatial derivatives of Navier & Stockes equations. The error will be proportional to the square of the time step and to the square of the cell size (5). A grid sensitivity analysis in order to determine an appropriate mesh needs to be carried out for each series of simulations. This will be done in the first series, and will allow the estimation of the required computer power for all the simulations.

Several studies have been carried out concerning the size of the grid, and one of the techniques to determine the grid spacing, is the following obtain ratio $D^*/dx$, where $dx$ is the grid spacing and $D^*$ the characteristic diameter of the fire that is equal to

$$D^* = \left(\frac{Q}{\rho_\infty \cdot c_p \cdot T_\infty \cdot \sqrt{g}}\right)^{2/5}$$

is in the range of 4 to 16 (19) . Another way of checking that the grid resolution is fine enough consists of plotting a slice file called TURBULENCE RESOLUTION, and compared the Measure of Turbulence Resolution (MTR) value to 0,2 : if in the slice there is some area where the MTR is inferior to 0,2, it means that the turbulence is badly resolved in this part of the domain. On the other hand, if the MTR is superior to 0,2 it can be expected that the size of the grid allow a fair resolution of the turbulence phenomenon within the fluid.

However it should be kept in mind that the grid size will not have the same influence on all the output quantities: the heat flux to a target will require a finer mesh than the hot gas layer temperature or height. This has to be taken into account for the results analysis.

### B) Ventilation conditions

As mentioned in FDS user's guide (19), it is assumed that the combustion process is infinitely fast and the reaction rate is mixing-controlled. The mixture fraction model used by FDS is such that the combustion model assumption is good for large-scale, well-ventilated fires. As the fires that will be modelled have an important HRR, caution should be taken to make sure that the combustion is not limited by the oxidizer.

Low oxygen concentration models exist and are available in FDS version 5, however the aim of the numerical simulations is to prescribe a fire with a constant HRR, and that the correct amount energy will be released in a specific area, and not close to the opening because of the lack of oxygen. In an effort to make sure that the ventilation conditions are good enough to have a complete combustion inside the compartment, engineering tools will be set up, and calculations will be carried out before starting the simulations.

### C) Radiation/temperature close to the flames

The temperature field and the radiation predicted by FDS away from the fire are in general in better agreement with experiments than the one close to the flames. This is because of the steep gradients in temperature that we can find close to the flames that are more sensitive to subtle changes in the combustion model than where the temperature gradients are lower.

# CHAPTER 3: Unconfined ceiling jet

## 1) Methodology

The main objective associated with this series of simulations is the determination of the fire parameters that have a great impact on the hot gases temperature field, in order to know which ones are necessary to be taken into account and which ones are not. Those parameters mainly concern the fire source. The compartment geometry (apart from the ceiling height) aspects will be considered later on.

In this first set of numerical simulations, a fire impinging on a single ceiling will be represented in order to check if the CFD software represents well the analytical methods for unconfined ceiling jet (Alpert (5)/ Heskestad (10)). Then, another set of simulations will focus on the smoke accumulation.

One of the main advantages of running simulations without any walls is that the ventilation conditions are such that incomplete combustion cannot happen, representing good fire conditions for the FDS solver.

## 2) Input data

### a) Geometry of the compartment

The studied compartment consists of a 14,5 m * 14,5 m square floor and ceiling, with open boundaries on the four sides. Three extra open meters have been added on each side of the domain, and on top of the ceiling, to represent the same conditions as the experiments carried out by Alpert, while he was developing his formulas. The ceiling thickness is 0,50 m (that is the thinner wall possible for the coarse grid). The fire source is located in the middle of the floor, and consists of a default FDS burner (propane), where the only defined parameter is the HRR per unit area is defined.

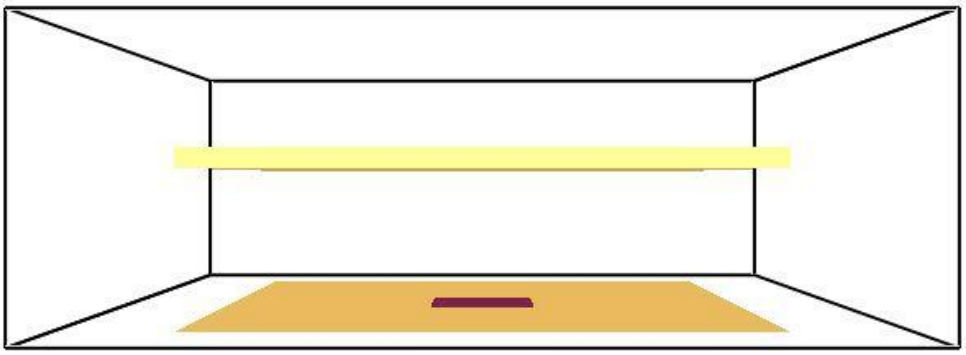

*Figure 5 : Geometry of the first set of simulations*

### b) Fire scenarios

The following fire scenarios have been simulated:

*Table 1: Fire scenarios modelled for the first set of simulations*

| **HRR (kW)** | 1000 | 1000 | 1000 | 1000 | 2250 | 2250 | 4000 | 4000 |
|---|---|---|---|---|---|---|---|---|
| **Burning surface ($m^2$)** | 4 | 4 | 4 | 4 | 9 | 9 | 16 | 16 |
| **Ceiling height (m)** | 4 | 6 | 8 | 10 | 4 | 6 | 4 | 6 |

The HRR per unit area was kept constant for all the simulations and was equal to 250kW/m$^2$, as recommended in Eurocode 1,1991-1-2:2002 Part 1-2 for office buildings (1).

The simulation time is 30 seconds that is enough to have the ceiling entirely full of smoke, and to have stabilized temperatures under the ceiling. The temperatures are averaged on the last 10 to 15 seconds, depending on the travel time of the smoke to cover the whole ceiling.

Then, a sensibility analysis has been carried out on the heat of combustion (20MJ/kg; 30MJ/kg; 46 MJ/kg), the soot yield (0,01 kg/kg ; 0,05 kg/kg ; 0,1 kg/kg) and the HRR per unit area (111kW/m$^2$; 250 kW/m$^2$; 444kW/m$^2$ ; 562,5 kW/m$^2$).

### c) Grid resolution

Three different grid sizes have been used for the simulations, in order to carry a grid sensitivity analysis:

- Coarse : dx = 0,50 m
- Medium : dx = 0,25 m
- Fine : dx = 0,10 m

### d) Ceiling thermal properties

The ceiling that is considered in the simulations is made of concrete. The thermal properties have been defined following Eurocode 2, 1992-1-2:2004 Part 1-2 guidance (20) .Those thermal properties are the following ones:

- Heat capacity : $c_p = 900\, J/kg.K$
- Density : $\rho = 2300\, kg/m^3$
- Thermal Conductivity : $k = 1{,}585\, W/m.K$

## 3) Results & analysis of the results

The temperature profiles under the ceiling have been obtained from the first set of simulations are shown in Appendix A. They will be analysed as a function of the studied parameters.

### a) Grid size

From Appendix A, it can be noticed that the coarse grid generally underestimates the temperatures compared to the medium and fine ones, and compared to Alpert temperature profiles. This is partly due to the discretization process that is increasing the errors proportionally to the size of the cell (50cm cell seems not suitable to represent a 1MW fire). Given that Alpert's expressions have been validated by experiments, it can be concluded that the grid resolution for the coarse grid is not good enough to capture all the major phenomena occurring in the gas phase.

There is no clear trend to define which of the two other grids (medium and fine) are representing the phenomenon the best: sometimes one temperature profile fits better than the other one, and sometimes that is the contrary. So the grid size will be fixed depending of the time available for the simulations compared to the required computational time.

The errors between the different simulations and the theory represented by Alpert are decreasing with the radial distance to the fire plume that was expectable given the FDS limitations to predict accurately the temperatures close to the flames. So, the conclusions for temperatures close to the flame need to be done carefully. However, this will not be a problem by the end since the focus of the master thesis is the far field temperature characterisation.

Concerning the turbulence resolution problem, the characteristic diameter $D^*$ over the grid size

$dx$ has been calculated for all the fire, and a slice of the TURBULENCE RESOLUTION output quantity has been calculated with FDS. The values of $\frac{D^*}{dx}$ are sum-up in the following table:

*Table 2: Grid resolution factors for the first set of simulations*

| **D*/dx** | **Coarse** | **Medium** | **Fine** |
|---|---|---|---|
| **1 MW fire** | 1,99 | 3,98 | 9,96 |
| **2,25 MW fire** | 2,75 | 5,51 | 13,78 |
| **4 MW fire** | 3,47 | 6,93 | 17,35 |

It is stated in FDS user guide (19) that the values of $\frac{D^*}{dx}$ used for validation were between 4 and 16, and in other documents like "Fire Dynamics and Forensic Analysis of Limited Ventilation Compartment Fires Volume 2: Modeling" (21) it can be found that the grid size that allows a correct resolution of the fire physics has a value of $\frac{D^*}{dx}$ between 5 and 10. From Table 2, it is straightforward to conclude that the coarse grid is not appropriate for this analysis. Concerning the medium and the fine grid, no conclusions can be drawn: the medium one does not seem suitable for small fires, but on the other hand the fine one seems to be over-accurate for big fires, that will result in a lot of time spent for the calculations.

The TURBULENCE resolution slices gives as an output the MTR value (Measure of Turbulence Resolution) that is small for well-resolved signals and close to unity for unresolved ones (19). As a reference, if the MTR is smaller than 0,2 give acceptable results concerning mean field quantities. As we can see on figure 6 and 7, the fine grid gives quite better results for small fires (1MW).

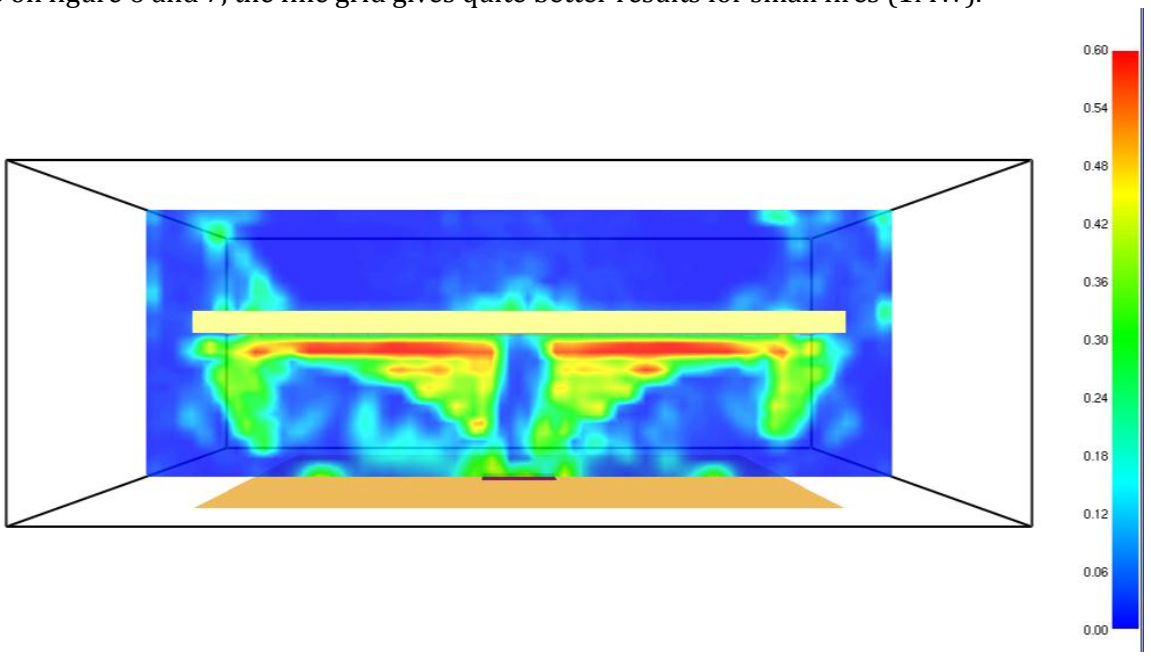


*Figure 6 : Turbulence resolution slice medium grid 1MW fire*

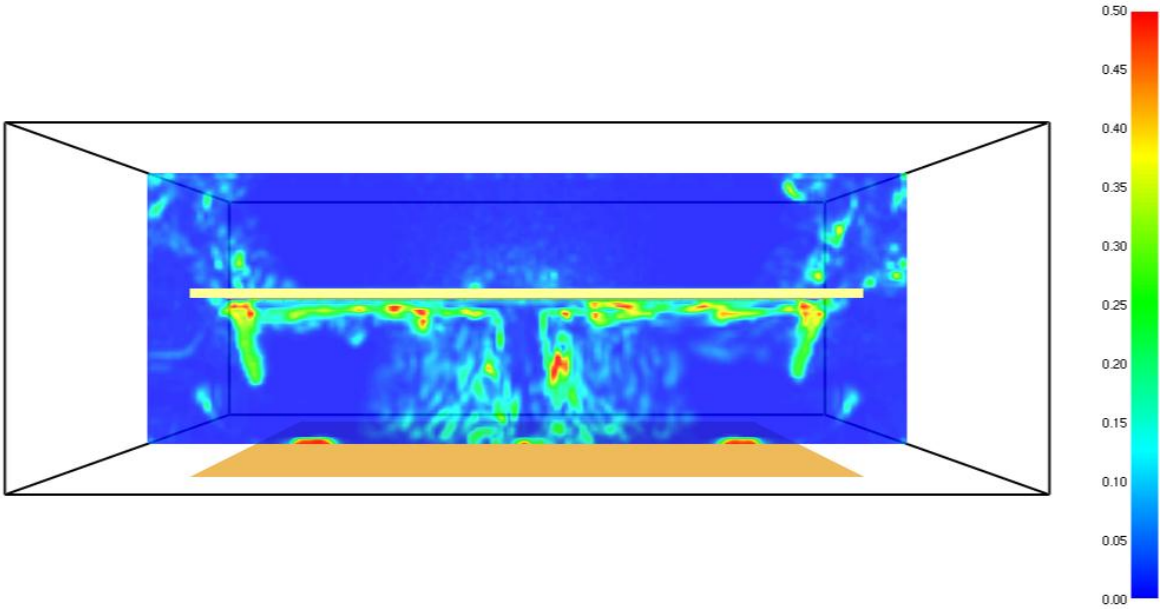


*Figure 7 : Turbulence resolution file fine grid 1MW fire*

However, for bigger fires (for instance 4MW in figure 9), the medium grid has a better resolution, so that both grids can be suitable to model the fire. Given that the HRR used to design the fires in the Travelling Fires methodology are quite important, using a medium size grid can be convenient to save time in computation.

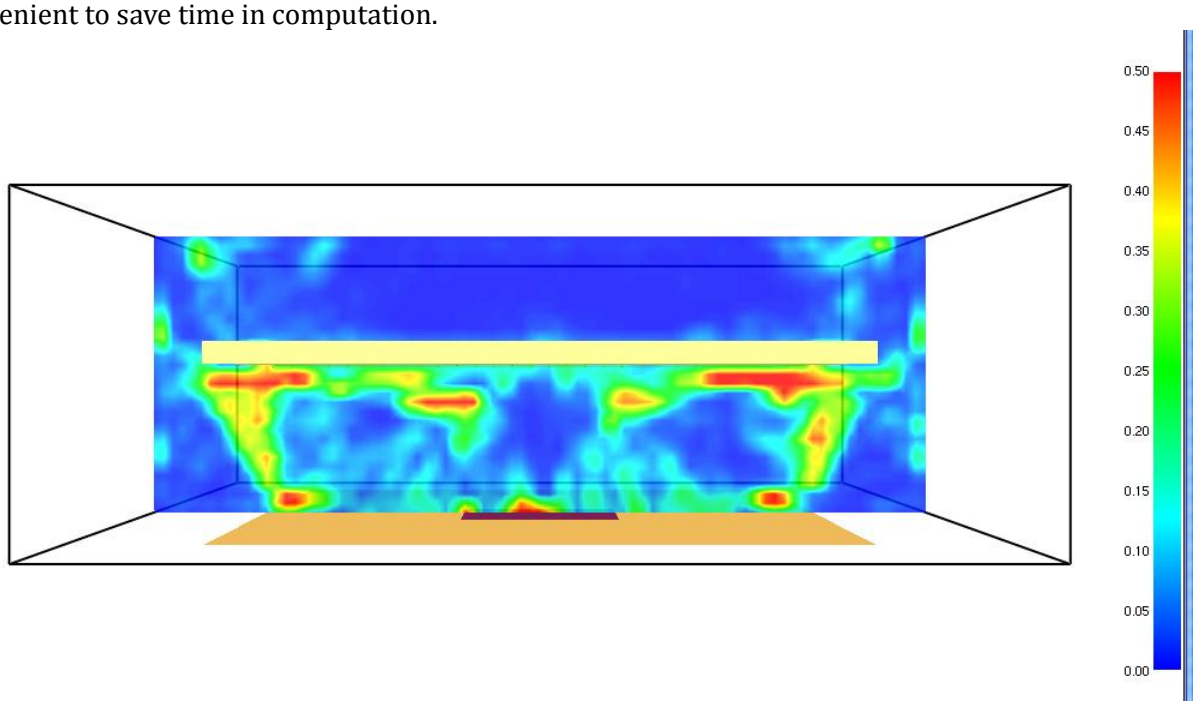


*Figure 8 : Turbulence resolution file medium grid 4MW*

### b) HRR and ceiling height: top hat profiles

The only noticeable effect when the HRR and the distance between the fire source and the ceiling increases is that the top-hat profiles shape used by Alpert in his unconfined expressions is not seen any more, and the shape of the temperature profiles resembles more the Gaussian profiles than the top-hat ones.

It has to be kept in mind that Alpert's top-hat profiles were use at that time to have quick and

simple calculations, but it is mentioned in the 1975 paper (6) that considering Gaussian profiles would be more accurate.

One of the reasons that cause the top-hat profiles not to be seen in the simulations can be the fact that Alpert considers the fire as a point energy source. When the HRR increases, the burning area increases (since the HRR per unit area is fixed at 250kW/m$^2$), up to a point where the point energy source assumption does not apply any more.

To sum up, the fire properties close to the flame, in Alpert's top hat profile region, have to be analysed with care.

### c) HRR per unit area

The HRR per unit area was varied from 111kW/m$^2$ to 562,5kW/m$^2$ for the same configurations concerning the ceiling height and the burning area. Table 1 represents the different simulations for the analysis of the impact of the HRR per unit area.

*Table 3 : Sensitivity analysis on HRR per unit area*

| **Fire n°** | **1_111kW/m²** | **5_562,5kW/m²** | **7_444kW/m²** |
|---|---|---|---|
| **HRR (kW)** | 1000 | 2250 | 4000 |
| **H(m)** | 4 | 4 | 4 |
| **Burning surface (m²)** | 9 | 4 | 9 |
| **HRR per unit area (kW/m²)** | 111 kW/m$^2$ | 562,5 kW/m$^2$ | 444 kW/m$^2$ |

Figures 9 shows that the differences for simulations with same HRR and ceiling height are important inside the fire plume and in the turning region, but reduces a lot as the radial distance to the fire axis increases, to be almost equivalent for $r/H \geqslant 0{,}5$.

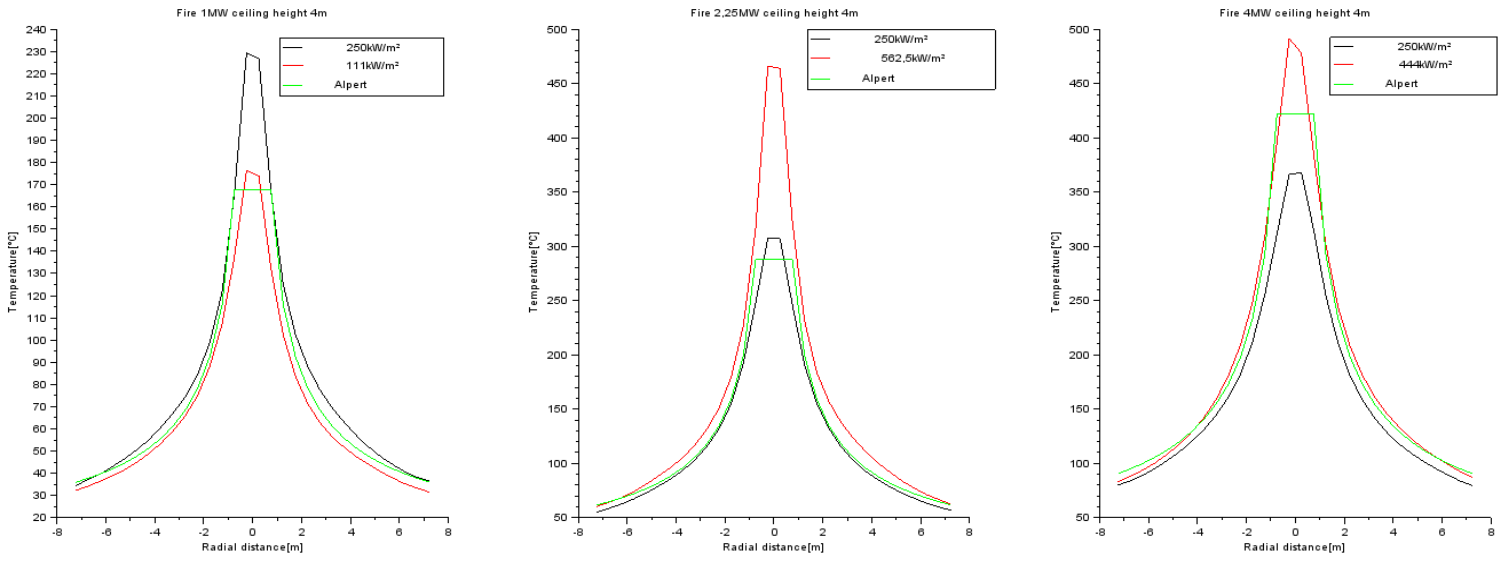


*Figure 9: Excess temperature of the hot gases for varying HRR*

A higher HRR per unit area means a higher quantity of energy released for the same area that will for most of the cases mean a higher flame height (the mean flame height formula from Zukoski, only depends on the HRR and the diameter of the fire source). The changes in the flame height will modify the interaction between the ceiling and the fire plume, and change the temperature field close

to the fire axis. The higher temperatures noticed for the simulations with an higher HRR per unit area, can be explained either by the phenomenon of flame impingement on the ceiling (for the 562,5kW/m$^2$ simulation for instance), or by the fact that the same quantity of energy is liberated in a smaller area, that causes the local gases temperatures to be higher close to the fire plume.

### d) Heat of combustion

Different heat of combustion were tested: 20 MJ/kg corresponding to the burning of wood, 30 MJ/m$^2$ corresponding to a mix of wood and hydrocarbons burning and 46 MJ/kg corresponding to pure propane burning (default fuel from FDS). Since the HRR of the fire is prescribed, the variation of the heat of combustion will change the quantity of smoke produced by the fire and will perhaps have an influence on the temperature field under the ceiling.

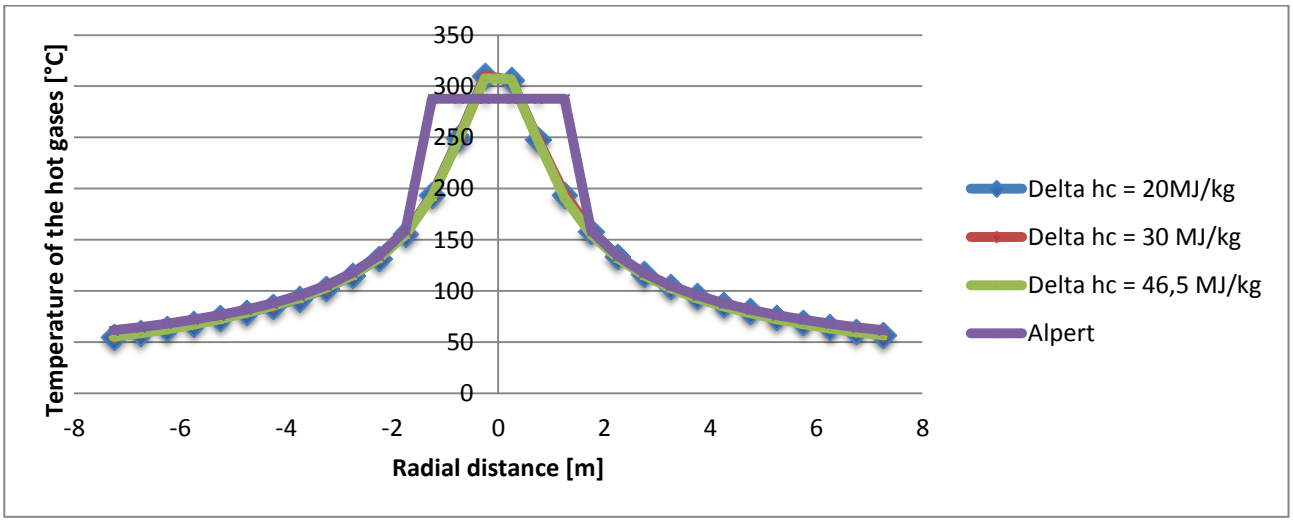


*Figure 10 : Excess temperature under the ceiling for various heat of combustion*

Figure 10 shows the maximum excess temperature under the ceiling for a 2,25MW fire and a 4m ceiling height. The temperature profiles under the ceiling are plotted for the three different heat of combustion. It can be seen that the differences between the three different profiles are very small so, this parameter will not be taken into account for the analysis and will be set at a default value for the next simulations.

### e) Soot yield

The same procedure as for the heat of combustion is repeated but for the soot yield. Three different values of soot yield (kg of smoke particles produced by kg of fuel burned) were tested : 0,01 kg/kg (default value from FDS suitable for a well-ventilated clean burning fuel), 0,05 kg/kg and 0,1 kg/kg (corresponding to a more common fire).

Figure 11 represents the temperature field under the ceiling for these variations in the soot yield. As the previous parameter, it can be concluded that the soot yield does not have an important impact on the temperature distribution under the ceiling. The soot yield will not be taken into account further ahead, and will be set at 0,01 that is the default FDS value.

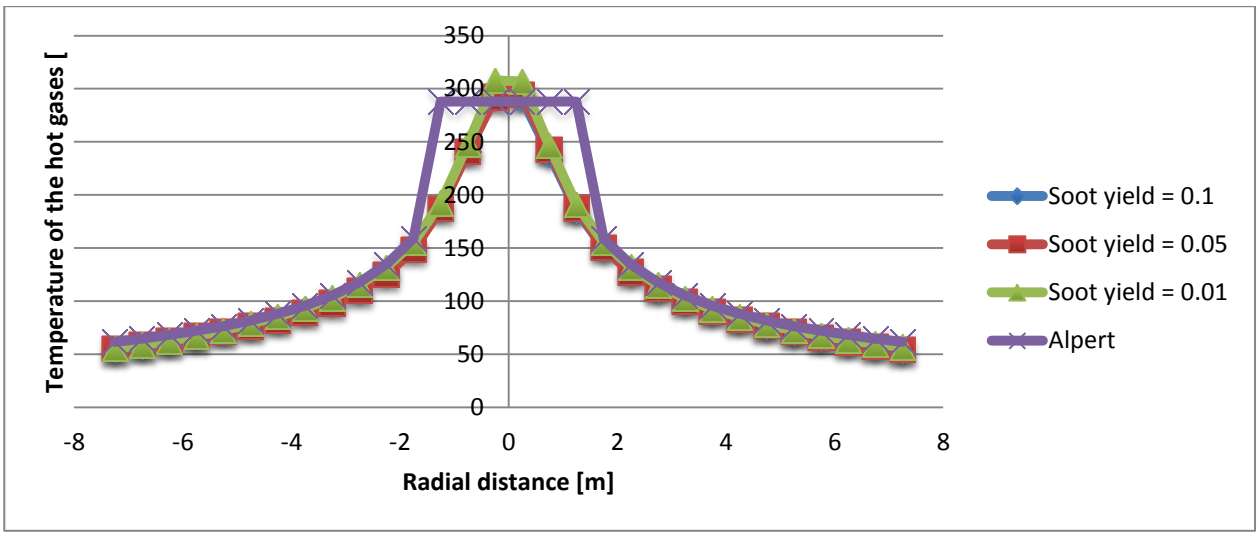


*Figure 11: Excess temperature under the ceiling for various soot yields*

## 4) Uncertainties from Alpert correlations

The different experiments carried out by Alpert generated a cloud of points from which a straight line trend was taken to represent the evolution of temperature and velocity under the ceiling. This trend was found as the best compromise to represent the different experimental results, but it implies that some uncertainties are present in the unconfined ceiling jet equations.

In an attempt to quantify those uncertainties, one graph representing the results of the series of experiments has been studied and the envelope of the points has been plotted in order to determine the range of trend lines that could have been picked up to represent the excess temperature under the ceiling. Power regression has been used on this log-log graph.

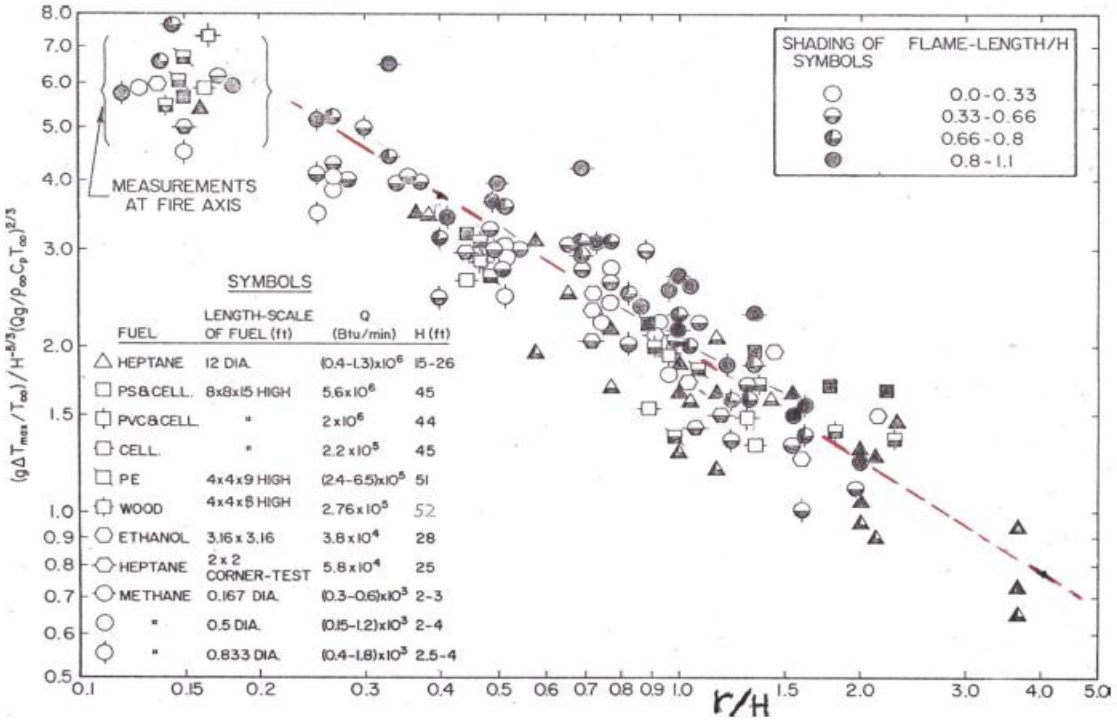


*Figure 12 : Alpert experimental results*

Then, from the results of the regression, the different expressions for the excess temperature were calculated, leading to the following equations (note that the calculated data for Alpert's original experiments are slightly different, but the original expression will be used for more consistency with the comparisons done beforehand):

- Superior limit : $\Delta T = 6{,}107 * \frac{\frac{(\dot{Q})^{2/3}}{H^{5/3}}}{(\frac{r}{H})^{0{,}96}}$ for $\frac{r}{H} > 0{,}18$

- Inferior limit : $\Delta T = 4{,}821 * \frac{\frac{(\dot{Q})^{2/3}}{H^{5/3}}}{(\frac{r}{H})^{0{,}52}}$ for $\frac{r}{H} > 0{,}18$

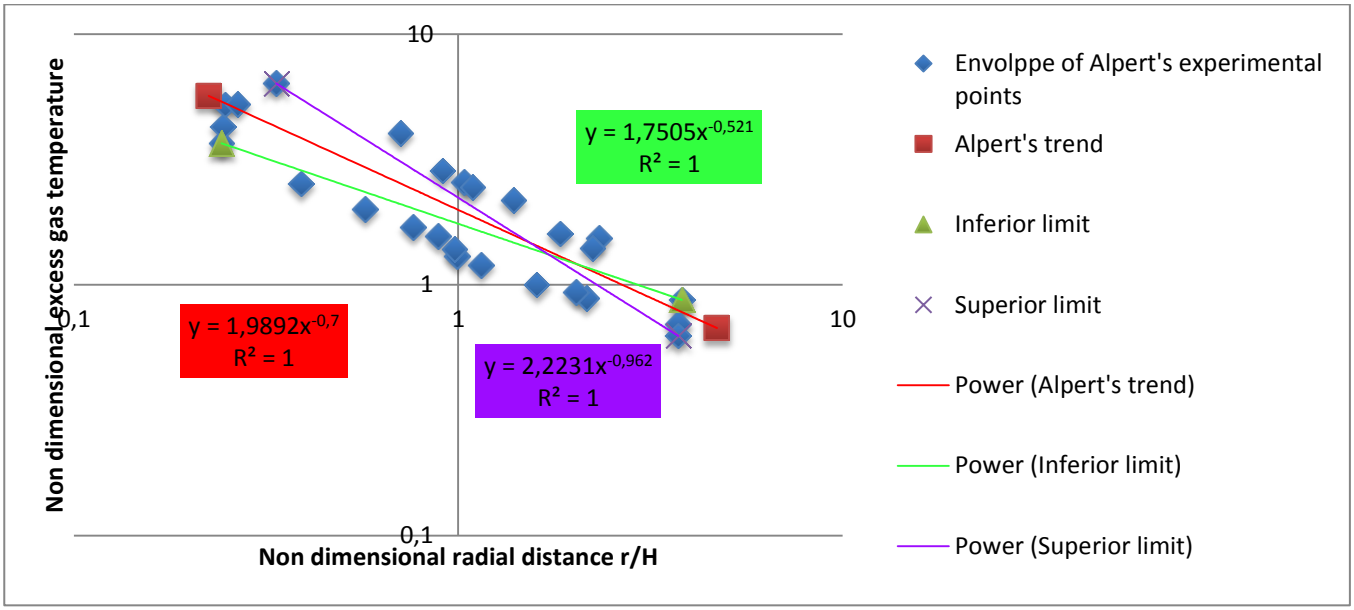


*Figure 13 : Uncertainties from Alpert experiment results*

The relative error between those equations and Alpert's original ones is 13,5% for the superior limit and 10,4% for the inferior limit. So, from this small study it can be considered that the ceiling jet properties are for the majority of the cases, well represented by FDS since in the errors are in the range of the uncertainties from Alpert experiments.

From this first series of simulations it can point out that FDS represents quite fairly the unconfined ceiling jet temperature field under the ceiling, especially from a radial distance of 2 meters away from the fire plume axis for the studied fires. However, it should be kept in mind for further analysis that the top-hat profile is not well represented by FDS for large fires, or for high ceilings and that temperatures close to the flames are not accurately predicted.

The fire parameters such as the heat of combustion, the soot yield or the HRR per unit are will not be taken into account in the next steps of this analysis, since they have very limited effects on the results. The fire power and the ceiling height remain the important parameters that influence the temperature distribution under the ceiling, as stated in the theory developed a few decades ago. The spatial discretization of the temperature in this quite small compartment (14,5 m * 14,5 m) is already noticeable, as predicted by the unconfined ceiling jet theories (Alpert (5), Heskestad (10)). Given that the final compartment is 14,25 m * 30,25 m, it can be expected that the discretization will be more important. Nevertheless, the smoke accumulation and the compartment can have a homogeneous effect on the temperature field under the ceiling. In order to quantify this effect, screens will be added to the compartment, in order create a deeper smoke layer, while keeping good ventilation conditions.

# CHAPTER 4: Smoke accumulation under the ceiling

## 1) Methodology

Now that it is known that FDS can represent the unconfined ceiling jet quite fairly, it is time to study the impact of smoke accumulation on the temperature distribution under the ceiling. The development of an upper layer in an enclosure will increase the ceiling jet temperatures, modifying the heat transfer to the structure (22). Moreover, it can be expected that this upper layer will have a homogenous effect on the gas field, since the uniformity of the smoke layer is often used in analytical models (15), (16) or in zone models.

In an effort to characterise the smoke accumulation effect, screens will be added to the geometry of the first set of simulations. It will make it possible to determine whether or not the temperature variation in space is still present and to study the heat fluxes to the ceiling (convective and radiative), to try to understand which phenomenon is predominant in the heat transfer to the structure. The addition of the screens is very convenient since it allows the study of the impact of a smoke layer while still being in good ventilation conditions.

It has been decided that the height of the compartment, being one of the main parameters in the determination of the temperature distribution for the unconfined ceiling jet, will be fixed at 4 meters, since the final aim of this master thesis is to study the gas field in the compartment fixed by CERIB. It will be easier to plan then the last set of simulations inside the studied compartment.

## 2) Input data

### a) Geometry of the compartment

As said before, the geometry of this new set of simulations is quite similar to the previous one, but 4 concrete screens have been added to the ceiling in order to keep under the ceiling a significant smoke layer.

The height of the screens was varied for a sensibility analysis, and it was then decided to leave a clear height of 2 meters that corresponds to the door soffit in most of the actual compartments. So, the screens height will be 2 meters for all the simulations.

The thickness of the screens is the same as the ceiling, that is 0,5 m.

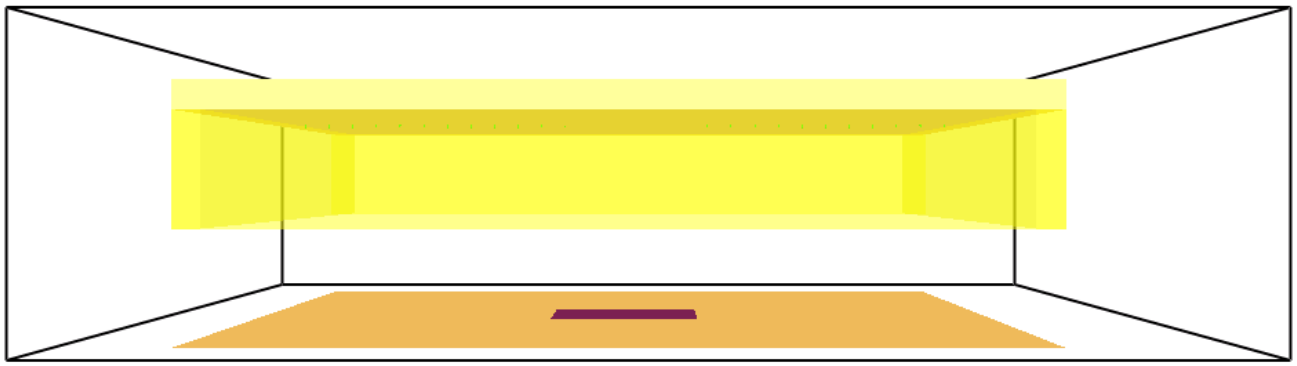

*Figure 14 : Geometry of the second set of simulations*

### b) Fire scenarios

Since the ceiling height is fixed, the only parameter that is varying is the HRR of the fire. The

HRR per unit area is kept constant and equal to 250 kW/m² for the same reasons explained in chapter 1. The chosen HRR are 1MW – 2,25 MW – 4MW – 6,25 MW that corresponds respectively to 4 m² - 9 m² – 16 m² – 25 m² of burning area.

The screens height was varied from 1 to 3 meters for the 1MW fire, in order to understand the impact of the thickness of the smoke layer on the temperature field under the ceiling.

The simulation time is 150 seconds, where a quasi-steady state is reached for the gas field. 'Quasi' is used because the heat transfer to the ceiling is a transient phenomenon that depends on the ceiling temperature, and the steady state for the gases will be only reached when the solid phase is at the steady state. The thermal-penetration time of a 0,5 m thick concrete slab is so long that it is not suitable for CFD calculations, since the computational time will be too large for each simulation. The gas field reaches a quasi-steady state after around 100 seconds, and increases very slowly then, that is why 150 seconds should be sufficient to have a good estimate of the temperature distribution close to the ceiling.

To accelerate the process in the heat solid phase, the SHRINK FACTOR tool (19) from FDS was used: this parameter multiplies the thermal properties of the solid boundaries by a chosen factor. A value of 10 was chosen in this set of simulations.

#### c) Grid resolution

From the last set of simulations, the medium and fine grids look suitable to run the simulations, with a recommendation of the fine grid for small HRR fires. Since the computation time was quite reasonable with the fine grid, all the simulations were carried out with this 10 cm cell mesh.

#### d) Ceiling thermal properties

The ceiling that is considered in the simulations is made of concrete. The thermal properties has been defined following Eurocode 2, 1992-1-2:2004 Part 1-2 guidance (20) .Those thermal properties are the following ones:

- Heat capacity : $c_p = 900\, J/kg.K$
- Density : $\rho = 2300\, kg/m^3$
- Thermal Conductivity : $k = 1{,}585\, W/m.K$

## 3) Results & analysis of the results

### a) Screens height

As it can be seen from figure 15, the increase in the screen height involves a small increase in the temperatures under the ceiling everywhere except close to the flames where the differences are even smaller. This was expectable since a thicker smoke layer would mean that the losses by mixing with cold air because of entrainment will happen further away from the ceiling, allowing more important temperatures close to the ceiling. Concerning the turning region, the mixing is so important in this area that the differences are really small.

Concerning the heat fluxes, there are almost no changes for the radiative and convective heat fluxes to the ceiling that is linked to the small differences in temperatures found under the ceiling.

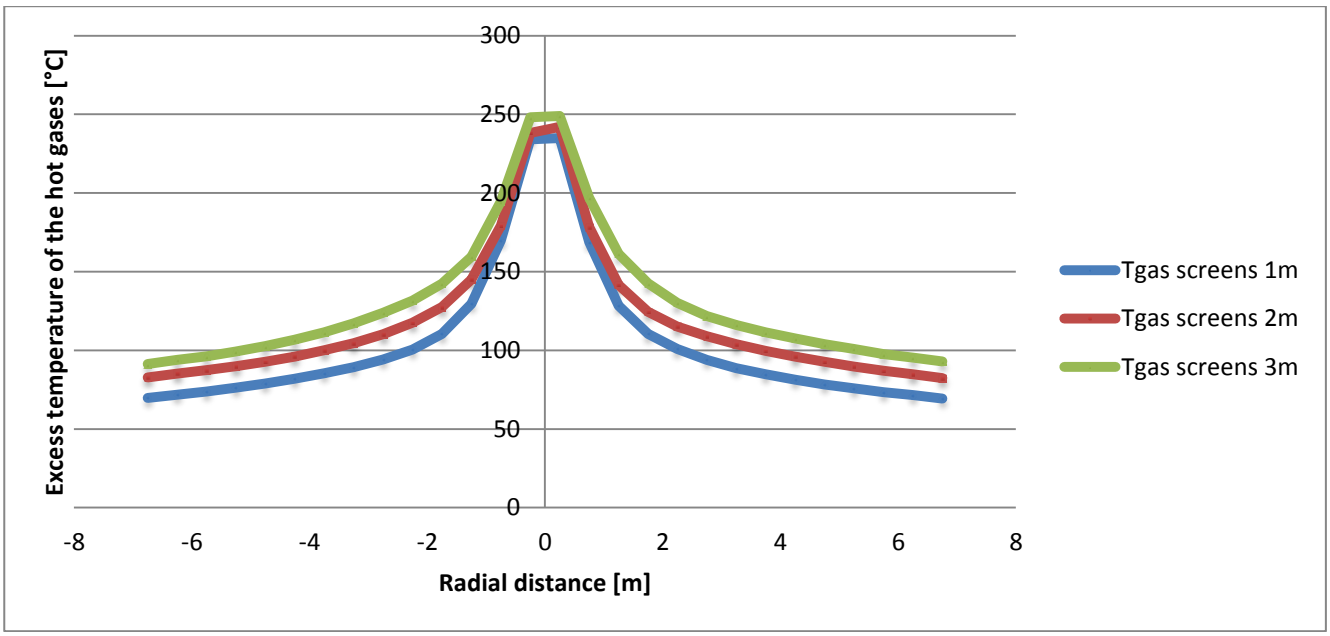


*Figure 15 : Excess temperature of the hot gases for different screen heights*

### b) Temperature field

The accumulation of a smoke layer under the ceiling results as predicted by an increase of the temperature field, compared to the unconfined ceiling configuration. All the simulations give gas temperatures under the ceiling higher than Alpert's predictions except for the temperature close to the flames for big fires (more than 4MW).

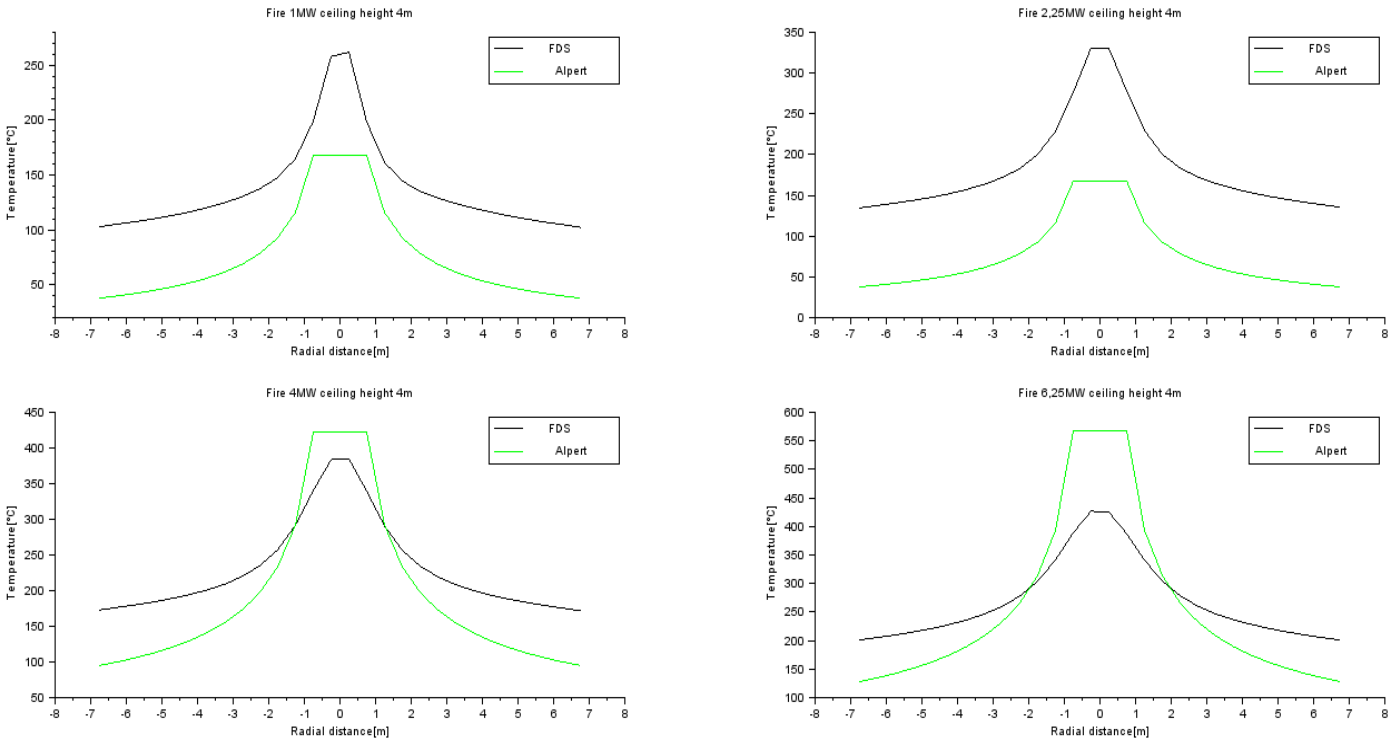


*Figure 16 : Excess temperature of the hot gases with screens*

For small fires (1 and 2,25MW), FDS temperatures are always bigger than Alpert ones, but the shape of the temperature profile is exactly the same as Alpert's one. For instance for the 1MW fire, the FDS predictions fit to the curve corresponding to Alpert +35°C (figure 17).

But this trend is not followed if the HRR of the fire is increased: for bigger fires Alpert's temperature profiles shape does not match the confined ceiling jet temperatures anymore. It looks that Alpert over predicts the temperatures close to the flames, and under predict the ones further away. As said earlier, this observation should be taken carefully important mistakes can be produced by FDS concerning the temperature field close to the flames. On top of that, the Travelling Fires methodology uses a constant value to define the Near Field temperature (1200°C) that is not the focus point of this thesis. However, FDS is supposed to predict accurately the ceiling jet temperatures away from the flames. The fact that the far field temperatures are higher than the one predicted by Alpert is very important to be taken into account, since this gas temperature field is the main input for the heat transfer calculations inside the solid phase, that will determine or not the failure of the structural elements.

Moreover, with the smoke accumulation, the Gaussian profile of the temperature field under the ceiling for big HRR fires is even more noticeable.

After this set of simulations, it is clear that the temperature of the hot gases under the ceiling for a confined ceiling jet is spatially discretized, since the temperature difference between the edge of the compartment to the limit between the turning region and the ceiling jet are ranging approximately from 40°C to 100°C for the studied fires.

### c) Heat fluxes

The radiative and convective heat fluxes to the ceiling have been studied in order to determine if there is a predominant phenomenon, and how do the heat fluxes to the ceiling evolve with time. Concerning the convective heat transfer coefficient h, comparisons will be made with the h used in the heat transfer calculations of the Travelling Fires method (25W/m²K for exposed surfaces).

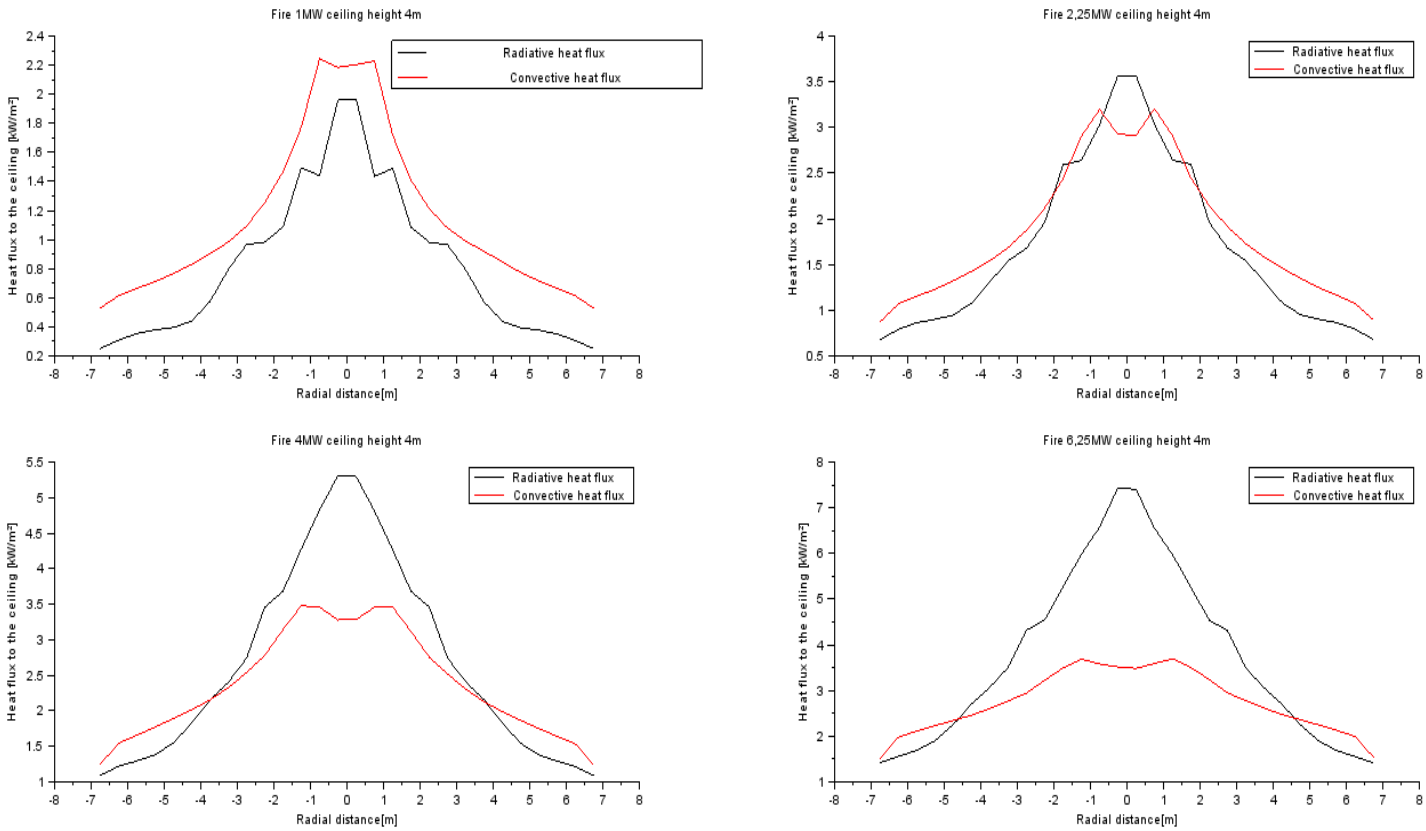


*Figure 17: Heat fluxes to the ceiling with screens*

It was observed for the different simulations that the convective heat fluxes are more important than the radiative ones for small fires. When the HRR is increased, the radiative fluxes close to the flames are becoming a lot bigger than the convective ones, this is understandable given that radiative fluxes are proportional to $T^4$ and convective fluxes are proportional to T. Since the radiation decreases rapidly with the distance, it can be noticed that for radial distances bigger than 4 meters, the convective heat fluxes are more important than the radiative ones.

# CHAPTER 5: Fire within the compartment

## 1) Methodology

Now that the unconfined ceiling jet and the smoke accumulation have been studied, the fire behaviour in the compartment can be modelled and analysed. A burner with various HRR will be placed in the centre of the compartment, and the area of the openings (located on a single wall) will be varied to determine the influence of ventilation on the temperature profiles and heat fluxes.

Then a correlation valid for a range of HRR will be extracted to characterise the temperature field under the ceiling, aiming at obtaining a fair estimate of the temperature distribution under the ceiling without having to perform the CFD simulations. Afterwards, the limitations and the quality of the correlation will be discussed.

## 2) Input data

### A) Geometry & fire scenarios

The final compartment is now modelled: it has the dimensions of 14,25 m * 30,25 m * 4m, with concrete walls of 0,20 m of thickness. The fire is still located in the middle of the compartment so that no interactions with the laterals walls are modelled. The HRR of the fires were chosen in the similar way of the Travelling Fires design, so that the burning area of the fire represents 1%, 5%, 7,5%, 10%, 15%, 20% and 25% of the entire floor plate. This gives the respective HRR of 1MW; 5,5 MW; 8 MW, 10,8MW, 16,2MW, 21,5MW and 27,8MW (cf table 4).

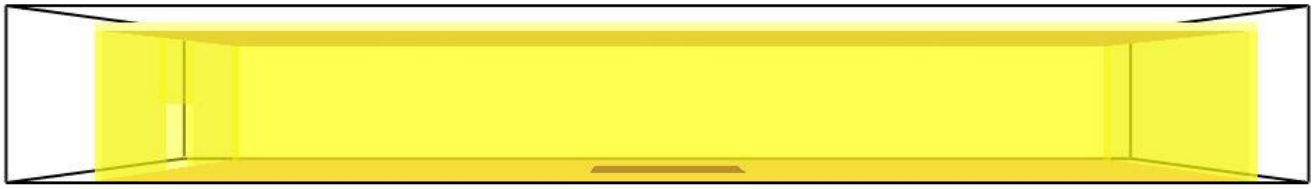

*Figure 18: Compartment geometry for the third set of simulations*

The openings of the compartments will be located only on one side, and will be representing regular double-doors of 1,5m width * 2m high (the single opening being representative of regular office configuration). Several ventilation conditions will be tested for the same HRR, in order to examine the effects of the ventilation on the temperature field and heat fluxes. As said in the FDS limitation part, the software is suitable for well ventilated fires (22), so the simulations will be performed for fuel limited fires and not at all for ventilation limited fires. To achieve these conditions, rapid hand calculations have been carried out in order to determine the minimum of opening areas needed for the different HRR chosen. It was observed by Kawagoe (23) that the rate of burning of wood cribs under restricted ventilation conditions follows the relationship:

$$\dot{m} = K.A_w\sqrt{H}$$

In Enclosure Fire Dynamics (24), the maximum energy rate released in a compartment, based on Kawagoe expression is:

$$\dot{m} = 0{,}09.A_w\sqrt{H}.\Delta H_{eff,wood}$$

So, the minimum opening area was determined, and is sum up in Table 4 :

*Table 4: Ventilation requirements for the different fires modelled*

| HRR (% of floor plate burning) | Minimum opening width | Equivalent number of doors |
|---|---|---|
| 1000kW (1%) | 0,46 m | 1 door |
| 5500kW (5%) | 1,27 m | 1 door |
| 8000 kW (7,5%) | 1,84 m | 2 doors |
| 10800kW (10%) | 2,5 m | 2 doors |
| 16200kW (15%) | 3,75 m | 3 doors |
| 21500kW (20%) | 4,97 m | 4 doors |
| 27800 kW (25%) | 6,43 m | 5 doors |

### B) Simulation time and steady state

The simulation time is 1000 seconds for the gas phase and 10000 seconds for the solid phase (a time shrink factor of 10 used as explained in chapter 4), that is going to give a fair estimate of the quasi-steady state temperatures for the gases. As said in chapter 4, given that the solid boundaries are made of concrete it will take a long time to reach the steady state, time that is not affordable for these CFD calculations. For instance, for the concrete ceiling of the simulation, the thermal penetration time is :

$$t_{p,wall} = \frac{\delta^2}{4\,.\,\alpha_{concrete}} = \frac{\delta^2}{4.\frac{k}{\rho.c_p}} = \frac{0.2^2}{4.\frac{1{,}585 * 10^{-3}}{2300 * \ 0{,}9}} = 52240\ sec$$

So, it obvious that the solid boundaries will not be in equilibrium after the 10000 seconds modelled, however, the heating process is so slow that the gas temperature is not going to increase a lot compared to the first 100 seconds of the simulation. Figure 20 represents the temperature evolution for radial position of 14,7 m away from the fire axis : it is obvious that first the gases are spreading under the ceiling and start to accumulate to form the smoke layer (important increase in temperatures) and then the gases are heating up more slowly, at the same time as the walls are heating up (slow increase of the temperatures from 200s to 1000s). It can be seen from figure 20 that between 200s and 1000s, the temperature increases of more or less 70°C, that represents a 15% increase for the last 800 seconds, that is why the fact that a quasi-steady state is reached instead of the traditional steady state has to be kept in mind concerning the following analyses.

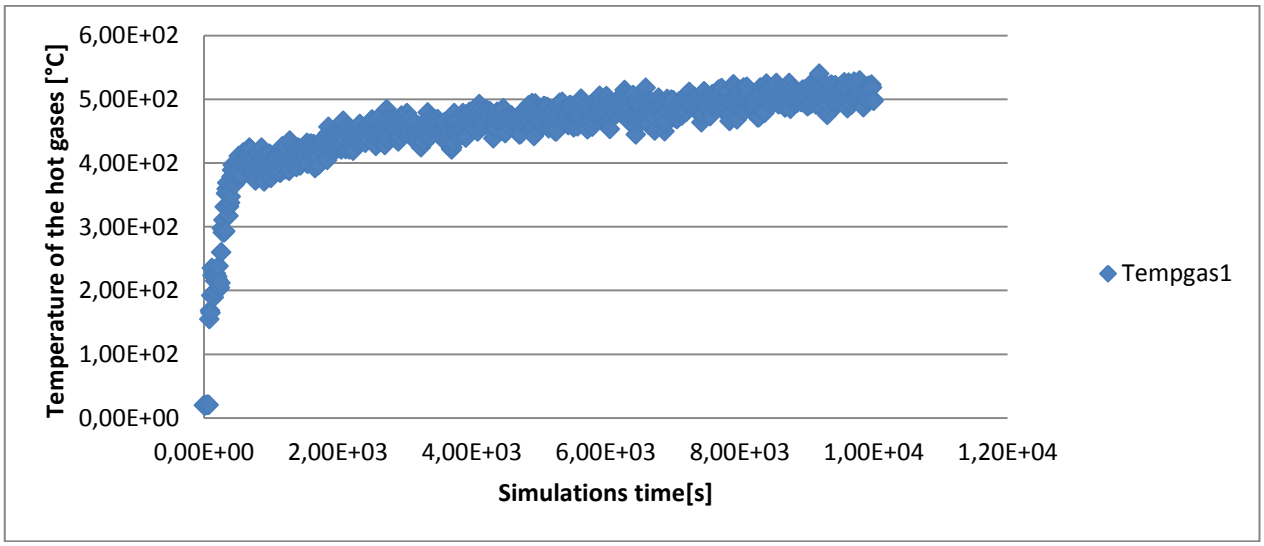


*Figure 19: Temperature evolution with time for r=14.7 m for the 21,5 MW*

### C) Grid size

The grid size was fixed at first at 10 cm but a single simulation taking more than 2 weeks to compute, it was decided to use a coarser grid of 20 cm that reduces the compilation time to 2-3 days, given that the different HRR used are high enough to make the 20 cm grid size suitable.

Figure 20 and 21 represent the turbulence resolution slices for the 5500kW fire and the 21500kW one. It can be seen that the MTR values close to the ceiling, are quite acceptable (closer to 0,20 than unity). The only places where there are some high values of MTR are the stagnation zone on the right of the compartment and close to the opening.

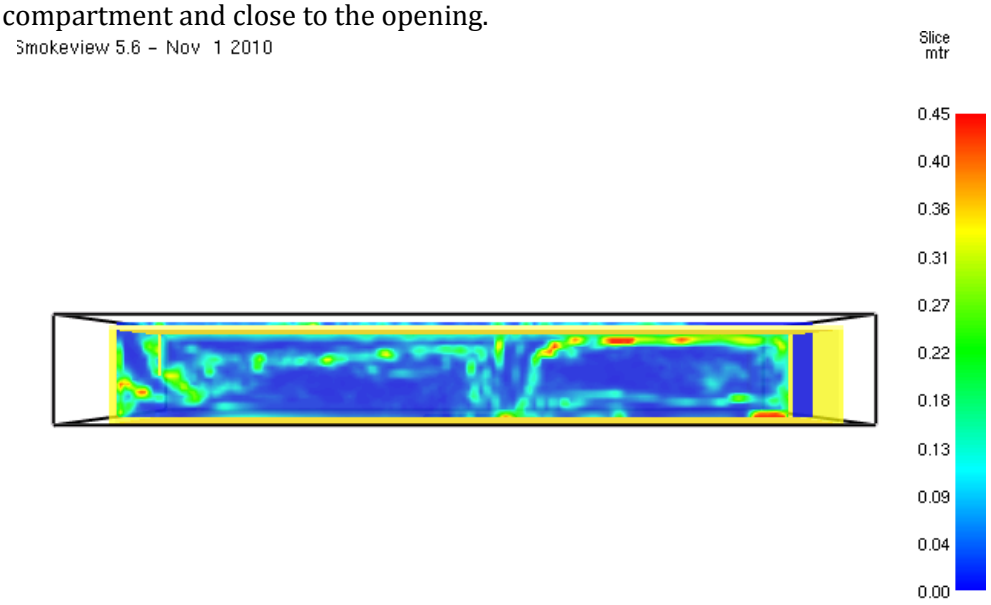


*Figure 20: Turbulence resolution slice for the 5500 kW fire - 20 cm grid*

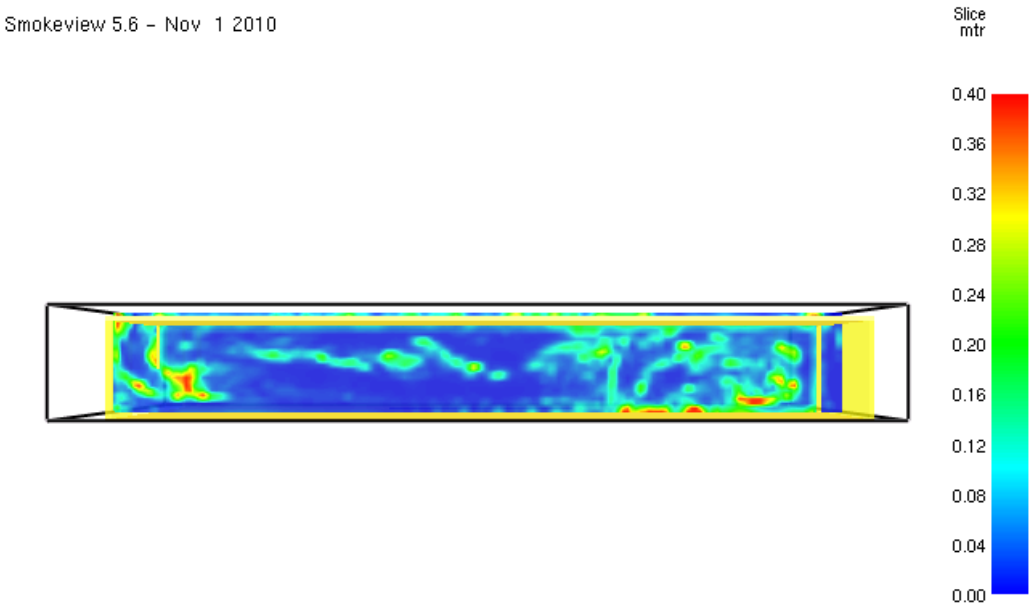


*Figure 21: turbulence resolution slice for the 21500kW - 20 cm grid*

Moreover, the results of the 10cm grid simulation and 20cm grid simulations have been compared in Appendix B, and it turns out that the results of the 20 grid are very similar to the 10 cm simulations. This means that the accuracy of the 20 cm grid given the reduced computation time is quite good compared to the 10 cm grid that is not affordable for this project.

### D) Ceiling thermal properties

The ceiling that is considered in the simulations is made of concrete. The thermal properties have been defined following Eurocode 2, 1992-1-2:2004 Part 1-2 guidance (20) .Those thermal properties are the following ones:

- Heat capacity : $c_p = 900\,J/kg.K$
- Density : $\rho = 2300\,kg/m^3$
- Thermal Conductivity : $k = 1{,}585\,W/m.K$

### E) Final set of simulations

The simulations for the different HRR were performed with the minimum number of doors required to be in fully combustion conditions within the compartment. However, for some of them the analytical calculations for the ventilation were not sufficient, and flames were going through the doorway and outside of the compartment. Since these conditions are not suitable for the analysis carried out, the number of doors was increased in order to reach good ventilation conditions. To sum up, the following simulations have been computed:

*Table 5: Simulation list of the third set of simulations*

| Simulation number | HRR of the fire [kW] | Number of doors | Ventilation conditions OK? [Yes/No] | Percentage of the floor plate burning |
|---|---|---|---|---|
| 1 | 1000 | 1 | Yes | 1% |
| 2 | 1000 | 2 | Yes | 1% |
| 3 | 1000 | 3 | Yes | 1% |
| 4 | 1000 | 4 | Yes | 1% |
| 5 | 1000 | 5 | Yes | 1% |
| 6 | 5500 | 1 | No | 5% |
| 7 | 5500 | 2 | Yes | 5% |
| 8 | 5500 | 3 | Yes | 5% |
| 9 | 5500 | 4 | Yes | 5% |
| 10 | 8000 | 2 | No | 7,5% |
| 11 | 8000 | 3 | Yes | 7,5% |
| 12 | 10800 | 2 | No | 10% |
| 13 | 10800 | 3 | No | 10% |
| 14 | 10800 | 4 | Yes | 10% |
| 15 | 16200 | 3 | No | 15% |
| 16 | 16200 | 4 | Yes | 15% |
| 17 | 16200 | 5 | Yes | 15% |
| 18 | 21500 | 5 | No | 20% |
| 19 | 21500 | 6 | Yes | 20% |
| 20 | 27800 | 5 | No | 25% |
| 21 | 27800 | 6 | No | 25% |
| 22 | 27800 | 7 | Yes | 25% |

## 3) Results & analysis of the results

### A) Ventilation influence

The variation of the ventilation area while the opening height is kept the same, has impacts on the temperature field under the ceiling. As it can be seen in Appendix C, the larger the opening is the smaller the temperatures will be (the maximum temperature difference is 10% between the critical width configuration and wider opening configurations for radial distance superior than 3m from the

fire axis), because of a bigger mass flow of hot gases leaving the compartment and a thinner smoke layer within the compartment. The same trend is observed for the convective and radiative fluxes: there is a decrease in the fluxes when the opening gets wider (up to 0,17kW/m² difference for the convective heat fluxes and 0,7 kW/m² for the radiative heat fluxes).

It can be noticed as well from Appendix C that this phenomenon is more important for the 5,5MW fire than for the 1MW one, and can be expected to be more and more noticeable for bigger HRR. Given that we cannot characterise the temperature of the gases for all the ventilation configurations and that the profiles are following the same trend, the more conservative will be kept in the analysis, meaning the one with the highest temperature and heat fluxes. This means that for each fire, the critical opening width (the smaller opening width for which the complete combustion is taking place inside the compartment) will be chosen to correlate the data.

### B) Temperature field

Simulations with the critical width for the opening have been performed for the different HRR chosen. The results are summed up in the temperature profiles of figure 22.

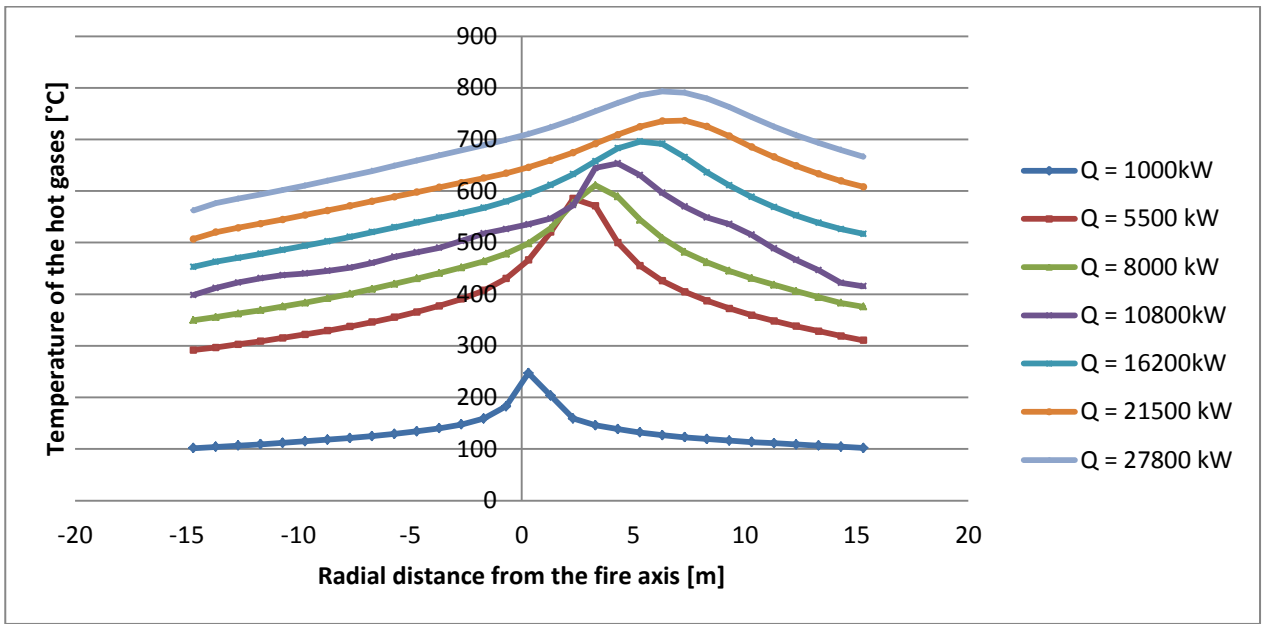


*Figure 22: Temperature profiles for critical width opening for different HRR*

First of all, it is visible that the temperature peak shifts on the right as the HRR increases. This phenomenon only happens when the opening is located on one side and can be explained by the fact that the burners used are so big (up to to 112 m²) that the side of the burner that is opposite to the opening receives quite less air than the side that is the closest to the opening. Because of that the volatiles are going to be more dispersed before burning, that it will create an higher flame on the bottom side of the burner. This high part of the flame is shifted on the right hand side compared to the middle of the burner, and is responsible of the shifting of the temperature profiles. This phenomenon becomes stronger and stronger when the HRR increases because the burner surface is increasing and the fire demands more and more oxygen for quite small openings. This can be seen on the velocity vectors from figure 23.

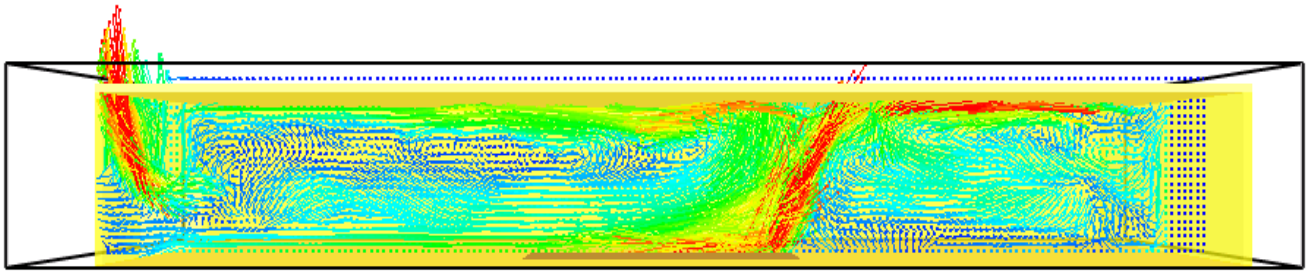

*Figure 23: Velocity vectors - 16200kW fire*

Then, as the HRR increases the shape of the temperature profile is changing from a power evolution as a function of the radial distance (1MW and 5,5MW fires) to a linear evolution (16,2MW , 21,5MW and 27,8MW fires).

Finally, if those results are compared to Alpert correlation (cf. Appendix D), it is obvious that Alpert's trends is followed for small fires (even if the temperatures are higher because of the smoke accumulation and the compartment effect). On the contrary for big HRR Alpert's temperature profile is not followed anymore: the flame temperatures predicted by Alpert are really higher than the one generated by FDS, and the temperature further away from the flames are under predicted by the ceiling jet correlation, that we can see in figure 24.

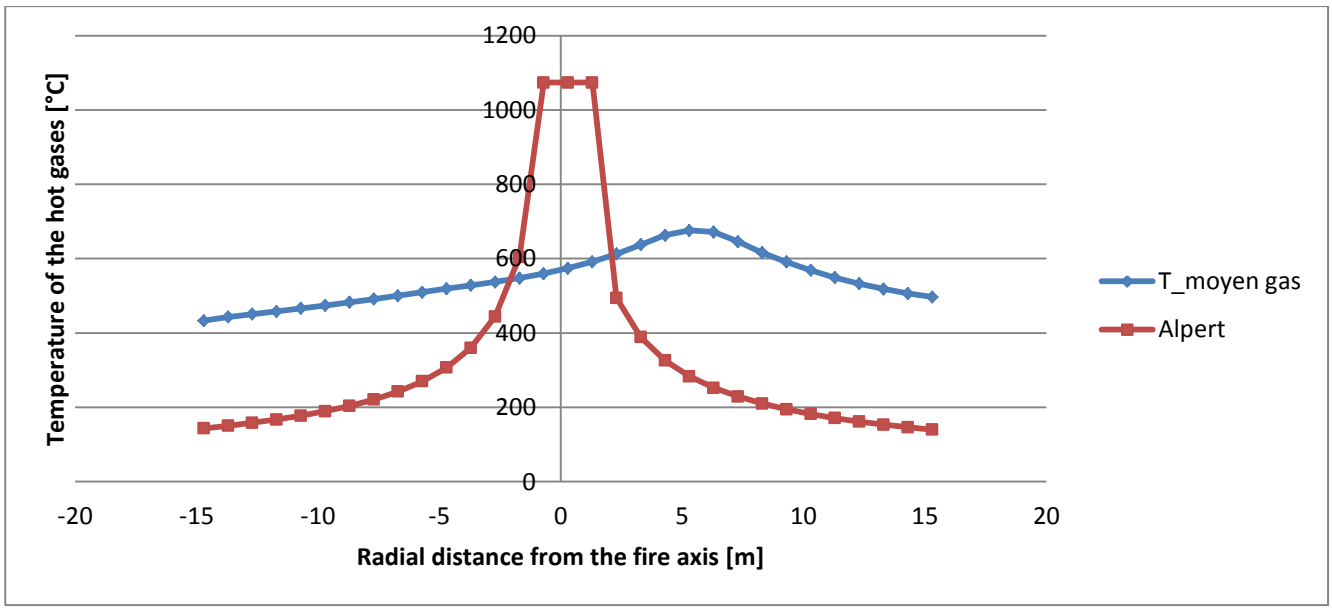


*Figure 24: Comparison between Alpert and FDS temperature profiles for the 16,2MW fire within the compartment*

### C) Heat fluxes

It can be first noted that the heat fluxes to the ceiling are varying in time, as it can be seen in figure 25 that represent the evolution in time of the heat fluxes to the ceiling for a given radial position.

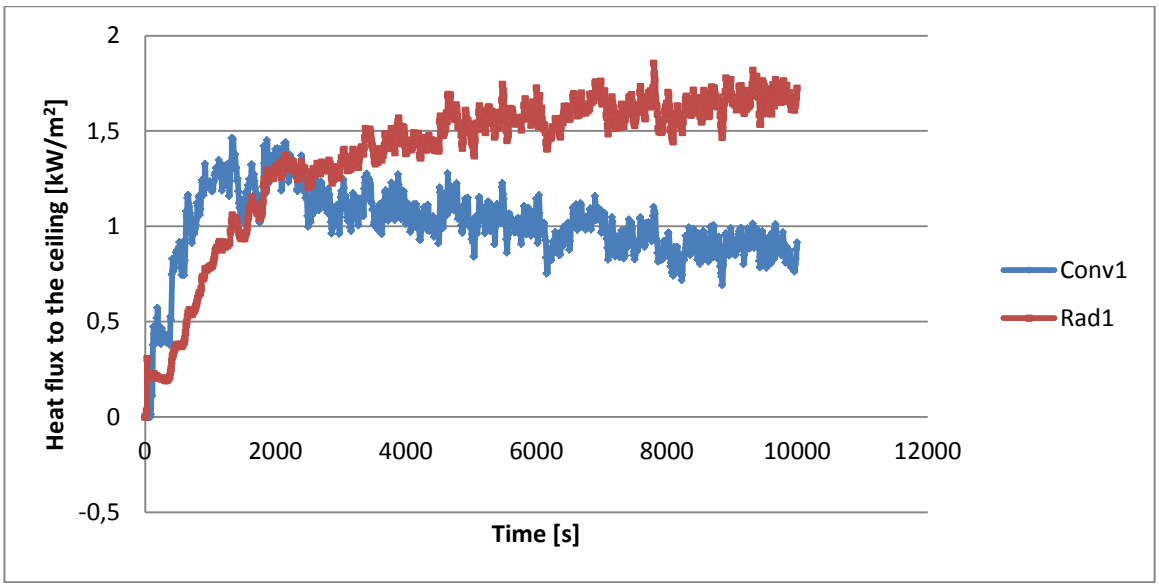


*Figure 25: time evolution of the heat fluxes - 5,5 MW fire*

The convective fluxes are decreasing as the wall is heating up, and that the temperature difference between the hot gases and the wall is decreasing, whereas the radiative heat fluxes are increasing as smoke that is becoming hotter and hotter is accumulating under the ceiling. This time evolution makes the comparison between heat fluxes tricky and it is not possible to compare with analytical formulas expressed in chapter 2, since it is not clearly stated in which conditions the formula should be used. The averaged heat fluxes on the last 100 seconds of the simulation are plotted in Appendix E, to have an estimation of the order of magnitude between radiation and convection, since the Travelling Fires can last up to several hours.

From this appendix, it is clear that the radiative fluxes become more and more important as the HRR of the fire increases, whereas the convective fluxes after 1000 seconds are quite constant for different HRR and equal more or less to 1kW/m².

Concerning the convective heat transfer coefficient, that was extracted from FDS, it can be observed on figure 26 that shape is more or less similar for all the HRR, but it is shifted on the right and side as the HRR increases, such as the temperature peak. Moreover, the convective heat transfer coefficient globally reduces as the HRR increases. The value of 25 W/m².K is chosen for the exposed face in the Travelling Fires methodology (3) that clearly overestimates the rate of heat transfer by convection compared to the FDS simulations.

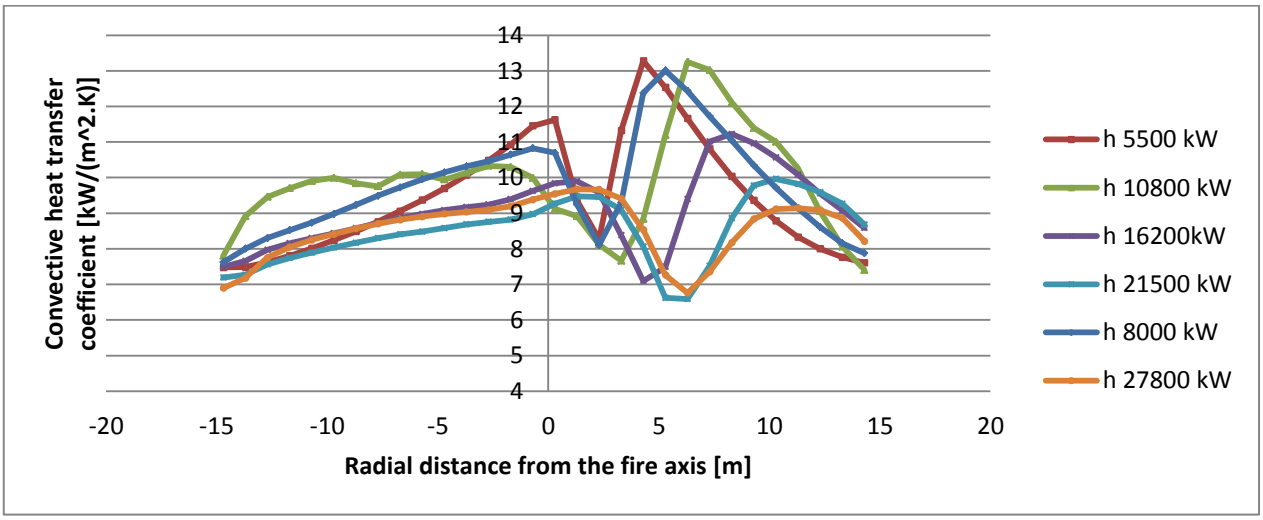


*Figure 26: Convective heat transfer coefficient distribution for different HRR*

## 4) Correlation for the temperature field

Since Alpert correlation does not seem appropriate to characterise properly the temperature environment of the gases under the ceiling, an attempt has been made to create an alternative correlation that would be more suitable for the Travelling Fires methodology.

### A) Non dimensional temperature profile

First of all, in an order to have similar temperature profiles, the radial distance from the fire axis r used (that corresponds to the middle of the burner) was changed to the radial distance from the temperature peak $r^*$, that we can see on figure 27.

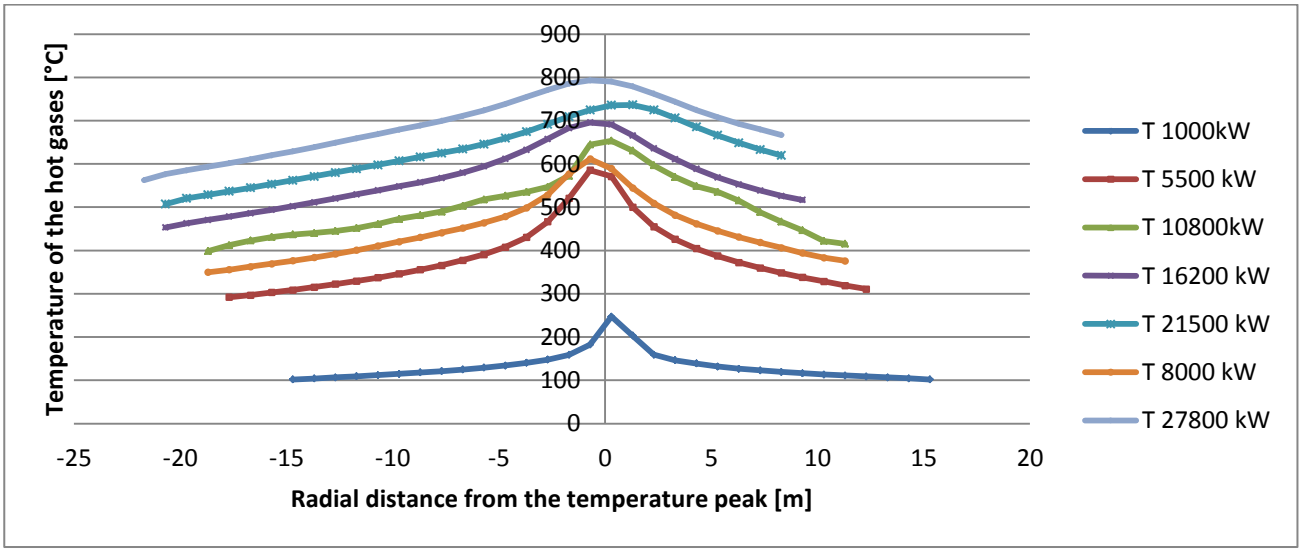


*Figure 27: Temperature profiles as a function of the distance from the temperature peak*

Then, the temperature profiles for the different HRR have been transformed in non-dimensional temperatures profiles by dividing each by their peak temperature called $T_{max}$ , and multiplied by the non dimensional HRR, $Q^* = \frac{\dot{Q}}{\rho_\infty * c_p * T_\infty * \sqrt{gD} * D^2}$ . On figure 28, the quantity $\frac{T_{gas} \cdot Q^*}{T_{max}}$ was plotted as a function of the radial distance r.

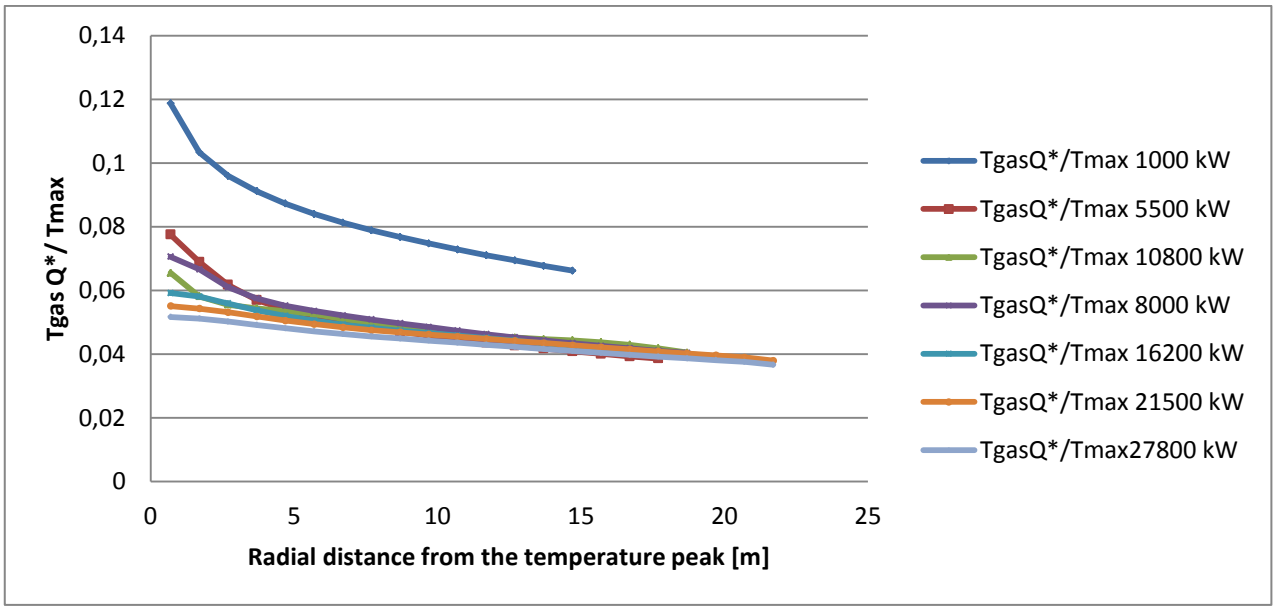


*Figure 28: Quantity (Tgas.Q*)/Tmax as a function of the radial distance from the temperature peak*

From figure 28, it can be noticed that fire with a HRR equals or bigger than 5,5MW follow the same trend for the quantity $\frac{T_{gas}.Q^*}{T_{max}}$. A small divergence can be seen for short radial distance from the temperature peak, especially for the 5,5MW fire. From this graph, a curve fitting can be done (figure 29) in order to link the temperature of the hot gases $T_{gas}$ as a function of the radial distance r, the fire power $\dot{Q}$ and the peak temperature$T_{max}$. The data for radial distance from the temperature peak inferior to 2,5 m will be ignored in the curve fitting, because it is diverging too much for small HRR, and this area will be included in the near field zone in the Travelling Fires methodology.

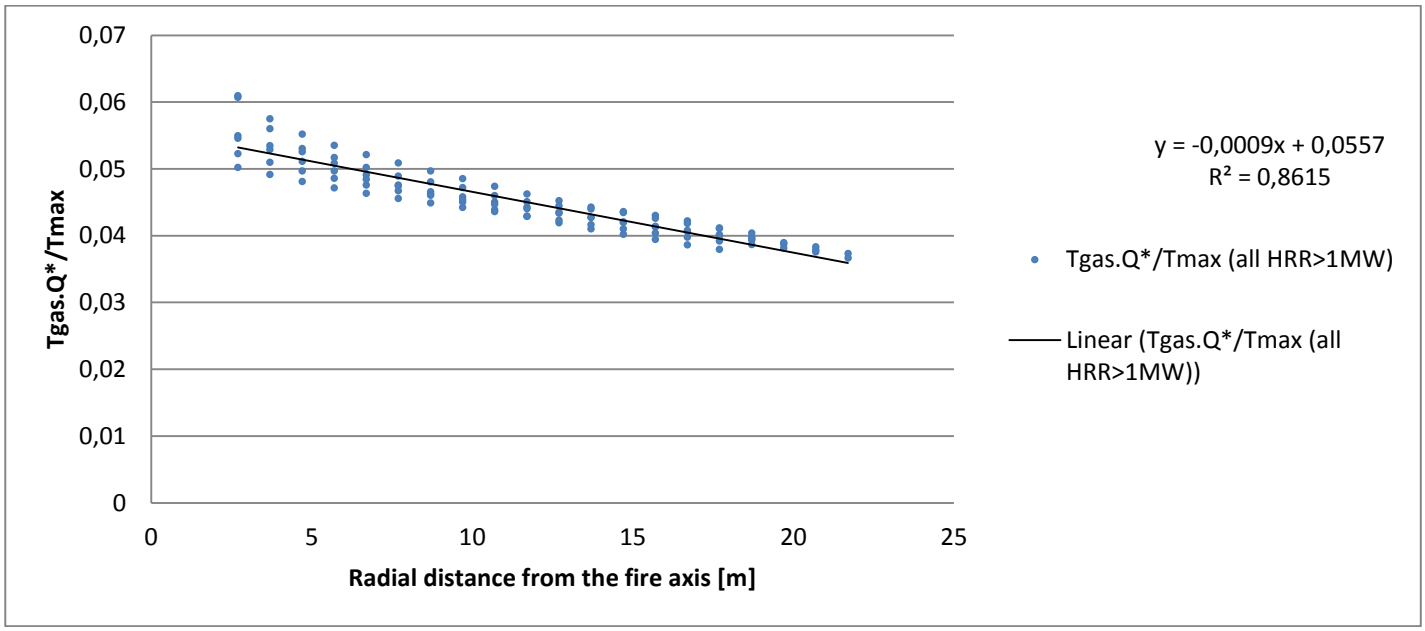


*Figure 29: Curve fitting of the data*

The fitting gives the following relation for HRR bigger than 1MW and r* bigger than 2,5 m :

$$\frac{T_{gas}.Q^*}{T_{max}} = -0{,}0009\, r^* + 0{,}0557$$

So, the temperature of the gases under the ceiling is :

$$T_{gas} = \frac{T_{max}}{Q^*}\,(-0{,}0009\, r^* + 0{,}0557)$$

### B) Peak temperature definition

A relation between the temperature of the hot gases $T_{gas}$ as a function of the radial distance r*, the fire power $\dot{Q}$ and the peak temperature$T_{max}$ has been set up. The radial distance and fire power are known quantities, whereas the peak temperature of the gases under the ceiling is not.

The different temperature peak were multiplied by the non-dimensional HRR $Q^*$, and plotted as a function of the fire power $\dot{Q}$ on figure 30. A logarithmic curve fitting was done, allowing the determination of a relationship between $T_{max}$ and the fire power $\dot{Q}$ :

$$T_{max}\,.\,Q^* = -2{,}737\ln(\dot{Q}) + 68{,}145$$

Yielding to

$$T_{max} = \frac{-2{,}737\ln(\dot{Q}) + 68{,}145}{Q^*}$$

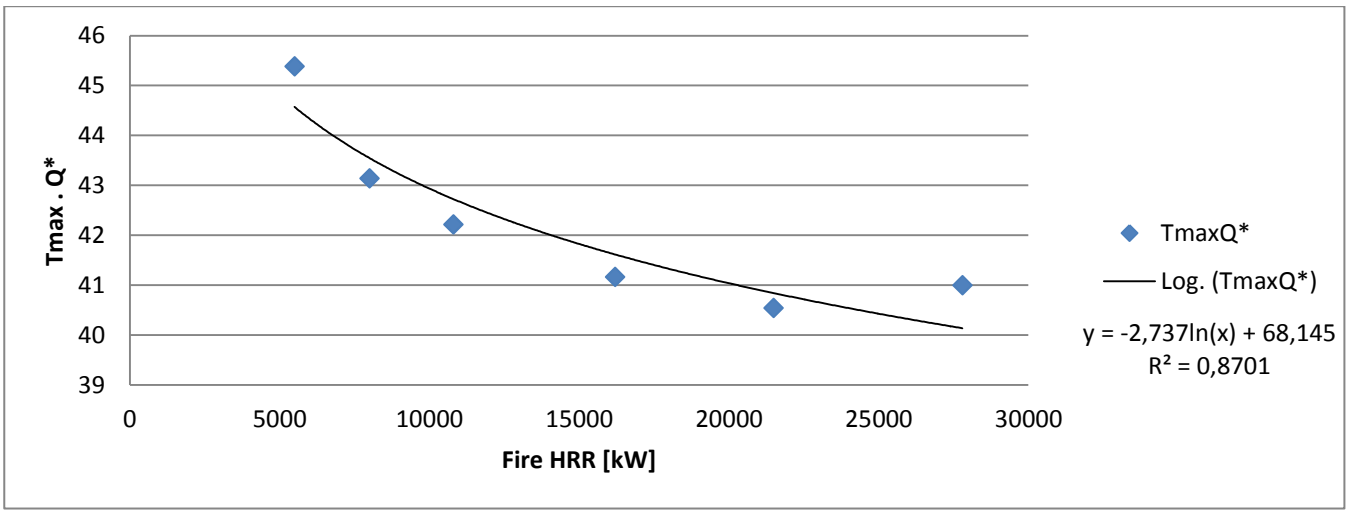


*Figure 30: the quantity Tmax.Q* as a function of the HRR*

### C) Combination of the 2 expressions

The two previous relations can be combined to end up in a single equation that allows the determination of the temperature distribution of the hot gases under the ceiling as a function of the fire power $\dot{Q}$, the non dimensional fire power $Q^*$ and the radial distance from the peak temperature r*.

$$T_{gas} = \left(\frac{-2{,}737\ln(\dot{Q}) + 68{,}145}{Q^{*2}}\right) * (-0{,}0009\, r^* + 0{,}0557)$$

This expression is valid for fire powers bigger or equal to 5,5MW, and for a radial distance from the temperature peak that is bigger than 2,5 m. It has to be taken into account that the far-field zone starts at a radial distance equal to half of the burner width, and that for fires equal or bigger than 5,5MW this correlation is characterising the whole far field zone.

Calculations were performed using the proposed equation, and compared to the results from FDS simulations in figure 31. The relative errors ($\frac{T_{FDS}-T_{model}}{T_{FDS}}$) between the model and the simulation were calculated in Appendix E, and it turns out that the differences go up to 15% maximum of relative error, and the mean relative error for all the HRR is 2,5%, that is quite acceptable for such a simple formula.

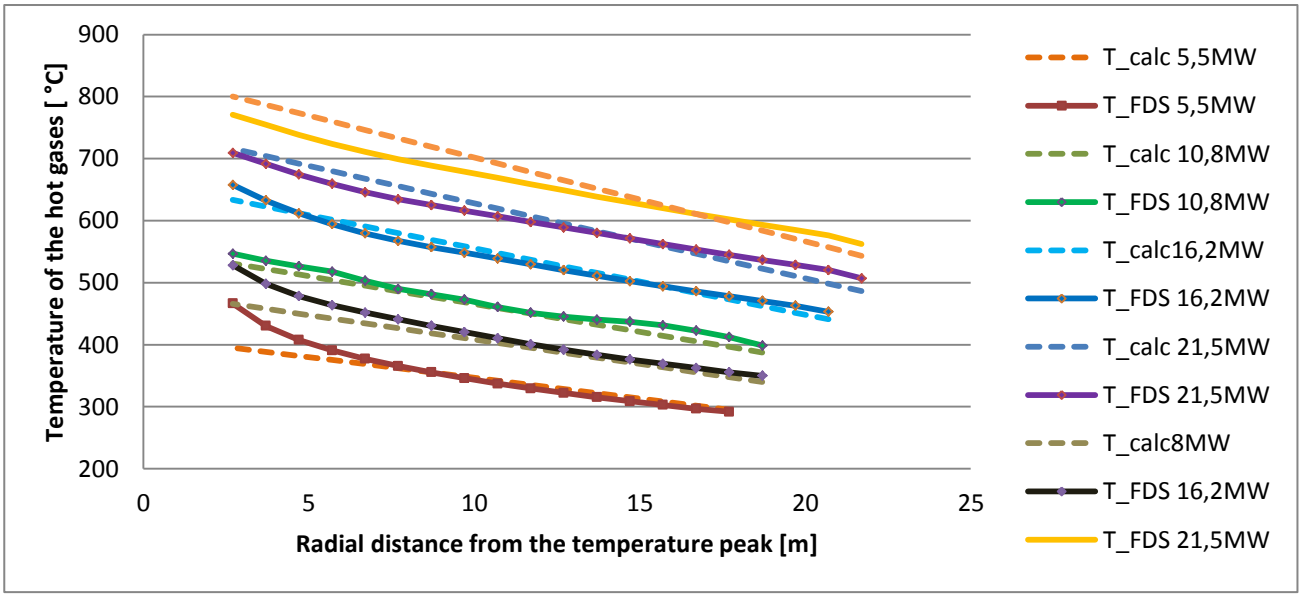


*Figure 31: Comparison of the correlation with the FDS simulation results*

### D) Radial distance from the axis r and radial distance from the temperature peak $r^*$

The previous equation uses $r^*$ the radial distance from the temperature peak to express the temperature of the hot gases under the ceiling. As seen in figure 23, the temperature peak shifts as the HRR of the fire increases, so it is not convenient to have an expression using to $r^*$ instead of the radial distance from the fire axis r.

However, the radial distance from the fire axis can be expressed as a function of $r^*$ as follows:

$$r = r^* - d_{shift}$$

where $d_{shift}$ represents the distance from the fire axis to the temperature peak, as it can be seen in figure 32.

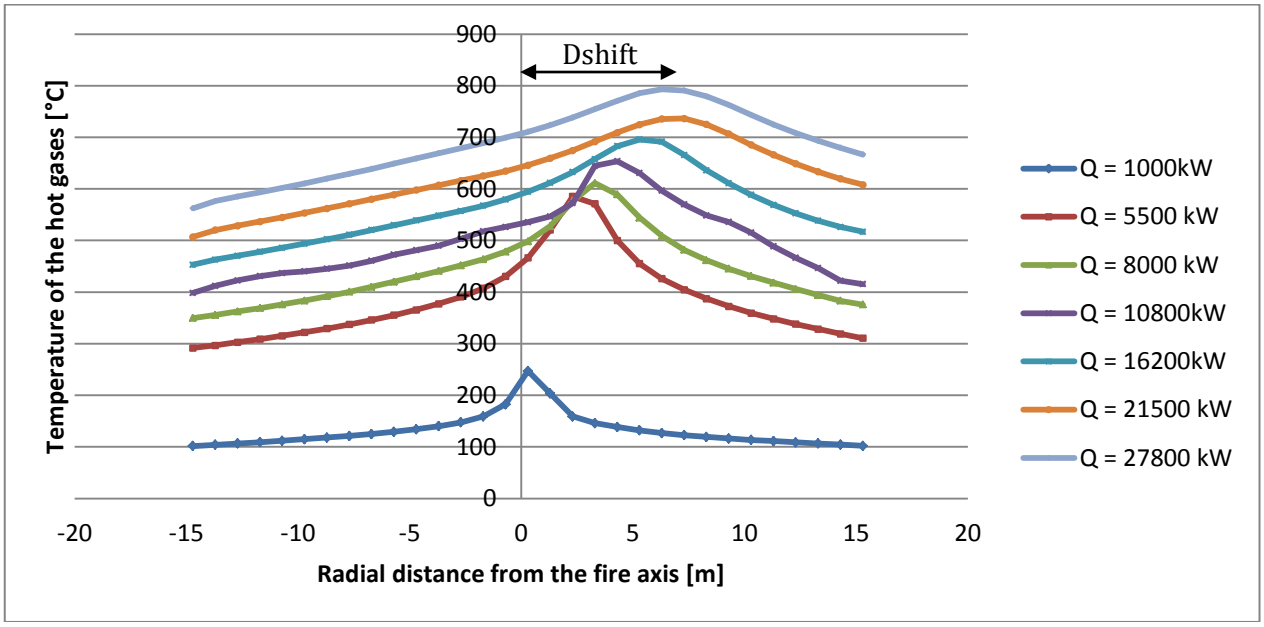


*Figure 32: Dshift = distance between temperature peak and fire axis*

The distance between the maximum of temperature and the fire axis was plotted as a function of the heat release rate of the fire, and it was observed that it follow a linear trend, meaning that:

$$d_{shift} = 0{,}0002\ \dot{Q} + 1{,}8265$$

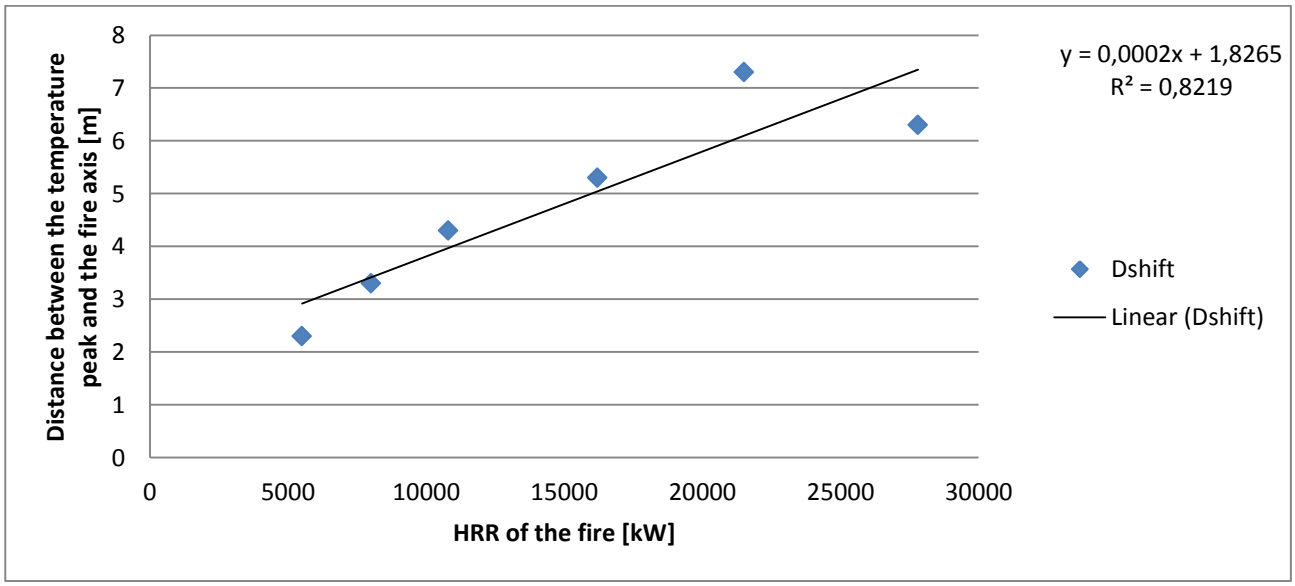


*Figure 33: Dshift as a function of the HRR of the fire*

### E) Final form of the correlation

To sum up, this correlation enables to express the temperature of the hot gases under the ceiling as a function of the HRR of the fire and the radial distance from the fire axis:

$$T_{gas} = \left(\frac{-2{,}373\ \ln(\dot{Q})+68{,}145}{{Q^*}^2}\right) * (-0{,}0009\, r^* + 0{,}0557) \text{ with } r = r^* - (0{,}0002\, \dot{Q} + 1{,}8265)$$

It should be kept in mind that this relation is suitable for :

- Fire powers from 5,5 MW to 7,8 MW
- Radial distance from the peak temperatures $r^*$ bigger than 2,5 m

Moreover, it has to be taken into account that in the Travelling Fires Methodology, the near field is represented by a constant temperature of 1200 °C, and has a length corresponding to the burner width. The results from the FDS simulations and the previous expression combined with the near field from the Travelling Fires methodology are plotted in figure 34.

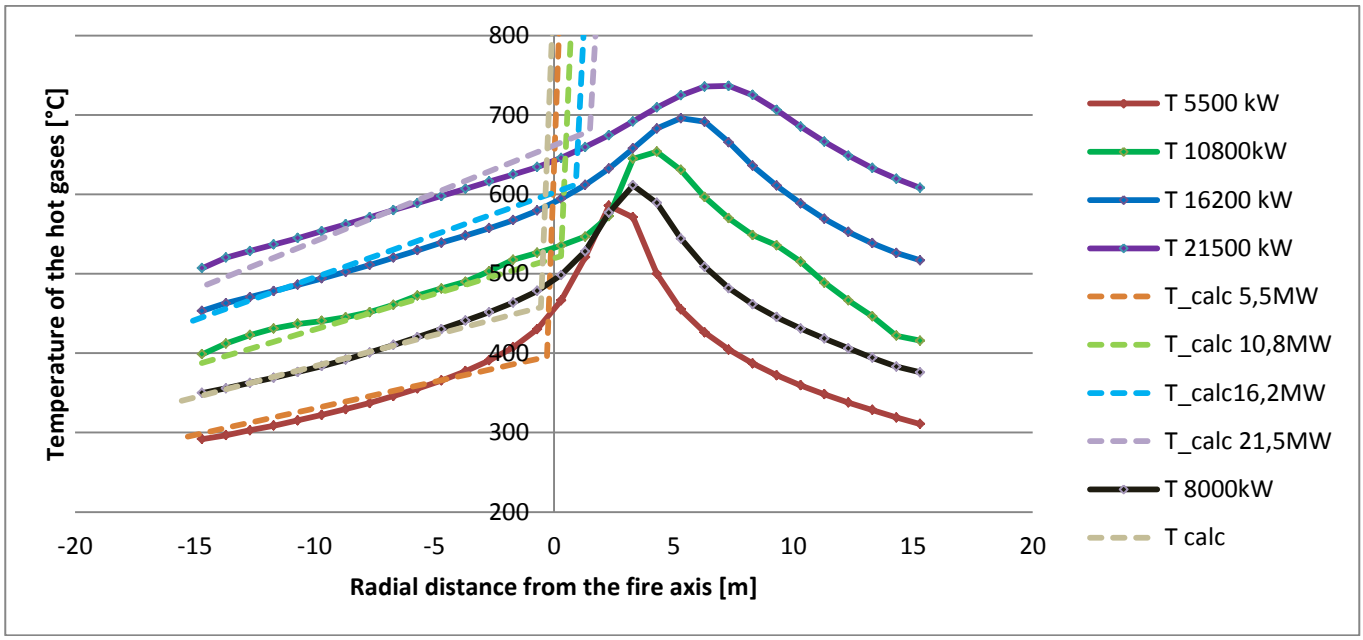


*Figure 34: Comparison of FDS values and the correlation as a function of r*

## 5) Symmetric opening configuration

It has been decided earlier that the opening of the compartment was located only on one side of it, making that the temperature distribution is not axis-symmetric anymore but shifted toward the opposite side of the opening. Some extra simulations have been carried out to investigate on the temperature distribution when the openings are located on two symmetric walls of the compartment that would avoid the shifting of the temperature profile.

### a) Input data

The settings of the simulation are kept the same as for the previous compartment simulations but the openings are split into two doors located on symmetric walls, and that have a width equal to half of the single opening configuration, so that the amount of air going in and hot gases going out is kept the same compared to the single opening simulations. The geometry of the compartment is represented in figure 35.

*Figure 35: Geometry of the simulation with symmetric openings*

Four simulations of different HRR of 5500 kW, 10800 kW, 16200 kW, and 21500 kW were carried out.

### b) Results and analysis of the results

` As it can be seen in figure 36, the temperature profiles are axis symmetric with the two openings configuration, and there is no shifting of the flames anymore.

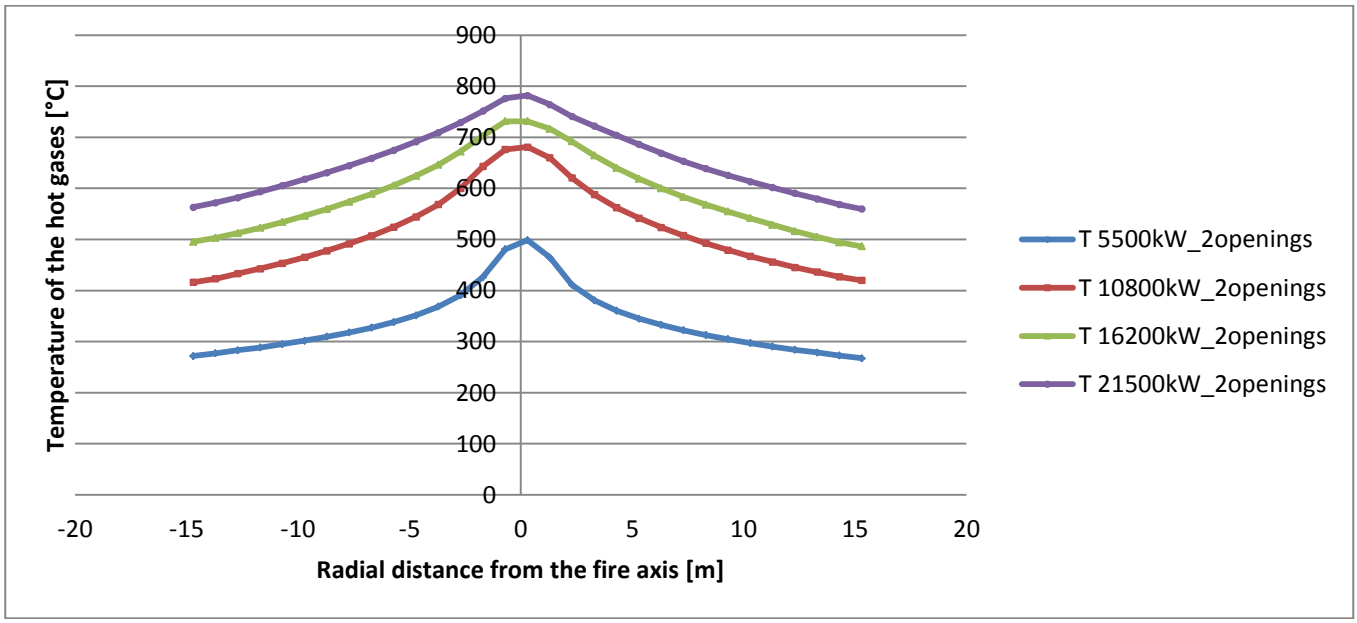


*Figure 36: Temperature profiles for different HRR - 2 symmetric openings*

Apart from geometrical differences, there is not much difference in the magnitude of the results compared to the single opening simulations. This is true for heat fluxes and for the convective heat flux distribution as well.

From those observations, it can be expected that the former correlation can also apply to the 2 symmetric openings configuration. The only change that has to be done is to ignore the shifting parameter $r^*$ and set it up as $r^* = r$. Figure 37 shows the results of the calculations compared with the results from the simulation.

The correlation represents quite fairly the temperature distribution under the ceiling, with a maximum relative error of 16% for the smaller HRR, and an averaged relative error of 3,5% for all the simulations (cf Appendix G). This means that the correlation is suitable for the one opening configuration or on the two symmetric openings one, with $r = r^* - (0{,}0002\ \dot{Q} + 1{,}8265)$ for the single opening configuration and $r = r^*$ for the two symmetric openings one.

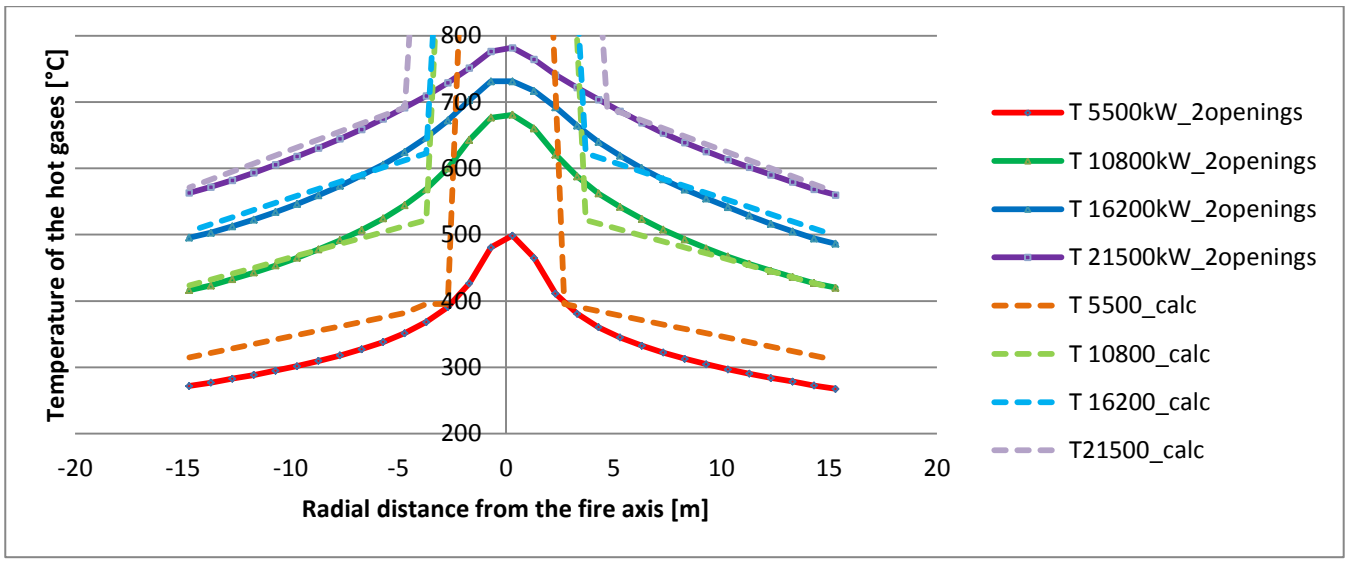


*Figure 37: Comparison of the FDS values and the correlation as a function of r - 2 openings configuration*

## 6) Discussions about the correlation

### A) Comments relative on the studied compartment

The equation found previously has some limitations that make it no applicable in several conditions. First of all, if the HRR of the fire need to be equal or bigger than 5,5 MW. It has been observed in the previous chapters and in the simulations for the 1MW fire within the compartment that the temperature distribution has a shape that is very similar to Alpert temperature profile, but the smoke accumulation makes the temperatures higher, as it can be seen from figure 38, where a modified version of Alpert correlation ( $\Delta T = \frac{5{,}38\,(\dot{Q}/r)^{2/3}}{H} + 70°C$ ) has been plotted .

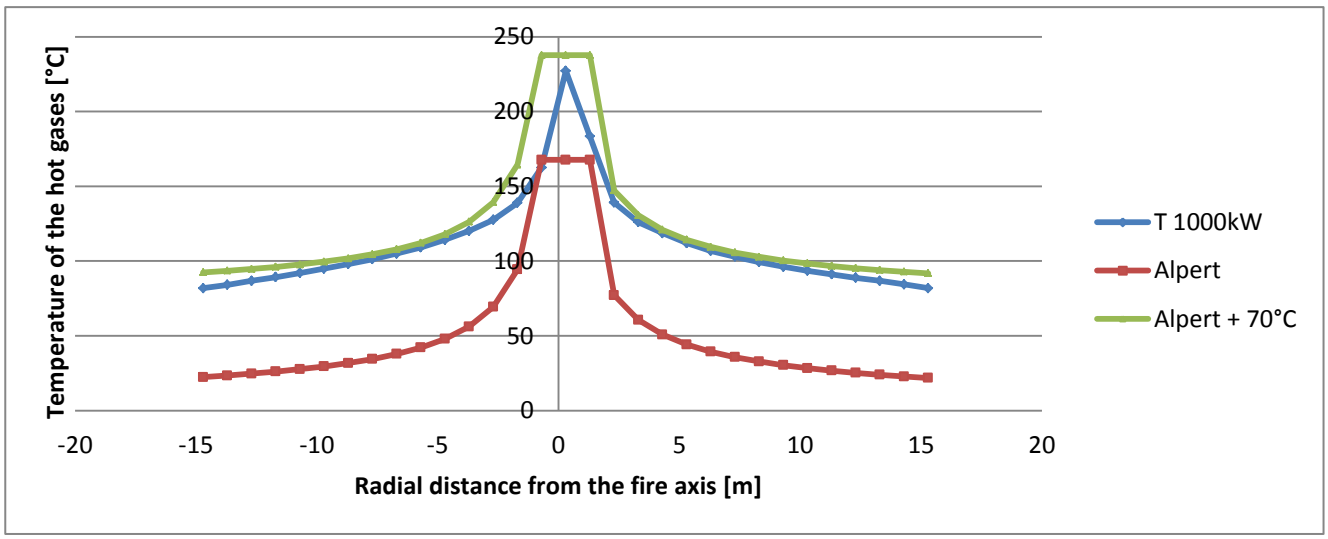


*Figure 38: Temperature profile for the 1MW fire - comparison with Alpert and a modified version of Alpert*

Since no other simulations have been performed for a HRR between 1MW and 5,5MW, no solutions can be provided for this kind of fires, but a quick series of 3 or 4 simulations would allow to determine the increase in temperature compared to Alpert that should be used to characterise the ceiling jet .

The second limitation is that the formula can only be used to characterise the temperature field for $r^* > 2{,}5\,m$ .However, this does not address any other problems since the near field zone characterised by a constant temperature of 1200°C is in general bigger than the 2,5 m gap where the temperature field cannot be estimated.

Then, this formula does not characterise the temperature in the recirculation zone (right hand side of the compartment) that has higher temperatures than the left hand side, where the opening is located. It is expected that the temperature distribution in this zone is depending a lot on the geometry of the compartment that is why no attempt to characterise the temperature distribution on this side of the compartment has been done. Further studies need to be carried out to quantify the impact of the geometry on the recirculation, in order to determine whether or not it is possible to consider an axis symmetric temperature distribution.

### B) General comments

Given that all the simulations have been performed in a single compartment (because of the important computation time), the previous formula only apply to this general compartment geometry. Further work should be done to work on parameters such as the ceiling height, the compartment area and the ventilation configuration (the analysis carried out has analysed the impact of varying the opening area, however the ceiling height was not changed, so the pressure profile through the opening was kept more or less the same) .Moreover, some input data such as the HRR per unit area or the solid boundaries characteristics have been fixed for more clearance in this document, but still need to be investigated. For instance, changing the HRR per unit area is going change the flame geometry that will have an effect on the temperature distribution of the hot gases under the ceiling.

Nevertheless, the aim of this work was to investigate on the temperature distribution in the Travelling Fires framework in a more qualitative sense, and find a way to correlate the data that represent better the design fire, such that the sensitivity analyses can be carried out later, with the same methodology, and at the end create an analytical tool that give a fair approximation of the temperature distribution in all types of large enclosures.

Moreover, it is still needed to perform a quantitative analysis to determine if the quasi steady state of the solid boundaries is suitable. This is linked to the materials properties and the choice of the material does not fit in the scope of this master thesis. The impact of the materials of the compartment should be investigated as well.

Finally, as it was said in part 4 of this chapter, the convective heat transfer coefficient h varies in space and the values do not correspond to the 25 W/m².K used in the Travelling Fires methodology. The changes in this parameter will influence greatly the heat transfer between the hot gases and the solid boundaries, that will modify the result of the analysis regarding the structural failure criteria chosen in (3). A investigation on this parameter would be needed in future work, since the impact of h in the convective heat transfer coefficient is one of the parameters of the heat transfer calculation scheme of the Travelling Fires methodology.

# CHAPTER 6: General Conclusions

The results and conclusions of this master thesis can be sum up as follows:

- Alpert equation (5) that characterises unconfined ceiling jet has some limitations when the HRR of the fire increases for a constant ceiling height: the top-hat profile shape of the temperature profile is not present anymore, Gaussian profiles are appearing instead of the top hat ones. However, for small fire Alpert formula describes the unconfined ceiling jet perfectly.
- The analytical tools that are available in the literature for confined ceiling jets are not applicable for large enclosures (the size of the enclosure is such that it falls out of the range of the methods), and have been only validated for small compartments.
- The smoke accumulation increases the temperature under the ceiling, proportionally to the smoke layer thickness. If the fire is small enough, Alpert expression where a constant temperature has been added characterises perfectly the temperature field under the ceiling. However, this breaks down when the HRR of the fire is increased, the temperature profiles do not match exactly Alpert trend anymore.
- A single opening in a compartment causes, if the burning area is large enough, that the fire plume is shifted on the opposite side of the opening because of mixing and air movement reasons. This phenomenon is responsible of the shifting of the temperature profiles, and creates a recirculation zone within the compartment that leads to un-axis symmetric temperature profiles.
- The ventilation conditions are influencing the shape and the magnitude of the temperature profiles, and should be investigated more since it is not taken into account in the current Travelling Fires methodology.
- From a heat fluxes point of view, it has been observed that concerning travelling fires that have a quite high HRR, the radiative heat fluxes a predominant in most of the compartment especially close to the fire plume. The radiative heat fluxes are increasing in time whereas the convective ones are decreasing because of the solid boundaries becoming hotter and hotter. The convective heat transfer coefficient is not constant in space, and some work should be done in order to be able to approximate this parameter in a more precise way.
- A simple correlation has been extracted allowing to predict the temperature field of the hot gases under the ceiling in the studied compartment depending on input data such as the fire power $\dot{Q}$ and the radial distance from the fire axis $r$. Nevertheless, the quasi-steady states has been reached instead of the regular steady state, and this investigation only applies on one type of compartment. Further work need to be done to create a tool that can characterise the temperature field of the hot gases under the ceiling for a whole family of compartments.
- Finally, the temperature profiles from the obtained correlation should be compared to complete phenomenon of the travelling fires since the small burning areas fires can last up to several hours that changes the thermal conditions within the compartment and will influence the heat transfer to the structural elements.

# Acknowledgments

I would like to thank the following persons for all the support provided during this master thesis:

Prof. Bart Merci and Dr. Nicolas Bal for their supervision and guidance provided during the whole thesis. Thank you Nico to receive me at CERIB for those 2 months and for putting a lot of effort to create such good opportunities for IMFSE students.

People from CERIB for taking care of me during those 2 months in Epernon.

All the teachers, PhD, students and administrative people from the three universities for take care of us during those two years and teaching us some many interesting things.

All the IMFSE 2011-2013 team for turning this master in such a good life experience, and especially Luis, Evi and Roberto for this nice semester we had in Edinburg living together.

My friends from France and my family for visiting me that often, and for all the support they provided to me.

# Bibliography


1. *Eurocode 1 : Actions on structures, Part 1-2 : Actions on structures exposed to fire.* 1991. EN 1991-1-2-2002.
2. *Multi-story fire analysis for high rise buildings.* **al., G. Rein and.** s.l. : Proceedings of the 11th Interflam Conference, 2007 йил.
3. **Gottfried, J. Stern.** *Travelling fires for structural design.* s.l. : PhD report, 2011.
4. *Average centrelin temperatures of a buoyant pool fire obtained by image processing of video recordings.* **L. Audoin, G.Kolb, J.L Torero, J.M Most.** s.l. : Fire safety Journal, 1995 йил, Vol. 24.
5. *Calculation of response time of ceiling mounted fire detectors.* **Alpert, R. L.** s.l. : Fire Technology, 1972 йил, Vol. 8.
6. *Turbulent ceiling jet induced by large scale fires.* **Alpert, R. L.** s.l. : Combustion and Technology, 1975 йил, Vol. 11.
7. *Turbulent entrainment in stratified flows.* **T.H Ellison, J.S Turner.** s.l. : Journal of Fluid Mechanics, 1959 йил, Vol. 6.
8. **B.R Morton, G.I Tayler, J.S Turner.** s.l. : Proc.Royal.Soc, 1956 йил, Vol. 236.
9. *the fire induced ceiling jet revisited.* **Alpert, R.L.** s.l. : Fire Seat 2011, 2011 йил.
10. *Physical modelling of fire.* **Heskestad, G.** s.l. : Journal of Fire & Flammability, 1993 йил, Vol. 6.
11. *The initial convective flow in fire.* **G. Heskestad, M.A Delichatsios.** s.l. : factory Mutual Research Corporation, 1978 йил.
12. *the flow of fire gases under a beamed ceiling.* **Delichatsios, M.A.** 1, s.l. : Combustion and flames, 1981 йил, Vol. 43.
13. *Behaviour of a 2 dimensional ceiling jet flow : a beamed ceiling configuration.* **C. Koslowski, V.Motevalli.** s.l. : Fire Safety Science, Proceedings of the 4th International Symposium, IAFSS, 1994.
14. *Ceiling heat transfer during fire plume and fire impingement.* **H.Z Yu, G.M Feath.** 3, s.l. : Fire and Materials, 1979 йил, Vol. 140.
15. *Calculating sprinkler actuation time in compartments.* **Evans, D.** s.l. : Fire Safety Journal, 1985 йил, Vol. 9.
16. *A buoyant source in the lower of two, homogeneous, stably stratified layers.* **Cooper, L. Y.** 20th Internationam Symposium on Combustion : Combustion Institue, 1984 йил.
17. **Alpert, R.L.** *Ceiling jet flows - The SFPE Handbook of Fore Protection Engineering 3rd edition - chapter 2 sect 2.* s.l. : NFPA, 2002.
18. *Heat transfer from a buoyant plume to an unconfined ceiling.* **Cooper, L.Y.** 3, s.l. : Journal of Heat Transfer, 1982 йил, Vol. 104.
19. **Commerce, NIST - US department of.** *Fire Dynamics Simulator (version 5) user's guide.* 2010. NIST special publication 1019-5.
20. *Eurocode 2 : Design of concrete structures, Part 1-2.* 1992. EN 1992-1-2:2204.
21. **H. Boehmer, J. Floyd, D.T Gottuk.** *Fire dynamics and forsenic analysis of limited ventilation compartment fires - volume 2.* s.l. : Hughes Associates, Inc., 2009.
22. **V. Motevalli and C. Ricciuti.** *Chracterisation of the confined ceiling jet in the presence of an upper layer in transient and steady state conditions.* s.l. : NIST - US Department of Commerce, 1992.
23. **Kawagoe, K.** *Fire behaviour in rooms - report No 27.* s.l. : Building Research Institute, Tokyo, 1958.
24. **B. Karlsson, J.G Quitiere.** *Enclosure Fire Dynamics.* s.l. : CRC Press, 2000.
25. **Alpert, R.L.** *FMRC Technical Report 19722-2.* s.l. : Factory Mutual Research Corporation, 1984.
26. *Verification and validation of selected fire models for nuclear power plant applications - volume 7 : Fire Dynamics Simulator.* s.l. : S Nuclear Regulatory Commission, 2007.
27. **Alpert, R. L.** *Ceiling jet - SFPE Handbook of Fire Protection Engineering.*

## Appendix A : Excess temperature of the hot gases for the first set of simulations

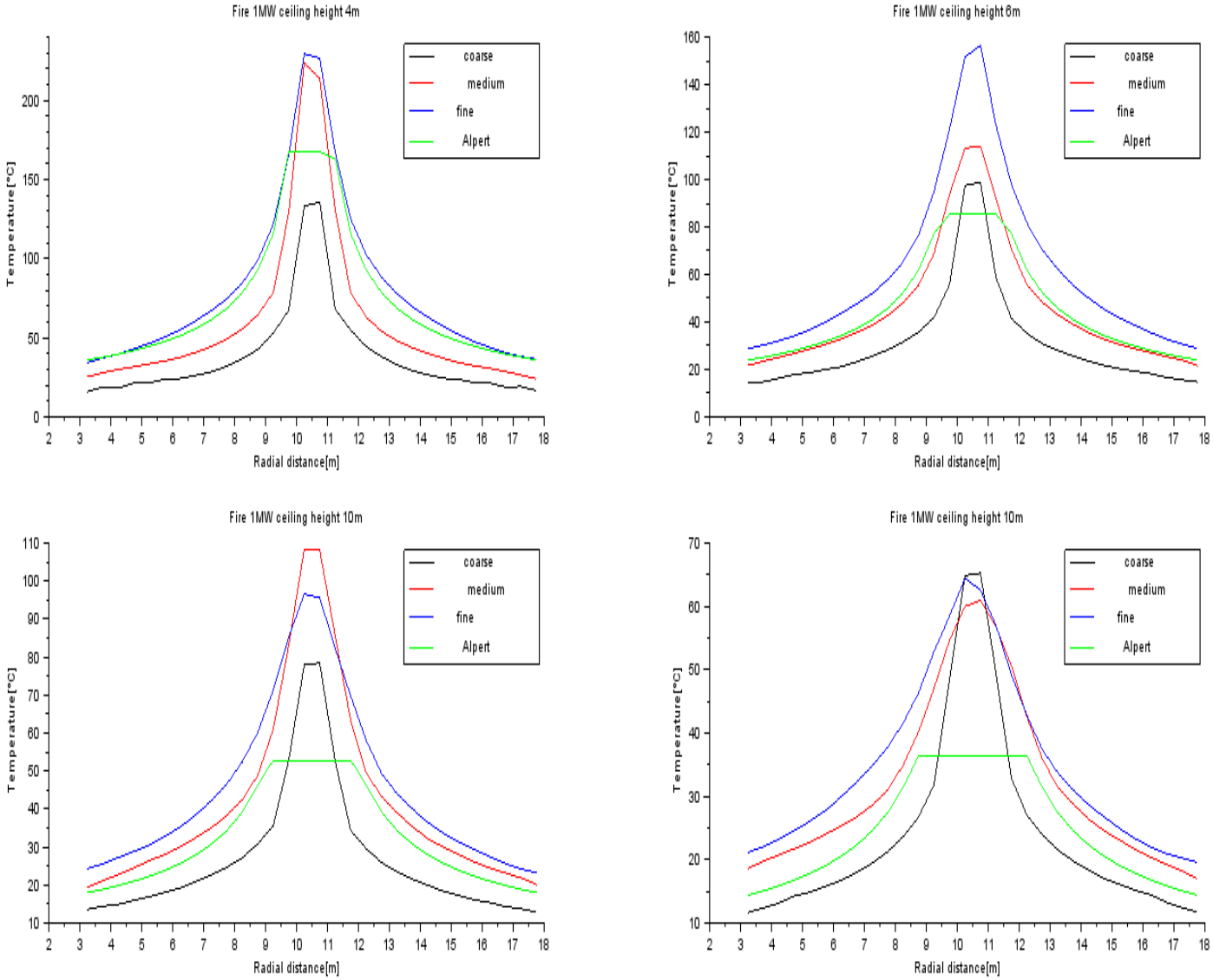


*Figure 39: Temperature profiles for all the grids 1MW fire - different ceiling heights*

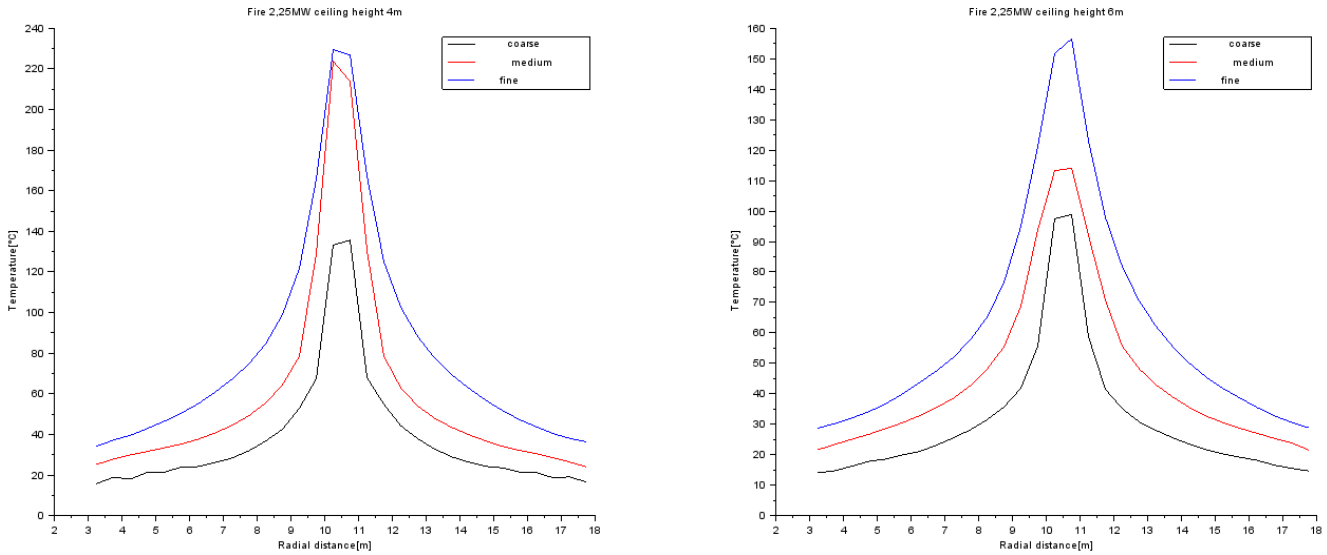


*Figure 40: Temperature profiles for all the grids 2,25MW fire - ceiling height 4m and 6m*

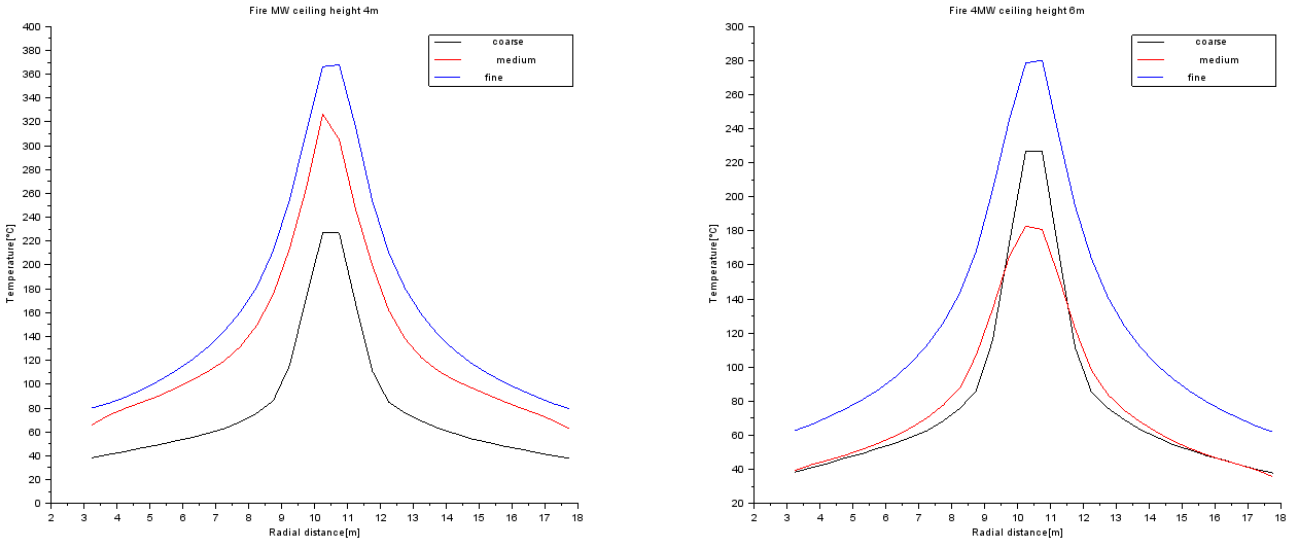


*Figure 41: Temperature profiles for all the grids - 4MW fire - ceiling heightm and 6m*

## Appendix B: Comparison 10 cm / 20 cm grid for the compartment simulations

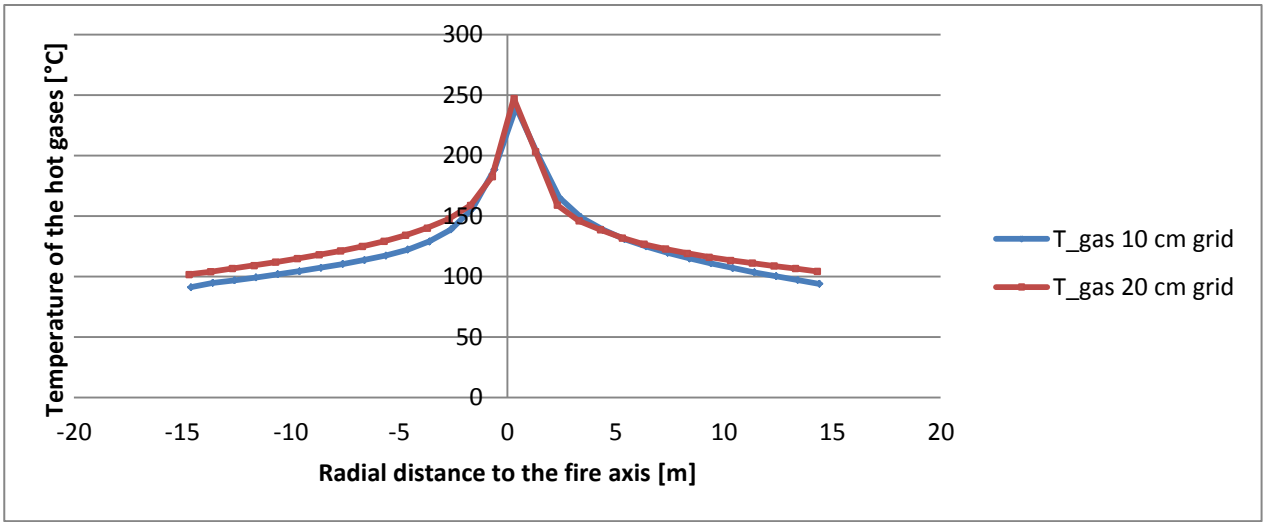


*Figure 42: Comparison temperature field 10 cm / 20 cm grid size*

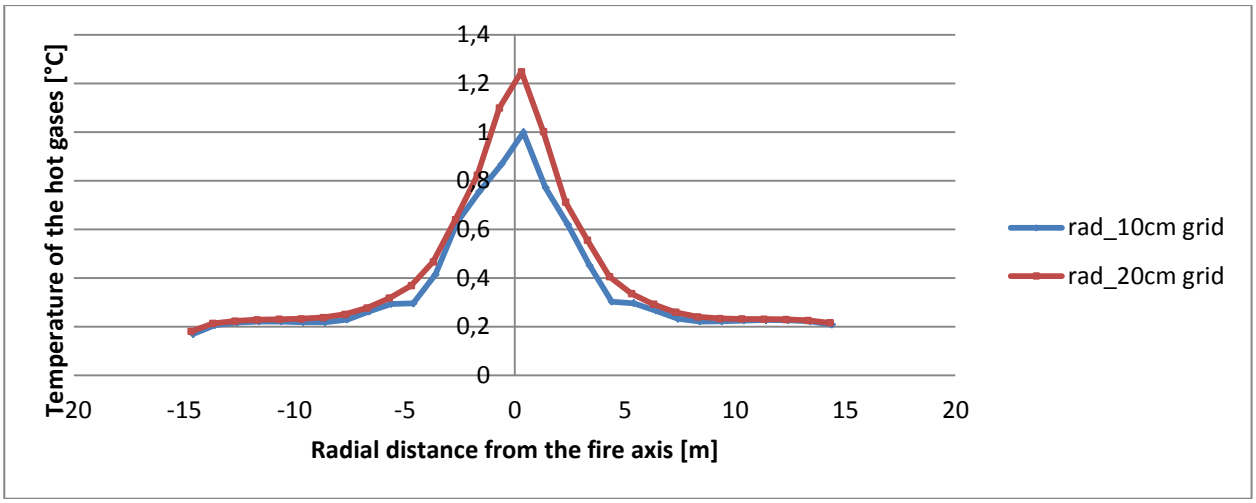


*Figure 43: Comparison radiative heat flux to the ceiling 10cm / 20 cm grid size*

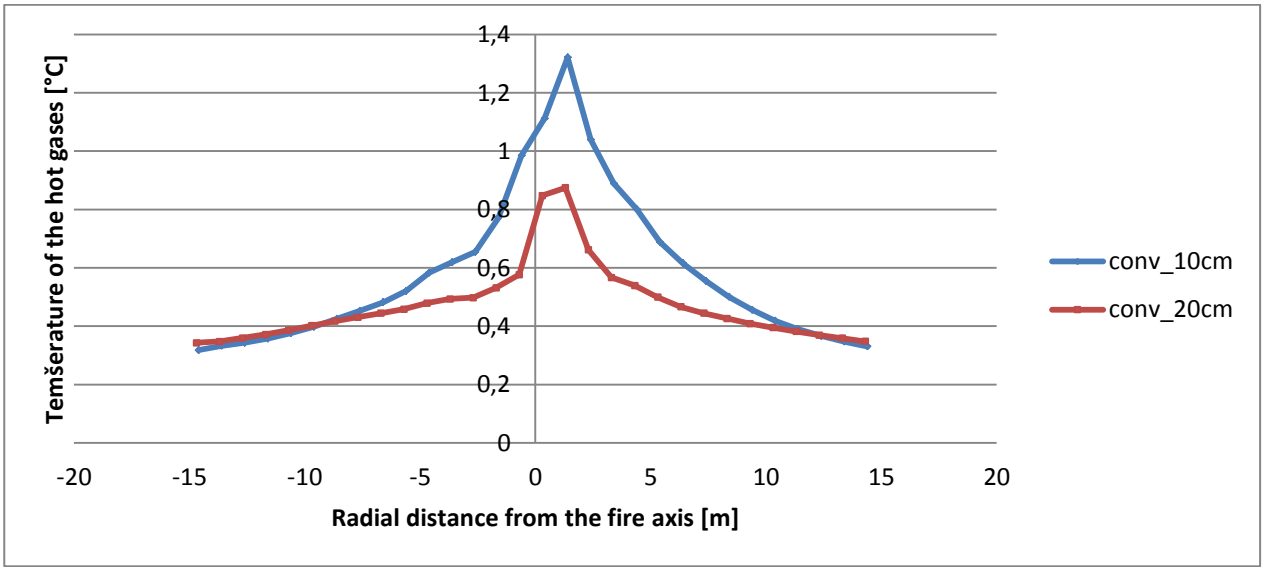


*Figure 44: Comparison convective heat flux to the ceiling 10 cm / 20 cm grid size*

**Appendix C : Variation of the opening width for the compartment simulations**

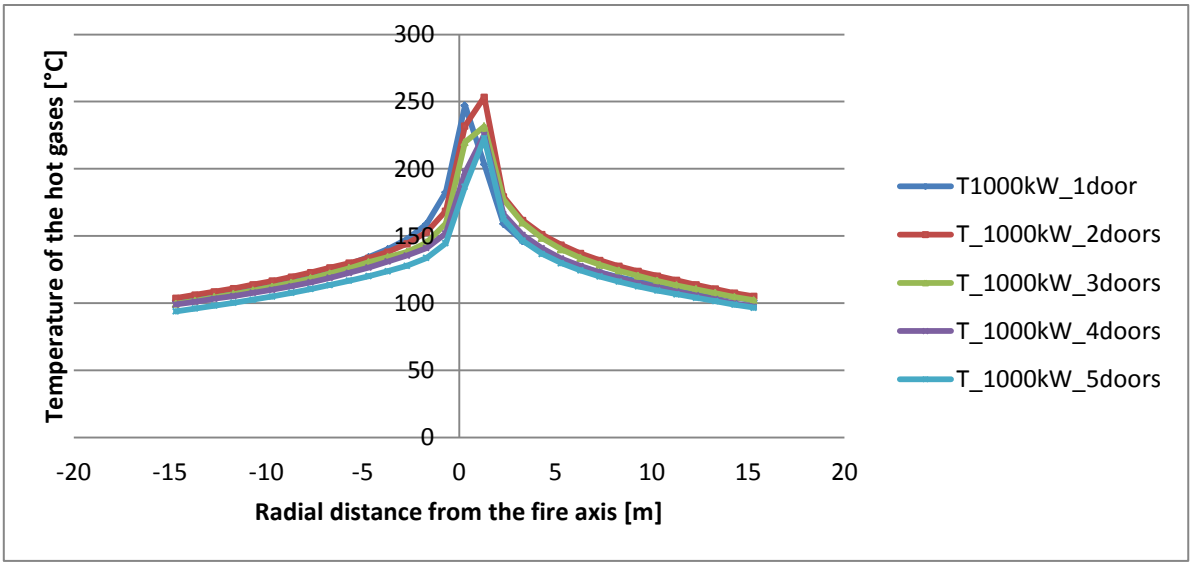


*Figure 45:Temperature distribution of the hot gases for different opening width - 1MW fire*

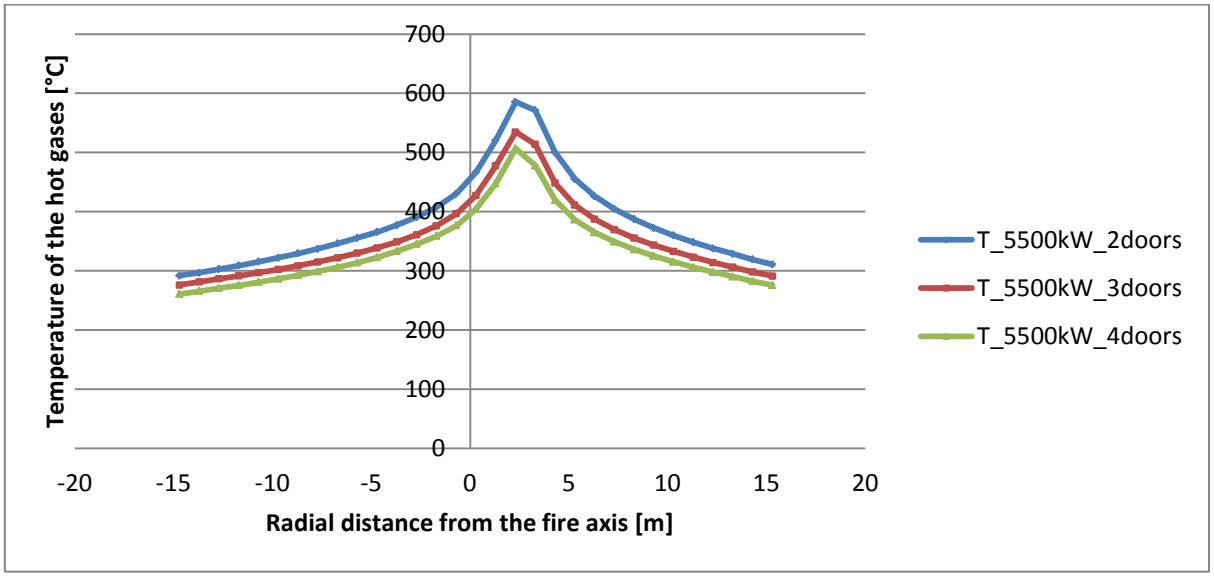


*Figure 46: Temperature distribution of the hot gases for different opening width - 5,5MW fire*

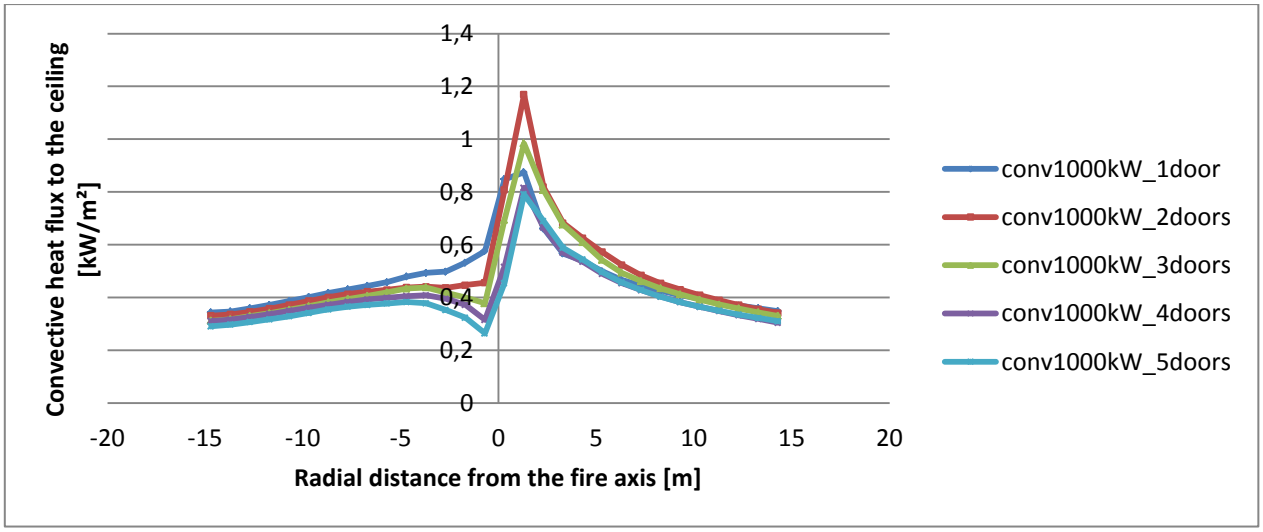


*Figure 47: Convective heat flux to the ceiling for different opening width - 1MW fire*

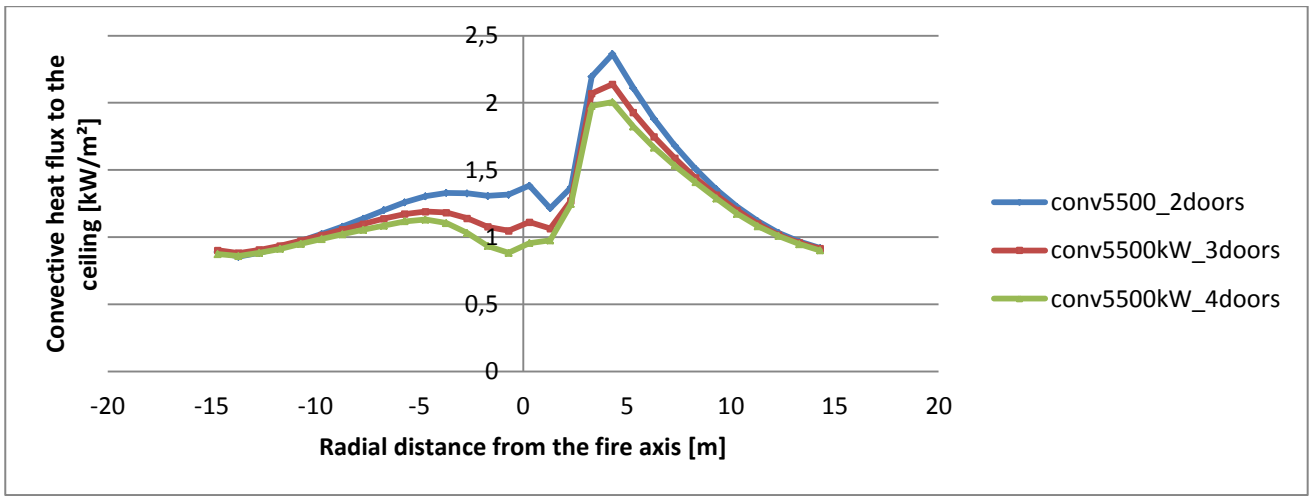


*Figure 48: Convective heat flux to the ceiling for different opening width – 5,5MW fire*

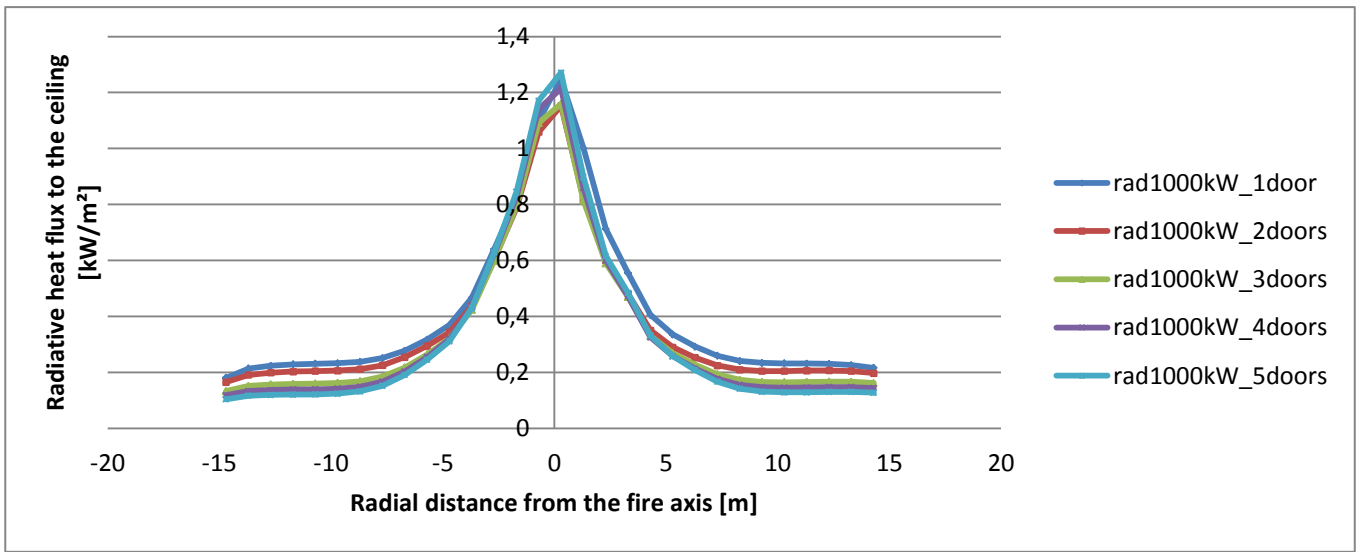


*Figure 49: Radiative heat flux to the ceiling for different opening width - 1MW fire*

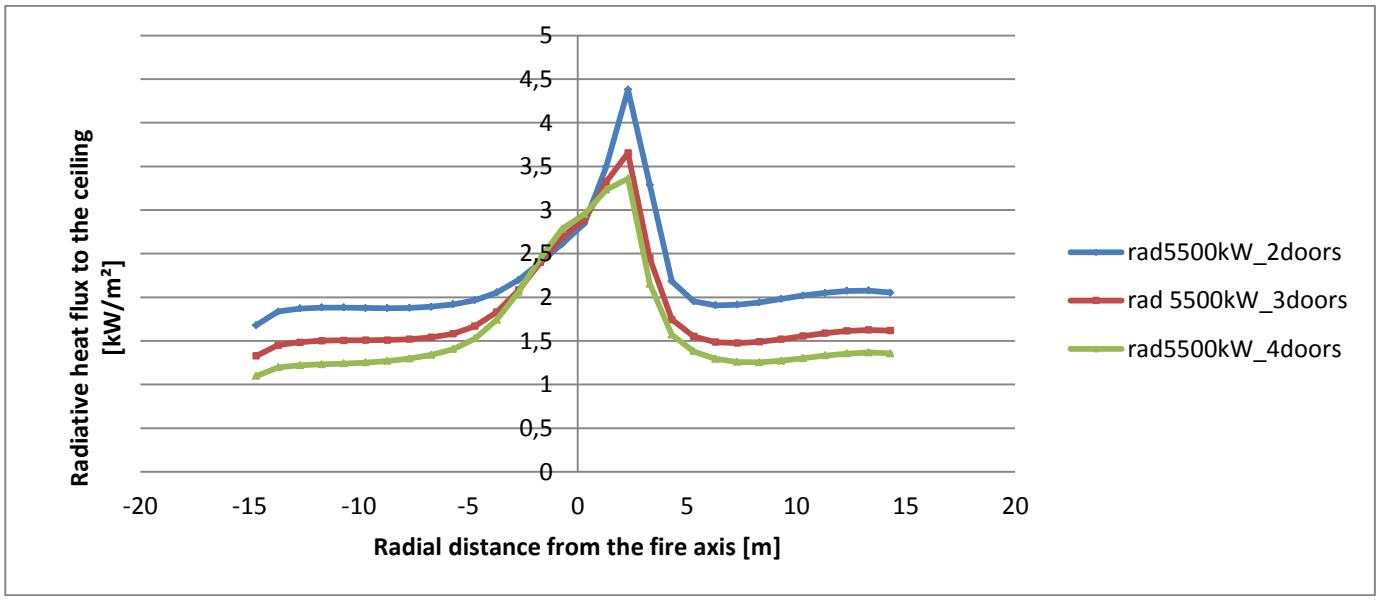


*Figure 50: Radiative heat flux to the ceiling for different opening width - 5,5MW fire*

**Appendix D : Comparison FDS and Alpert temperature profiles for compartment simulations**

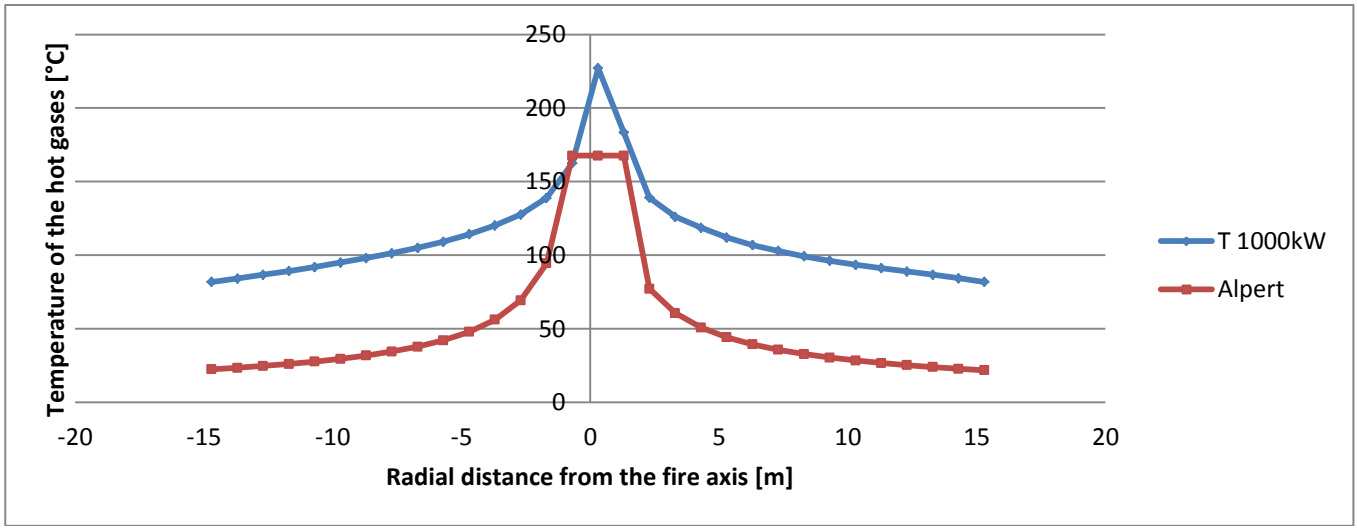


*Figure 51: Comparison FDS and Alpert temperature profiles - 1MW fire*

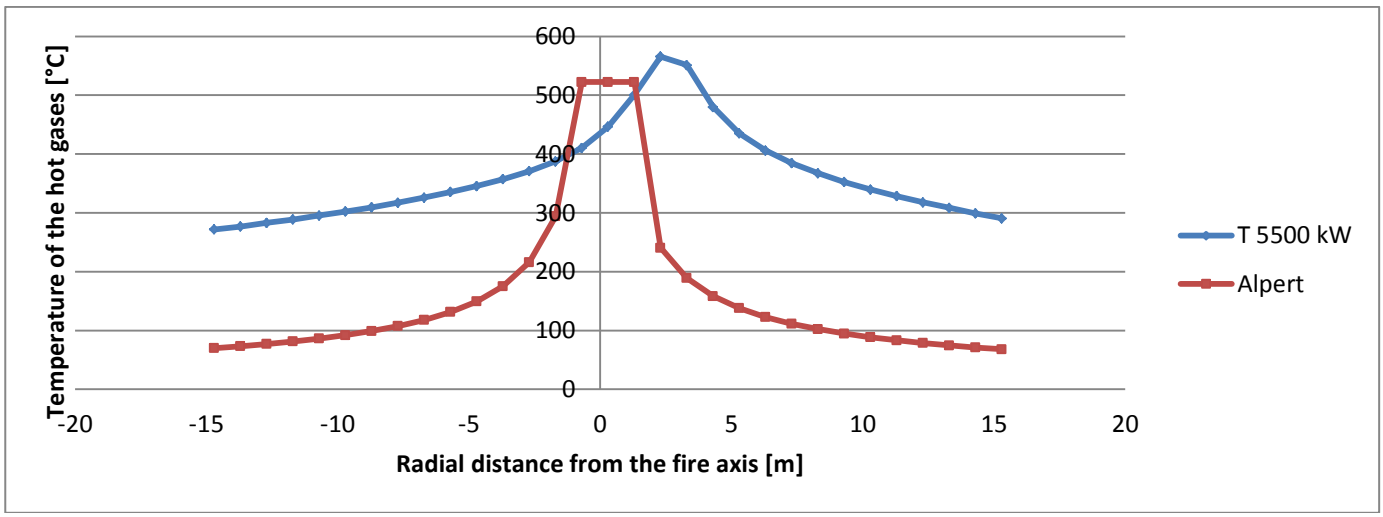


*Figure 52: Comparison FDS and Alpert temperature profiles - 5,5MW fire*

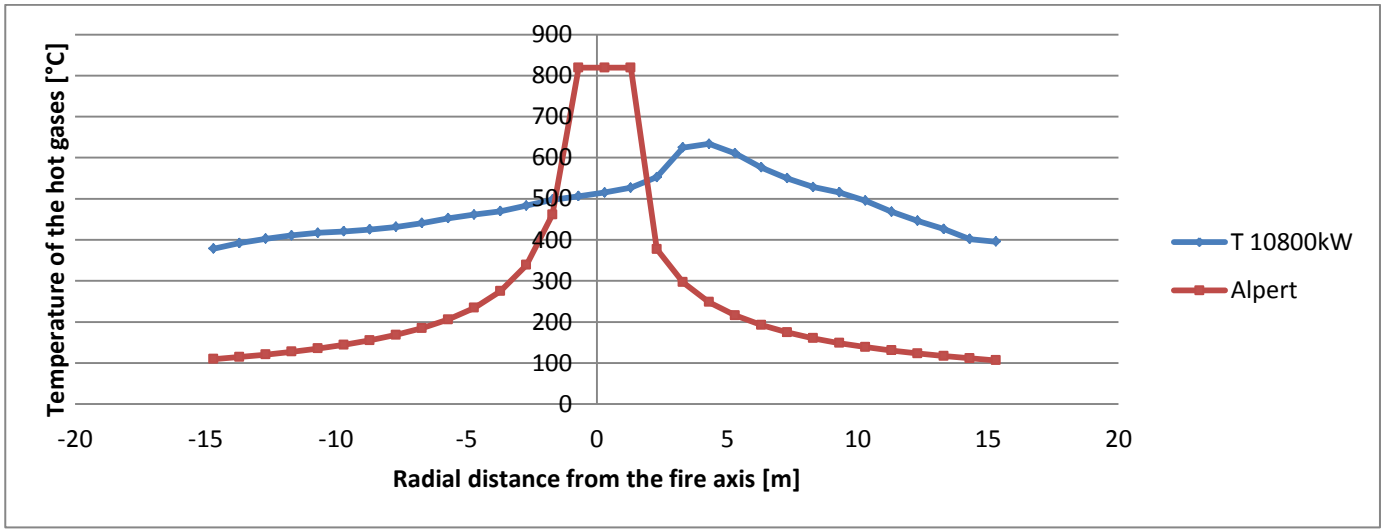


*Figure 53: Comparison FDS and Alpert temperature profiles - 10,8 MW fire*

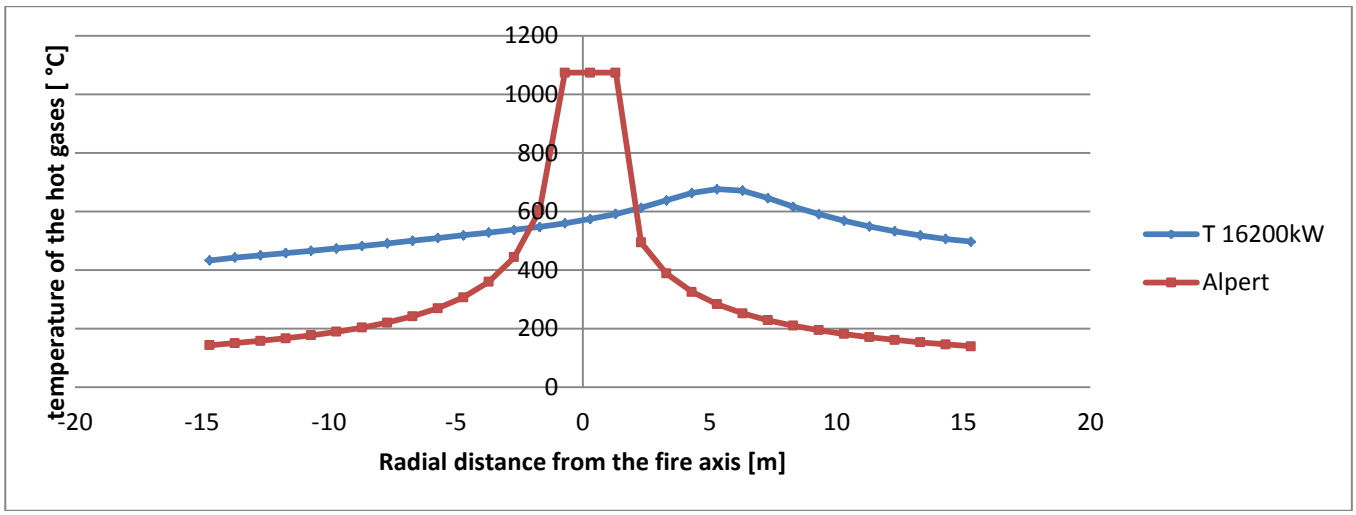


*Figure 54: Comparison FDS and Alpert temperature profiles - 16,2 MW fire*

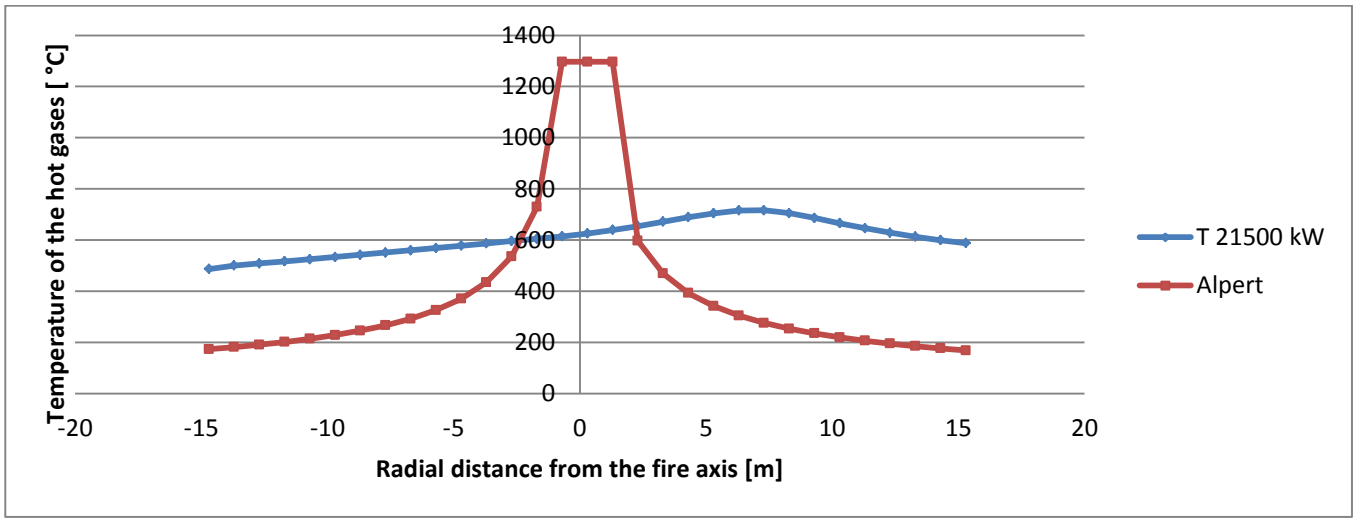


*Figure 55:Comparison FDS and Alpert temperature profiles - 21,5 MW fire*

**Appendix E : Heat fluxes to the ceiling – compartment simulations**

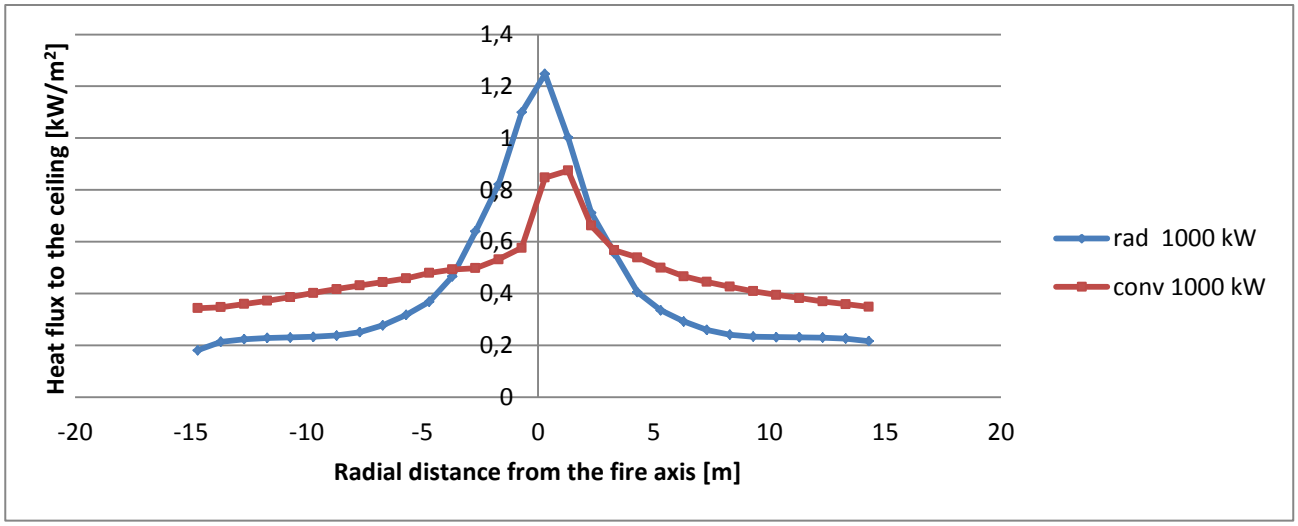


*Figure 56: Heat fluxes to the ceiling- 1000 sec - 1MW fire*

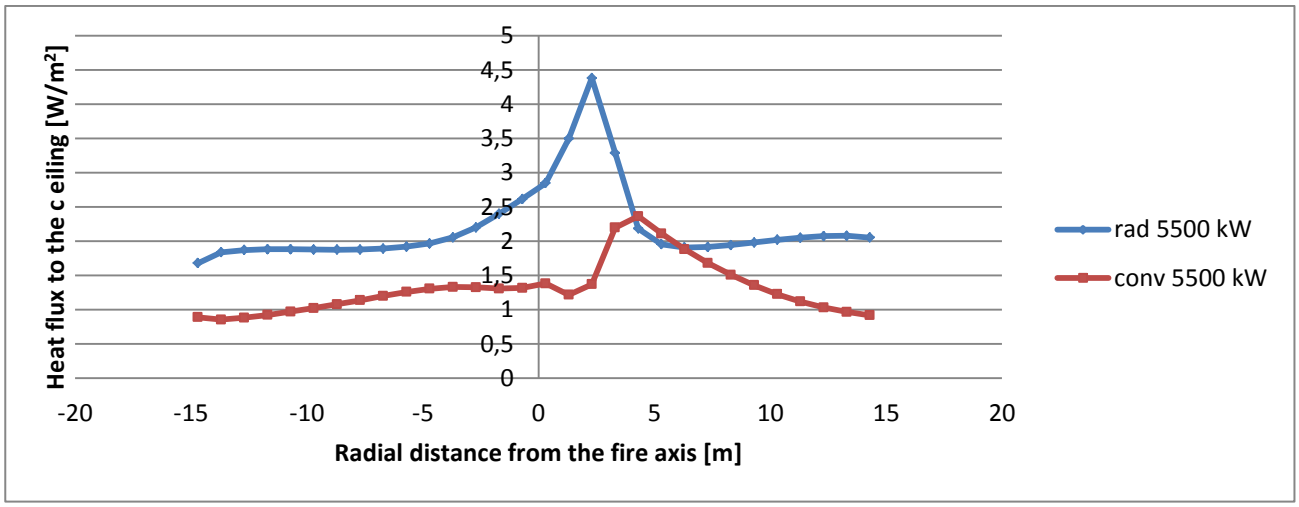


*Figure 57: Heat fluxes to the ceiling- 1000 sec - 5,5 MW fire*

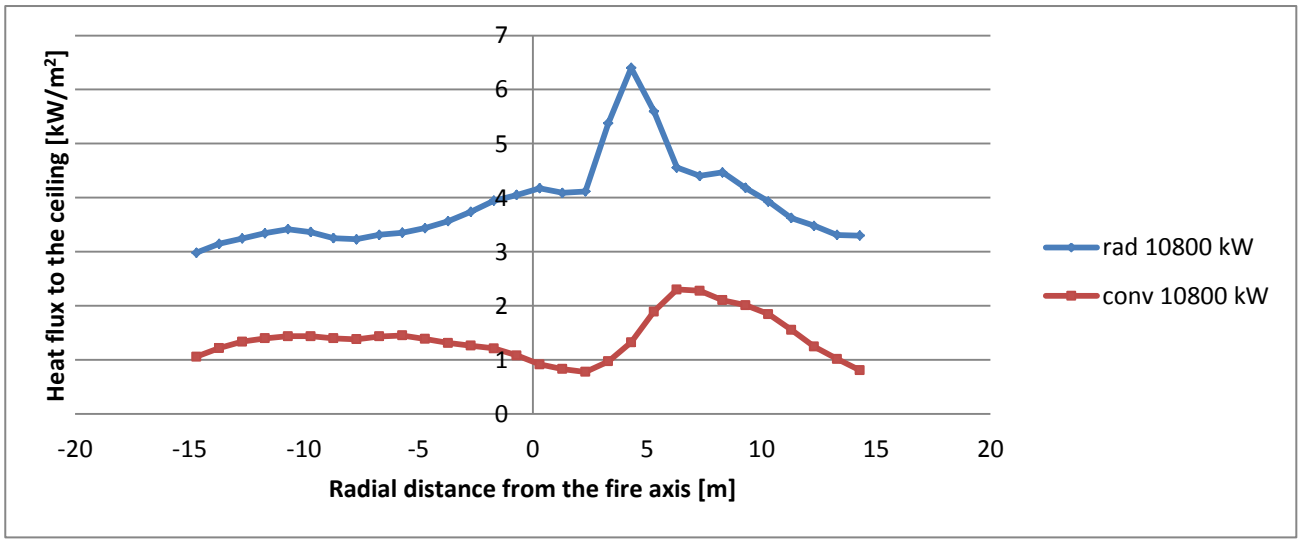


*Figure 58: Heat fluxes to the ceiling - 1000sec - 10,8 MW fire*

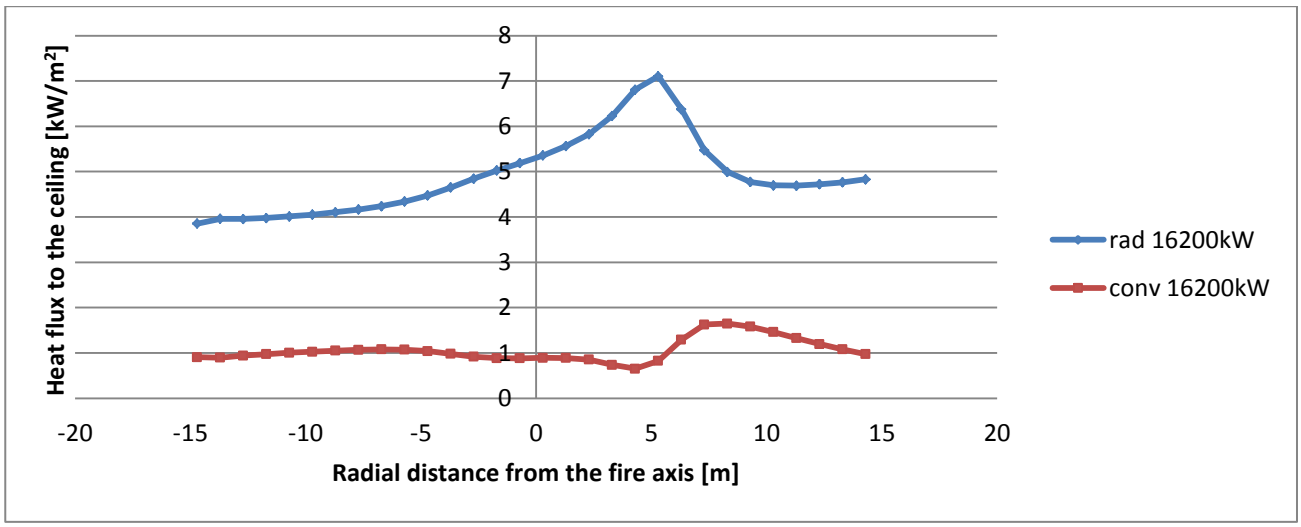


*Figure 59: Heat fluxes to the ceiling - 1000 sec - 16,2 MW fire*

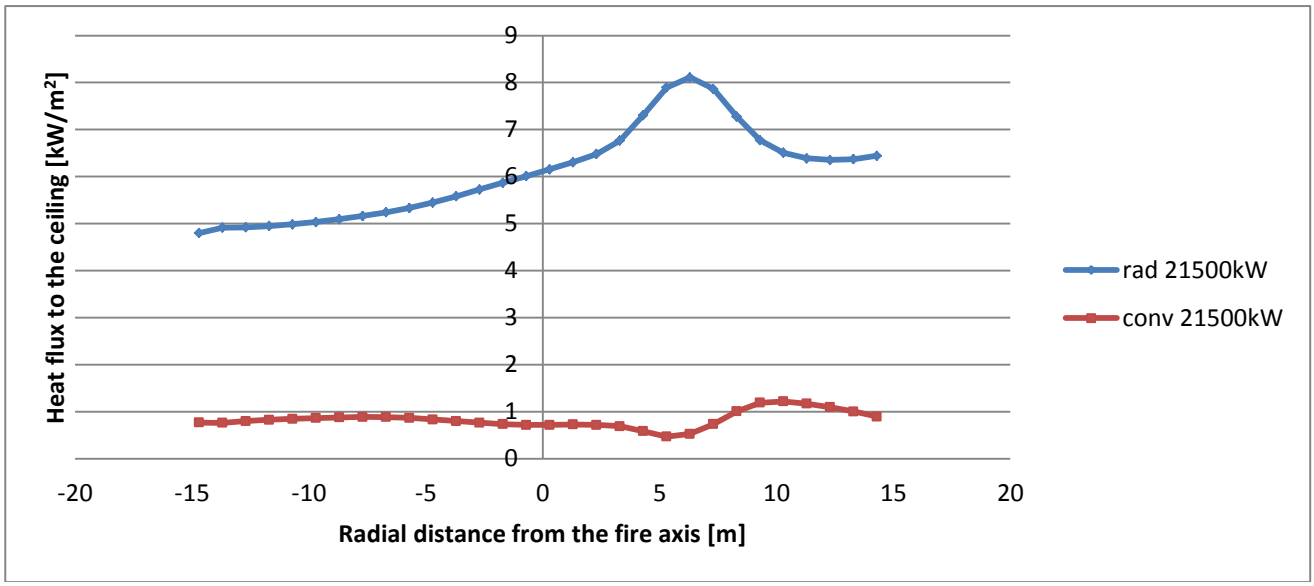


*Figure 60: Heat fluxes to the ceiling - 1000 sec - 21,5 MW fire*

Appendix F: Relative errors between the model and the simulations – single opening

| Q = 5500 kW | |
|---|---|
| r* | % of relative error |
| 17,7 | 1,14% |
| 16,7 | 1,73% |
| 15,7 | 1,85% |
| 14,7 | 2,07% |
| 13,7 | 2,05% |
| 12,7 | 1,98% |
| 11,7 | 1,76% |
| 10,7 | 1,37% |
| 9,7 | 0,71% |
| 8,7 | 0,06% |
| 7,7 | 1,01% |
| 6,7 | 2,30% |
| 5,7 | 3,98% |
| 4,7 | 6,28% |
| 3,7 | 9,68% |
| 2,7 | 15,24% |

| Q =10800 kW | |
|---|---|
| r* | % of relative error |
| 18,7 | 2,79% |
| 17,7 | 3,82% |
| 16,7 | 4,10% |
| 15,7 | 3,86% |
| 14,7 | 3,11% |
| 13,7 | 1,84% |
| 12,7 | 0,88% |
| 11,7 | 0,30% |
| 10,7 | 0,35% |
| 9,7 | 0,94% |
| 8,7 | 0,87% |
| 7,7 | 0,75% |
| 6,7 | 1,60% |
| 5,7 | 2,64% |
| 4,7 | 2,53% |
| 3,7 | 2,51% |
| 2,7 | 2,89% |

| Q = 8000 kW | |
|---|---|
| r* | % of relative error |
| 18,7 | 2,84% |
| 17,7 | 2,21% |
| 16,7 | 1,89% |
| 15,7 | 1,51% |
| 14,7 | 1,30% |
| 13,7 | 1,17% |
| 12,7 | 1,21% |
| 11,7 | 1,44% |
| 10,7 | 1,83% |
| 9,7 | 2,27% |
| 8,7 | 2,73% |
| 7,7 | 3,27% |
| 6,7 | 3,84% |
| 5,7 | 4,65% |
| 4,7 | 5,91% |
| 3,7 | 8,10% |
| 2,7 | 11,80% |

| Q =16200 kW | |
|---|---|
| r* | % of relative error |
| 20,7 | 2,71% |
| 19,7 | 2,47% |
| 18,7 | 1,77% |
| 17,7 | 1,10% |
| 16,7 | 0,50% |
| 15,7 | 0,06% |
| 14,7 | 0,52% |
| 13,7 | 0,90% |
| 12,7 | 1,19% |
| 11,7 | 1,41% |
| 10,7 | 1,63% |
| 9,7 | 1,89% |
| 8,7 | 2,14% |
| 7,7 | 2,21% |
| 6,7 | 1,92% |
| 5,7 | 1,17% |
| 4,7 | 0,06% |
| 3,7 | 1,55% |
| 2,7 | 3,68% |

| Q = 21500 kW | |
|---|---|
| **r*** | **% of relative error** |
| 21,7 | 4,09% |
| 20,7 | 4,23% |
| 19,7 | 3,44% |
| 18,7 | 2,64% |
| 17,7 | 1,89% |
| 16,7 | 1,22% |
| 15,7 | 0,60% |
| 14,7 | 0,03% |
| 13,7 | 0,50% |
| 12,7 | 1,06% |
| 11,7 | 1,57% |
| 10,7 | 2,03% |
| 9,7 | 2,48% |
| 8,7 | 2,95% |
| 7,7 | 3,36% |
| 6,7 | 3,40% |
| 5,7 | 3,09% |
| 4,7 | 2,61% |
| 3,7 | 1,78% |
| 2,7 | 0,97% |

| Q = 27800 kW | |
|---|---|
| **r*** | **% of relative error** |
| 21,7 | 3,40% |
| 20,7 | 3,39% |
| 19,7 | 2,52% |
| 18,7 | 1,59% |
| 17,7 | 0,71% |
| 16,7 | 0,06% |
| 15,7 | 0,75% |
| 14,7 | 1,40% |
| 13,7 | 1,99% |
| 12,7 | 2,49% |
| 11,7 | 2,97% |
| 10,7 | 3,45% |
| 9,7 | 3,93% |
| 8,7 | 4,41% |
| 7,7 | 4,78% |
| 6,7 | 4,99% |
| 5,7 | 4,96% |
| 4,7 | 4,73% |
| 3,7 | 4,25% |
| 2,7 | 3,85% |

**Appendix G: Relative errors between the model and the simulations – symmetric openings**

| Q = 5500 kW | |
|---|---|
| **R** | **% of relative error** |
| -14,7 | -15,88% |
| -13,7 | -16,19% |
| -12,7 | -16,08% |
| -11,7 | -16,17% |
| -10,7 | -15,90% |
| -9,7 | -15,48% |
| -8,7 | -14,72% |
| -7,7 | -13,85% |
| -6,7 | -12,60% |
| -5,7 | -10,94% |
| -4,7 | -8,66% |
| -3,7 | -5,47% |
| -2,7 | -1,16% |

| Q = 10800 kW | |
|---|---|
| **r** | **% of relative error** |
| -14,7 | -1,68% |
| -13,7 | -2,14% |
| -12,7 | -1,89% |
| -11,7 | -1,64% |
| -10,7 | -1,26% |
| -9,7 | -0,69% |
| -8,7 | 0,14% |
| -7,7 | 1,13% |
| -6,7 | 2,35% |
| -5,7 | 3,86% |
| -4,7 | 5,75% |
| -3,7 | 8,18% |

| Q = 16200 kW | |
|---|---|
| **R** | **% of relative error** |
| -14,7 | -1,90% |
| -13,7 | -2,54% |
| -12,7 | -2,71% |
| -11,7 | -2,76% |
| -10,7 | -2,57% |
| -9,7 | -2,27% |
| -8,7 | -1,77% |
| -7,7 | -1,08% |
| -6,7 | -0,23% |
| -5,7 | 0,72% |
| -4,7 | 2,01% |
| -3,7 | 3,62% |

| Q = 21500 | |
|---|---|
| **r** | **% of relative error** |
| -14,7 | -1,39% |
| -13,7 | -1,94% |
| -12,7 | -2,25% |
| -11,7 | -2,33% |
| -10,7 | -2,29% |
| -9,7 | -2,19% |
| -8,7 | -2,01% |
| -7,7 | -1,70% |
| -6,7 | -1,35% |
| -5,7 | -0,78% |
| -4,7 | -0,06% |

## Appendix H: samples of FDS Input code

### 1) *Ceiling only : 1MW fire – ceiling height 4m – fine grid*

```
 Square ceiling
&HEAD CHID='Fire1fine', TITLE='Fire1_fine' /

Grid (10 cm)
&MESH IJK = 210,210,75, XB=0,21,0,21,0,7.50/

Simulation time
&TIME T_END= 30/

&MATL ID = 'CONCRETE'
CONDUCTIVITY = 1.585
SPECIFIC_HEAT = 0.900
DENSITY = 2300/

&SURF ID = 'CONCRETE_CEILING'
MATL_ID = 'CONCRETE'
THICKNESS = 0.5/

&VENT MB=XMIN SURF_ID='OPEN'/
&VENT MB=XMAX SURF_ID='OPEN'/
&VENT MB=YMIN SURF_ID='OPEN'/
&VENT MB=YMAX SURF_ID='OPEN'/
&VENT MB=ZMIN SURF_ID='OPEN'/
&VENT MB=ZMAX SURF_ID='OPEN'/

Floor
&OBST XB= 3, 18, 3, 18, 0, 0,SURF_ID='CONCRETE_CEILING'/

Ceiling
&OBST XB= 3, 18, 3, 18, 4, 4.5,SURF_ID='CONCRETE_CEILING'/

Burner
&SURF_ID='FIRE', HRRPUA= 250 , COLOR='RASPBERRY' /
&OBST XB= 9.5, 11.5, 9.5, 11.5, 0, 0 , SURF_ID='FIRE' /

Velocity slice
&SLCF PBY=10.5, QUANTITY='VELOCITY',VECTOR= .TRUE. /
&SLCF PBY=10.5, QUANTITY='TEMPERATURE',/

Temperature of the gases
&DEVC ID='Tempgas1' , QUANTITY='TEMPERATURE', XYZ= 3.25,10.5,3.95 /
&DEVC ID='Tempgas2' , QUANTITY='TEMPERATURE', XYZ= 3.75,10.5,3.95 /
&DEVC ID='Tempgas3' , QUANTITY='TEMPERATURE', XYZ= 4.25,10.5,3.95 /
&DEVC ID='Tempgas4' , QUANTITY='TEMPERATURE', XYZ= 4.75,10.5,3.95 /
&DEVC ID='Tempgas5' , QUANTITY='TEMPERATURE', XYZ= 5.25,10.5,3.95 /
&DEVC ID='Tempgas6' , QUANTITY='TEMPERATURE', XYZ= 5.75,10.5,3.95 /
&DEVC ID='Tempgas7' , QUANTITY='TEMPERATURE', XYZ= 6.25,10.5,3.95 /
&DEVC ID='Tempgas8' , QUANTITY='TEMPERATURE', XYZ= 6.75,10.5,3.95 /
&DEVC ID='Tempgas9' , QUANTITY='TEMPERATURE', XYZ= 7.25,10.5,3.95 /
&DEVC ID='Tempgas10' , QUANTITY='TEMPERATURE', XYZ= 7.75,10.5,3.95 /
&DEVC ID='Tempgas11' , QUANTITY='TEMPERATURE', XYZ= 8.25,10.5,3.95 /
&DEVC ID='Tempgas12' , QUANTITY='TEMPERATURE', XYZ= 8.75,10.5,3.95 /
&DEVC ID='Tempgas13' , QUANTITY='TEMPERATURE', XYZ= 9.25,10.5,3.95 /
&DEVC ID='Tempgas14' , QUANTITY='TEMPERATURE', XYZ= 9.75,10.5,3.95 /
&DEVC ID='Tempgas15' , QUANTITY='TEMPERATURE', XYZ= 10.25,10.5,3.95 /
&DEVC ID='Tempgas16' , QUANTITY='TEMPERATURE', XYZ= 10.75,10.5,3.95 /
&DEVC ID='Tempgas17' , QUANTITY='TEMPERATURE', XYZ= 11.25,10.5,3.95 /
&DEVC ID='Tempgas18' , QUANTITY='TEMPERATURE', XYZ= 11.75,10.5,3.95 /
&DEVC ID='Tempgas19' , QUANTITY='TEMPERATURE', XYZ= 12.25,10.5,3.95 /
&DEVC ID='Tempgas20' , QUANTITY='TEMPERATURE', XYZ= 12.75,10.5,3.95 /
&DEVC ID='Tempgas21' , QUANTITY='TEMPERATURE', XYZ= 13.25,10.5,3.95 /
&DEVC ID='Tempgas22' , QUANTITY='TEMPERATURE', XYZ= 13.75,10.5,3.95 /
&DEVC ID='Tempgas23' , QUANTITY='TEMPERATURE', XYZ= 14.25,10.5,3.95 /
```

```
&DEVC ID='Tempgas24' , QUANTITY='TEMPERATURE', XYZ= 14.75,10.5,3.95 /
&DEVC ID='Tempgas25' , QUANTITY='TEMPERATURE', XYZ= 15.25,10.5,3.95 /
&DEVC ID='Tempgas26' , QUANTITY='TEMPERATURE', XYZ= 15.75,10.5,3.95 /
&DEVC ID='Tempgas27' , QUANTITY='TEMPERATURE', XYZ= 16.25,10.5,3.95 /
&DEVC ID='Tempgas28' , QUANTITY='TEMPERATURE', XYZ= 16.75,10.5,3.95 /
&DEVC ID='Tempgas29' , QUANTITY='TEMPERATURE', XYZ= 17.25,10.5,3.95 /
&DEVC ID='Tempgas30' , QUANTITY='TEMPERATURE', XYZ= 17.75,10.5,3.95 /


&TAIL/
```

### 2) *Screens : 2,25MW fire – ceiling height 4m – fine grid*

```
&HEAD CHID='Fire2_fine_screens_2m', TITLE='Fire2_fine_screens_2m' /

Grid (10 cm)
&MESH IJK = 210,210,75, XB=0,21,0,21,0,7.5/

Simulation time
&TIME T_END= 150/

&MATL ID = 'CONCRETE'
CONDUCTIVITY = 1.585
SPECIFIC_HEAT = 0.900
DENSITY = 2300/

&SURF ID = 'CONCRETE_CEILING'
MATL_ID = 'CONCRETE'
THICKNESS = 0.5/

&VENT MB=XMIN SURF_ID='OPEN'/
&VENT MB=XMAX SURF_ID='OPEN'/
&VENT MB=YMIN SURF_ID='OPEN'/
&VENT MB=YMAX SURF_ID='OPEN'/
&VENT MB=ZMIN SURF_ID='OPEN'/
&VENT MB=ZMAX SURF_ID='OPEN'/

Floor
&OBST XB= 3, 18, 3, 18, 0, 0,SURF_ID='CONCRETE_CEILING'/

Ceiling
&OBST XB= 3, 18, 3, 18, 6, 6.5,SURF_ID='CONCRETE_CEILING'/

Screens
&OBST XB=3,3.5,3,18,4,6,SURF_ID='CONCRETE_CEILING', COLOR='YELLOW', TRANSPARENCY=0.5/
&OBST XB=17.5,18,3,18,4,6,SURF_ID='CONCRETE_CEILING', COLOR='YELLOW', TRANSPARENCY=0.5/
&OBST XB=3,18,3,3.5,4,6,SURF_ID='CONCRETE_CEILING', COLOR='YELLOW', TRANSPARENCY=0.5/
&OBST XB=3,18,17.5,18,4,6,SURF_ID='CONCRETE_CEILING', COLOR='YELLOW', TRANSPARENCY=0.5/

Burner
&SURF ID='FIRE', HRRPUA= 250 , COLOR='RASPBERRY' /
&OBST XB= 9.5, 11.5, 9.5, 11.5, 0, 0 , SURF_IDS='FIRE','INERT','INERT' /

Velocity slice
&SLCF PBY=10.5, QUANTITY='VELOCITY',VECTOR= .TRUE. /
&SLCF PBY=10.5, QUANTITY='TEMPERATURE',/

Temperature of the gases

&DEVC ID='Tempgas2' , QUANTITY='TEMPERATURE', XYZ= 3.75,10.5,5.95 /
&DEVC ID='Tempgas3' , QUANTITY='TEMPERATURE', XYZ= 4.25,10.5,5.95 /
&DEVC ID='Tempgas4' , QUANTITY='TEMPERATURE', XYZ= 4.75,10.5,5.95 /
&DEVC ID='Tempgas5' , QUANTITY='TEMPERATURE', XYZ= 5.25,10.5,5.95 /
&DEVC ID='Tempgas6' , QUANTITY='TEMPERATURE', XYZ= 5.75,10.5,5.95 /
&DEVC ID='Tempgas7' , QUANTITY='TEMPERATURE', XYZ= 6.25,10.5,5.95 /
&DEVC ID='Tempgas8' , QUANTITY='TEMPERATURE', XYZ= 6.75,10.5,5.95 /
&DEVC ID='Tempgas9' , QUANTITY='TEMPERATURE', XYZ= 7.25,10.5,5.95 /
&DEVC ID='Tempgas10' , QUANTITY='TEMPERATURE', XYZ= 7.75,10.5,5.95 /
```

```
&DEVC ID='Tempgas11' , QUANTITY='TEMPERATURE', XYZ= 8.25,10.5,5.95 /
&DEVC ID='Tempgas12' , QUANTITY='TEMPERATURE', XYZ= 8.75,10.5,5.95 /
&DEVC ID='Tempgas13' , QUANTITY='TEMPERATURE', XYZ= 9.25,10.5,5.95 /
&DEVC ID='Tempgas14' , QUANTITY='TEMPERATURE', XYZ= 9.75,10.5,5.95 /
&DEVC ID='Tempgas15' , QUANTITY='TEMPERATURE', XYZ= 10.25,10.5,5.95 /
&DEVC ID='Tempgas16' , QUANTITY='TEMPERATURE', XYZ= 10.75,10.5,5.95 /
&DEVC ID='Tempgas17' , QUANTITY='TEMPERATURE', XYZ= 11.25,10.5,5.95 /
&DEVC ID='Tempgas18' , QUANTITY='TEMPERATURE', XYZ= 11.75,10.5,5.95 /
&DEVC ID='Tempgas19' , QUANTITY='TEMPERATURE', XYZ= 12.25,10.5,5.95 /
&DEVC ID='Tempgas20' , QUANTITY='TEMPERATURE', XYZ= 12.75,10.5,5.95 /
&DEVC ID='Tempgas21' , QUANTITY='TEMPERATURE', XYZ= 13.25,10.5,5.95 /
&DEVC ID='Tempgas22' , QUANTITY='TEMPERATURE', XYZ= 13.75,10.5,5.95 /
&DEVC ID='Tempgas23' , QUANTITY='TEMPERATURE', XYZ= 14.25,10.5,5.95 /
&DEVC ID='Tempgas24' , QUANTITY='TEMPERATURE', XYZ= 14.75,10.5,5.95 /
&DEVC ID='Tempgas25' , QUANTITY='TEMPERATURE', XYZ= 15.25,10.5,5.95 /
&DEVC ID='Tempgas26' , QUANTITY='TEMPERATURE', XYZ= 15.75,10.5,5.95 /
&DEVC ID='Tempgas27' , QUANTITY='TEMPERATURE', XYZ= 16.25,10.5,5.95 /
&DEVC ID='Tempgas28' , QUANTITY='TEMPERATURE', XYZ= 16.75,10.5,5.95 /
&DEVC ID='Tempgas29' , QUANTITY='TEMPERATURE', XYZ= 17.25,10.5,5.95 /

&DEVC ID='Tempwall2' , QUANTITY='WALL TEMPERATURE', XYZ= 3.75,10.5,5.95 IOR=-3/
&DEVC ID='Tempwall3' , QUANTITY='WALL TEMPERATURE', XYZ= 4.25,10.5,5.95 IOR=-3/
&DEVC ID='Tempwall4' , QUANTITY='WALL TEMPERATURE', XYZ= 4.75,10.5,5.95 IOR=-3/
&DEVC ID='Tempwall5' , QUANTITY='WALL TEMPERATURE', XYZ= 5.25,10.5,5.95 IOR=-3/
&DEVC ID='Tempwall6' , QUANTITY='WALL TEMPERATURE', XYZ= 5.75,10.5,5.95 IOR=-3/
&DEVC ID='Tempwall7' , QUANTITY='WALL TEMPERATURE', XYZ= 6.25,10.5,5.95 IOR=-3/
&DEVC ID='Tempwall8' , QUANTITY='WALL TEMPERATURE', XYZ= 6.75,10.5,5.95 IOR=-3/
&DEVC ID='Tempwall9' , QUANTITY='WALL TEMPERATURE', XYZ= 7.25,10.5,5.95 IOR=-3/
&DEVC ID='Tempwall10' , QUANTITY='WALL TEMPERATURE', XYZ= 7.75,10.5,5.95 IOR=-3/
&DEVC ID='Tempwall11' , QUANTITY='WALL TEMPERATURE', XYZ= 8.25,10.5,5.95 IOR=-3/
&DEVC ID='Tempwall12' , QUANTITY='WALL TEMPERATURE', XYZ= 8.75,10.5,5.95 IOR=-3/
&DEVC ID='Tempwall13' , QUANTITY='WALL TEMPERATURE', XYZ= 9.25,10.5,5.95 IOR=-3/
&DEVC ID='Tempwall14' , QUANTITY='WALL TEMPERATURE', XYZ= 9.75,10.5,5.95 IOR=-3/
&DEVC ID='Tempwall15' , QUANTITY='WALL TEMPERATURE', XYZ= 10.25,10.5,5.95 IOR=-3/
&DEVC ID='Tempwall16' , QUANTITY='WALL TEMPERATURE', XYZ= 10.75,10.5,5.95 IOR=-3/
&DEVC ID='Tempwall17' , QUANTITY='WALL TEMPERATURE', XYZ= 11.25,10.5,5.95 IOR=-3/
&DEVC ID='Tempwall18' , QUANTITY='WALL TEMPERATURE', XYZ= 11.75,10.5,5.95 IOR=-3/
&DEVC ID='Tempwall19' , QUANTITY='WALL TEMPERATURE', XYZ= 12.25,10.5,5.95 IOR=-3/
&DEVC ID='Tempwall20' , QUANTITY='WALL TEMPERATURE', XYZ= 12.75,10.5,5.95 IOR=-3/
&DEVC ID='Tempwall21' , QUANTITY='WALL TEMPERATURE', XYZ= 13.25,10.5,5.95 IOR=-3/
&DEVC ID='Tempwall22' , QUANTITY='WALL TEMPERATURE', XYZ= 13.75,10.5,5.95 IOR=-3/
&DEVC ID='Tempwall23' , QUANTITY='WALL TEMPERATURE', XYZ= 14.25,10.5,5.95 IOR=-3/
&DEVC ID='Tempwall24' , QUANTITY='WALL TEMPERATURE', XYZ= 14.75,10.5,5.95 IOR=-3/
&DEVC ID='Tempwall25' , QUANTITY='WALL TEMPERATURE', XYZ= 15.25,10.5,5.95 IOR=-3/
&DEVC ID='Tempwall26' , QUANTITY='WALL TEMPERATURE', XYZ= 15.75,10.5,5.95 IOR=-3/
&DEVC ID='Tempwall27' , QUANTITY='WALL TEMPERATURE', XYZ= 16.25,10.5,5.95 IOR=-3/
&DEVC ID='Tempwall28' , QUANTITY='WALL TEMPERATURE', XYZ= 16.75,10.5,5.95 IOR=-3/
&DEVC ID='Tempwall29' , QUANTITY='WALL TEMPERATURE', XYZ= 17.25,10.5,5.95 IOR=-3/

&DEVC ID='Rad1' , QUANTITY='RADIATIVE HEAT FLUX', XYZ= 3.75,10.5,6 IOR=-3/
&DEVC ID='Rad2' , QUANTITY='RADIATIVE HEAT FLUX', XYZ= 4.25,10.5,6 IOR=-3/
&DEVC ID='Rad3' , QUANTITY='RADIATIVE HEAT FLUX', XYZ= 4.75,10.5,6 IOR=-3/
&DEVC ID='Rad4' , QUANTITY='RADIATIVE HEAT FLUX', XYZ= 5.25,10.5,6 IOR=-3/
&DEVC ID='Rad5' , QUANTITY='RADIATIVE HEAT FLUX', XYZ= 5.75,10.5,6 IOR=-3/
&DEVC ID='Rad6' , QUANTITY='RADIATIVE HEAT FLUX', XYZ= 6.25,10.5,6 IOR=-3/
&DEVC ID='Rad7' , QUANTITY='RADIATIVE HEAT FLUX', XYZ= 6.75,10.5,6 IOR=-3/
&DEVC ID='Rad8' , QUANTITY='RADIATIVE HEAT FLUX', XYZ= 7.25,10.5,6 IOR=-3/
&DEVC ID='Rad9' , QUANTITY='RADIATIVE HEAT FLUX', XYZ= 7.75,10.5,6 IOR=-3/
&DEVC ID='Rad10' , QUANTITY='RADIATIVE HEAT FLUX', XYZ= 8.25,10.5,6 IOR=-3/
&DEVC ID='Rad11' , QUANTITY='RADIATIVE HEAT FLUX', XYZ= 8.75,10.5,6 IOR=-3/
&DEVC ID='Rad12' , QUANTITY='RADIATIVE HEAT FLUX', XYZ= 9.25,10.5,6 IOR=-3/
&DEVC ID='Rad13' , QUANTITY='RADIATIVE HEAT FLUX', XYZ= 9.75,10.5,6 IOR=-3/
&DEVC ID='Rad14' , QUANTITY='RADIATIVE HEAT FLUX', XYZ= 10.25,10.5,6 IOR=-3/
&DEVC ID='Rad15' , QUANTITY='RADIATIVE HEAT FLUX', XYZ= 10.75,10.5,6 IOR=-3/
&DEVC ID='Rad16' , QUANTITY='RADIATIVE HEAT FLUX', XYZ= 11.25,10.5,6 IOR=-3/
&DEVC ID='Rad17' , QUANTITY='RADIATIVE HEAT FLUX', XYZ= 11.75,10.5,6 IOR=-3/
&DEVC ID='Rad18' , QUANTITY='RADIATIVE HEAT FLUX', XYZ= 12.25,10.5,6 IOR=-3/
&DEVC ID='Rad19' , QUANTITY='RADIATIVE HEAT FLUX', XYZ= 12.75,10.5,6 IOR=-3/
```

```
&DEVC ID='Rad20' , QUANTITY='RADIATIVE HEAT FLUX', XYZ= 13.25,10.5,6 IOR=-3/
&DEVC ID='Rad21' , QUANTITY='RADIATIVE HEAT FLUX', XYZ= 13.75,10.5,6 IOR=-3/
&DEVC ID='Rad22' , QUANTITY='RADIATIVE HEAT FLUX', XYZ= 14.25,10.5,6 IOR=-3/
&DEVC ID='Rad23' , QUANTITY='RADIATIVE HEAT FLUX', XYZ= 14.75,10.5,6 IOR=-3/
&DEVC ID='Rad24' , QUANTITY='RADIATIVE HEAT FLUX', XYZ= 15.25,10.5,6 IOR=-3/
&DEVC ID='Rad25' , QUANTITY='RADIATIVE HEAT FLUX', XYZ= 15.75,10.5,6 IOR=-3/
&DEVC ID='Rad26' , QUANTITY='RADIATIVE HEAT FLUX', XYZ= 16.25,10.5,6 IOR=-3/
&DEVC ID='Rad27' , QUANTITY='RADIATIVE HEAT FLUX', XYZ= 16.75,10.5,6 IOR=-3/
&DEVC ID='Rad28' , QUANTITY='RADIATIVE HEAT FLUX', XYZ= 17.25,10.5,6 IOR=-3/

&DEVC ID='Conv1' , QUANTITY='CONVECTIVE HEAT FLUX', XYZ= 3.75,10.5,6 IOR=-3/
&DEVC ID='Conv2' , QUANTITY='CONVECTIVE HEAT FLUX', XYZ= 4.25,10.5,6 IOR=-3/
&DEVC ID='Conv3' , QUANTITY='CONVECTIVE HEAT FLUX', XYZ= 4.75,10.5,6 IOR=-3/
&DEVC ID='Conv4' , QUANTITY='CONVECTIVE HEAT FLUX', XYZ= 5.25,10.5,6 IOR=-3/
&DEVC ID='Conv5' , QUANTITY='CONVECTIVE HEAT FLUX', XYZ= 5.75,10.5,6 IOR=-3/
&DEVC ID='Conv6' , QUANTITY='CONVECTIVE HEAT FLUX', XYZ= 6.25,10.5,6 IOR=-3/
&DEVC ID='Conv7' , QUANTITY='CONVECTIVE HEAT FLUX', XYZ= 6.75,10.5,6 IOR=-3/
&DEVC ID='Conv8' , QUANTITY='CONVECTIVE HEAT FLUX', XYZ= 7.25,10.5,6 IOR=-3/
&DEVC ID='Conv9' , QUANTITY='CONVECTIVE HEAT FLUX', XYZ= 7.75,10.5,6 IOR=-3/
&DEVC ID='Conv10' , QUANTITY='CONVECTIVE HEAT FLUX', XYZ= 8.25,10.5,6 IOR=-3/
&DEVC ID='Conv11' , QUANTITY='CONVECTIVE HEAT FLUX', XYZ= 8.75,10.5,6 IOR=-3/
&DEVC ID='Conv12' , QUANTITY='CONVECTIVE HEAT FLUX', XYZ= 9.25,10.5,6 IOR=-3/
&DEVC ID='Conv13' , QUANTITY='CONVECTIVE HEAT FLUX', XYZ= 9.75,10.5,6 IOR=-3/
&DEVC ID='Conv14' , QUANTITY='CONVECTIVE HEAT FLUX', XYZ= 10.25,10.5,6 IOR=-3/
&DEVC ID='Conv15' , QUANTITY='CONVECTIVE HEAT FLUX', XYZ= 10.75,10.5,6 IOR=-3/
&DEVC ID='Conv16' , QUANTITY='CONVECTIVE HEAT FLUX', XYZ= 11.25,10.5,6 IOR=-3/
&DEVC ID='Conv17' , QUANTITY='CONVECTIVE HEAT FLUX', XYZ= 11.75,10.5,6 IOR=-3/
&DEVC ID='Conv18' , QUANTITY='CONVECTIVE HEAT FLUX', XYZ= 12.25,10.5,6 IOR=-3/
&DEVC ID='Conv19' , QUANTITY='CONVECTIVE HEAT FLUX', XYZ= 12.75,10.5,6 IOR=-3/
&DEVC ID='Conv20' , QUANTITY='CONVECTIVE HEAT FLUX', XYZ= 13.25,10.5,6 IOR=-3/
&DEVC ID='Conv21' , QUANTITY='CONVECTIVE HEAT FLUX', XYZ= 13.75,10.5,6 IOR=-3/
&DEVC ID='Conv22' , QUANTITY='CONVECTIVE HEAT FLUX', XYZ= 14.25,10.5,6 IOR=-3/
&DEVC ID='Conv23' , QUANTITY='CONVECTIVE HEAT FLUX', XYZ= 14.75,10.5,6 IOR=-3/
&DEVC ID='Conv24' , QUANTITY='CONVECTIVE HEAT FLUX', XYZ= 15.25,10.5,6 IOR=-3/
&DEVC ID='Conv25' , QUANTITY='CONVECTIVE HEAT FLUX', XYZ= 15.75,10.5,6 IOR=-3/
&DEVC ID='Conv26' , QUANTITY='CONVECTIVE HEAT FLUX', XYZ= 16.25,10.5,6 IOR=-3/
&DEVC ID='Conv27' , QUANTITY='CONVECTIVE HEAT FLUX', XYZ= 16.75,10.5,6 IOR=-3/
&DEVC ID='Conv28' , QUANTITY='CONVECTIVE HEAT FLUX', XYZ= 17.25,10.5,6 IOR=-3/

&TAIL/
```

### *3) Compartment : 5500 kW fire – single opening*

```
Square ceiling
&HEAD CHID='Fire5500kW_2door_medium', TITLE='Fire5500kW_2door_medium' /

Grid (20 cm)
&MESH IJK = 170,85,23, XB=0,34,1,18,0,4.6/

Simulation time
&TIME T_END= 10000
TIME_SHRINK_FACTOR=10/

&MISC
CHECK_KINETIC_ENERGY=.TRUE./

&MATL ID = 'CONCRETE'
CONDUCTIVITY = 1.585
SPECIFIC_HEAT = 0.900
DENSITY = 2300/

&SURF ID = 'CONCRETE_CEILING'
MATL_ID = 'CONCRETE'
THICKNESS = 0.2/

&VENT MB=XMIN SURF_ID='OPEN'/
&VENT MB=XMAX SURF_ID='OPEN'/
&VENT MB=YMIN SURF_ID='OPEN'/
```

```
&VENT MB=YMAX SURF_ID='OPEN'/
&VENT MB=ZMIN SURF_ID='OPEN'/
&VENT MB=ZMAX SURF_ID='OPEN'/

Floor
&OBST XB= 2, 33, 2, 17, 0, 0,SURF_ID='CONCRETE_CEILING'/

Ceiling
&OBST XB= 2, 33, 2, 17, 4, 4.2,SURF_ID='CONCRETE_CEILING'/

Walls
&OBST XB=2,2.2,2,17,0,4,SURF_ID='CONCRETE_CEILING', COLOR='YELLOW', TRANSPARENCY=0.5/
&OBST XB=32.8,33,2,17,0,4,SURF_ID='CONCRETE_CEILING', COLOR='YELLOW', TRANSPARENCY=0.5/
&OBST XB=2,33,2,2.2,0,4,SURF_ID='CONCRETE_CEILING', COLOR='YELLOW', TRANSPARENCY=0.5/
&OBST XB=2,33,16.8,17,0,4, SURF_ID='CONCRETE_CEILING', COLOR='YELLOW', TRANSPARENCY=0.5/

Openings
&HOLE XB=2,2.2,7.9,10.9,0,2/

Burner
&SURF ID='FIRE', HRRPUA= 250 , COLOR='RASPBERRY' /
&OBST XB= 15, 19.6, 6.8, 11.6, 0, 0 , SURF_IDS='FIRE','INERT','INERT' /

Velocity slice
&SLCF PBY=9.2, QUANTITY='VELOCITY',VECTOR= .TRUE. /
&SLCF PBY=9.2, QUANTITY='TEMPERATURE'/
&SLCF PBY=9.2, QUANTITY='MIXTURE FRACTION'/
&SLCF PBY=9.2, QUANTITY='TURBULENCE RESOLUTION'/

&DEVC ID='HRRperUnitVolume', QUANTITY='HRRPUV',STATISTICS='VOLUME INTEGRAL', XB=2.2,32.8,2.2,16.8,0,4 /

Temperature of the gases
&DEVC ID='Tempgas1' , QUANTITY='TEMPERATURE', XYZ= 2.5,9.3,3.95 /
&DEVC ID='Tempgas2' , QUANTITY='TEMPERATURE', XYZ= 3.5,9.3,3.95 /
&DEVC ID='Tempgas3' , QUANTITY='TEMPERATURE', XYZ= 4.5,9.3,3.95 /
&DEVC ID='Tempgas4' , QUANTITY='TEMPERATURE', XYZ= 5.5,9.3,3.95 /
&DEVC ID='Tempgas5' , QUANTITY='TEMPERATURE', XYZ= 6.5,9.3,3.95 /
&DEVC ID='Tempgas6' , QUANTITY='TEMPERATURE', XYZ= 7.5,9.3,3.95 /
&DEVC ID='Tempgas7' , QUANTITY='TEMPERATURE', XYZ= 8.5,9.3,3.95 /
&DEVC ID='Tempgas8' , QUANTITY='TEMPERATURE', XYZ= 9.5,9.3,3.95 /
&DEVC ID='Tempgas9' , QUANTITY='TEMPERATURE', XYZ= 10.5,9.3,3.95 /
&DEVC ID='Tempgas10' , QUANTITY='TEMPERATURE', XYZ= 11.5,9.3,3.95 /
&DEVC ID='Tempgas11' , QUANTITY='TEMPERATURE', XYZ= 12.5,9.3,3.95 /
&DEVC ID='Tempgas12' , QUANTITY='TEMPERATURE', XYZ= 13.5,9.3,3.95 /
&DEVC ID='Tempgas13' , QUANTITY='TEMPERATURE', XYZ= 14.5,9.3,3.95 /
&DEVC ID='Tempgas14' , QUANTITY='TEMPERATURE', XYZ= 15.5,9.3,3.95 /
&DEVC ID='Tempgas15' , QUANTITY='TEMPERATURE', XYZ= 16.5,9.3,3.95 /
&DEVC ID='Tempgas16' , QUANTITY='TEMPERATURE', XYZ= 17.5,9.3,3.95 /
&DEVC ID='Tempgas17' , QUANTITY='TEMPERATURE', XYZ= 18.5,9.3,3.95 /
&DEVC ID='Tempgas18' , QUANTITY='TEMPERATURE', XYZ= 19.5,9.3,3.95 /
&DEVC ID='Tempgas19' , QUANTITY='TEMPERATURE', XYZ= 20.5,9.3,3.95 /
&DEVC ID='Tempgas20' , QUANTITY='TEMPERATURE', XYZ= 21.5,9.3,3.95 /
&DEVC ID='Tempgas21' , QUANTITY='TEMPERATURE', XYZ= 22.5,9.3,3.95 /
&DEVC ID='Tempgas22' , QUANTITY='TEMPERATURE', XYZ= 23.5,9.3,3.95 /
&DEVC ID='Tempgas23' , QUANTITY='TEMPERATURE', XYZ= 24.5,9.3,3.95 /
&DEVC ID='Tempgas24' , QUANTITY='TEMPERATURE', XYZ= 25.5,9.3,3.95 /
&DEVC ID='Tempgas25' , QUANTITY='TEMPERATURE', XYZ= 26.5,9.3,3.95 /
&DEVC ID='Tempgas26' , QUANTITY='TEMPERATURE', XYZ= 27.5,9.3,3.95 /
&DEVC ID='Tempgas27' , QUANTITY='TEMPERATURE', XYZ= 28.5,9.3,3.95 /
&DEVC ID='Tempgas28' , QUANTITY='TEMPERATURE', XYZ= 29.5,9.3,3.95 /
&DEVC ID='Tempgas29' , QUANTITY='TEMPERATURE', XYZ= 30.5,9.3,3.95 /
&DEVC ID='Tempgas30' , QUANTITY='TEMPERATURE', XYZ= 31.5,9.3,3.95 /
&DEVC ID='Tempgas31' , QUANTITY='TEMPERATURE', XYZ= 32.5,9.3,3.95 /

Wall temperature
&DEVC ID='Wall1' , QUANTITY='WALL TEMPERATURE', XYZ= 2.5,9.3,4 IOR=-3/
&DEVC ID='Wall2' , QUANTITY='WALL TEMPERATURE', XYZ= 3.5,9.3,4 IOR=-3/
&DEVC ID='Wall3' , QUANTITY='WALL TEMPERATURE', XYZ= 4.5,9.3,4 IOR=-3/
```

&DEVC ID='Wall4' , QUANTITY='WALL TEMPERATURE', XYZ= 5.5,9.3,4 IOR=-3/
&DEVC ID='Wall5' , QUANTITY='WALL TEMPERATURE', XYZ= 6.5,9.3,4 IOR=-3/
&DEVC ID='Wall6' , QUANTITY='WALL TEMPERATURE', XYZ= 7.5,9.3,4 IOR=-3/
&DEVC ID='Wall7' , QUANTITY='WALL TEMPERATURE', XYZ= 8.5,9.3,4 IOR=-3/
&DEVC ID='Wall8' , QUANTITY='WALL TEMPERATURE', XYZ= 9.5,9.3,4 IOR=-3/
&DEVC ID='Wall9' , QUANTITY='WALL TEMPERATURE', XYZ= 10.5,9.3,4 IOR=-3/
&DEVC ID='Wall10' , QUANTITY='WALL TEMPERATURE', XYZ= 11.5,9.3,4 IOR=-3/
&DEVC ID='Wall11' , QUANTITY='WALL TEMPERATURE', XYZ= 12.5,9.3,4 IOR=-3/
&DEVC ID='Wall12' , QUANTITY='WALL TEMPERATURE', XYZ= 13.5,9.3,4 IOR=-3/
&DEVC ID='Wall13' , QUANTITY='WALL TEMPERATURE', XYZ= 14.5,9.3,4 IOR=-3/
&DEVC ID='Wall14' , QUANTITY='WALL TEMPERATURE', XYZ= 15.5,9.3,4 IOR=-3/
&DEVC ID='Wall15' , QUANTITY='WALL TEMPERATURE', XYZ= 16.5,9.3,4 IOR=-3/
&DEVC ID='Wall16' , QUANTITY='WALL TEMPERATURE', XYZ= 17.5,9.3,4 IOR=-3/
&DEVC ID='Wall17' , QUANTITY='WALL TEMPERATURE', XYZ= 18.5,9.3,4 IOR=-3/
&DEVC ID='Wall18' , QUANTITY='WALL TEMPERATURE', XYZ= 19.5,9.3,4 IOR=-3/
&DEVC ID='Wall19' , QUANTITY='WALL TEMPERATURE', XYZ= 20.5,9.3,4 IOR=-3/
&DEVC ID='Wall20' , QUANTITY='WALL TEMPERATURE', XYZ= 21.5,9.3,4 IOR=-3/
&DEVC ID='Wall21' , QUANTITY='WALL TEMPERATURE', XYZ= 22.5,9.3,4 IOR=-3/
&DEVC ID='Wall22' , QUANTITY='WALL TEMPERATURE', XYZ= 23.5,9.3,4 IOR=-3/
&DEVC ID='Wall23' , QUANTITY='WALL TEMPERATURE', XYZ= 24.5,9.3,4 IOR=-3/
&DEVC ID='Wall24' , QUANTITY='WALL TEMPERATURE', XYZ= 25.5,9.3,4 IOR=-3/
&DEVC ID='Wall25' , QUANTITY='WALL TEMPERATURE', XYZ= 26.5,9.3,4 IOR=-3/
&DEVC ID='Wall26' , QUANTITY='WALL TEMPERATURE', XYZ= 27.5,9.3,4 IOR=-3/
&DEVC ID='Wall27' , QUANTITY='WALL TEMPERATURE', XYZ= 28.5,9.3,4 IOR=-3/
&DEVC ID='Wall28' , QUANTITY='WALL TEMPERATURE', XYZ= 29.5,9.3,4 IOR=-3/
&DEVC ID='Wall29' , QUANTITY='WALL TEMPERATURE', XYZ= 30.5,9.3,4 IOR=-3/
&DEVC ID='Wall30' , QUANTITY='WALL TEMPERATURE', XYZ= 31.5,9.3,4 IOR=-3/

Convective heat transfer coefficient
&DEVC ID='HT1' , QUANTITY='HEAT TRANSFER COEFFICIENT', XYZ= 2.5,9.3,4 IOR=-3/
&DEVC ID='HT2' , QUANTITY='HEAT TRANSFER COEFFICIENT', XYZ= 3.5,9.3,4 IOR=-3/
&DEVC ID='HT3' , QUANTITY='HEAT TRANSFER COEFFICIENT', XYZ= 4.5,9.3,4 IOR=-3/
&DEVC ID='HT4' , QUANTITY='HEAT TRANSFER COEFFICIENT', XYZ= 5.5,9.3,4 IOR=-3/
&DEVC ID='HT5' , QUANTITY='HEAT TRANSFER COEFFICIENT', XYZ= 6.5,9.3,4 IOR=-3/
&DEVC ID='HT6' , QUANTITY='HEAT TRANSFER COEFFICIENT', XYZ= 7.5,9.3,4 IOR=-3/
&DEVC ID='HT7' , QUANTITY='HEAT TRANSFER COEFFICIENT', XYZ= 8.5,9.3,4 IOR=-3/
&DEVC ID='HT8' , QUANTITY='HEAT TRANSFER COEFFICIENT', XYZ= 9.5,9.3,4 IOR=-3/
&DEVC ID='HT9' , QUANTITY='HEAT TRANSFER COEFFICIENT', XYZ= 10.5,9.3,4 IOR=-3/
&DEVC ID='HT10' , QUANTITY='HEAT TRANSFER COEFFICIENT', XYZ= 11.5,9.3,4 IOR=-3/
&DEVC ID='HT11' , QUANTITY='HEAT TRANSFER COEFFICIENT', XYZ= 12.5,9.3,4 IOR=-3/
&DEVC ID='HT12' , QUANTITY='HEAT TRANSFER COEFFICIENT', XYZ= 13.5,9.3,4 IOR=-3/
&DEVC ID='HT13' , QUANTITY='HEAT TRANSFER COEFFICIENT', XYZ= 14.5,9.3,4 IOR=-3/
&DEVC ID='HT14' , QUANTITY='HEAT TRANSFER COEFFICIENT', XYZ= 15.5,9.3,4 IOR=-3/
&DEVC ID='HT15' , QUANTITY='HEAT TRANSFER COEFFICIENT', XYZ= 16.5,9.3,4 IOR=-3/
&DEVC ID='HT16' , QUANTITY='HEAT TRANSFER COEFFICIENT', XYZ= 17.5,9.3,4 IOR=-3/
&DEVC ID='HT17' , QUANTITY='HEAT TRANSFER COEFFICIENT', XYZ= 18.5,9.3,4 IOR=-3/
&DEVC ID='HT18' , QUANTITY='HEAT TRANSFER COEFFICIENT', XYZ= 19.5,9.3,4 IOR=-3/
&DEVC ID='HT19' , QUANTITY='HEAT TRANSFER COEFFICIENT', XYZ= 20.5,9.3,4 IOR=-3/
&DEVC ID='HT20' , QUANTITY='HEAT TRANSFER COEFFICIENT', XYZ= 21.5,9.3,4 IOR=-3/
&DEVC ID='HT21' , QUANTITY='HEAT TRANSFER COEFFICIENT', XYZ= 22.5,9.3,4 IOR=-3/
&DEVC ID='HT22' , QUANTITY='HEAT TRANSFER COEFFICIENT', XYZ= 23.5,9.3,4 IOR=-3/
&DEVC ID='HT23' , QUANTITY='HEAT TRANSFER COEFFICIENT', XYZ= 24.5,9.3,4 IOR=-3/
&DEVC ID='HT24' , QUANTITY='HEAT TRANSFER COEFFICIENT', XYZ= 25.5,9.3,4 IOR=-3/
&DEVC ID='HT25' , QUANTITY='HEAT TRANSFER COEFFICIENT', XYZ= 26.5,9.3,4 IOR=-3/
&DEVC ID='HT26' , QUANTITY='HEAT TRANSFER COEFFICIENT', XYZ= 27.5,9.3,4 IOR=-3/
&DEVC ID='HT27' , QUANTITY='HEAT TRANSFER COEFFICIENT', XYZ= 28.5,9.3,4 IOR=-3/
&DEVC ID='HT28' , QUANTITY='HEAT TRANSFER COEFFICIENT', XYZ= 29.5,9.3,4 IOR=-3/
&DEVC ID='HT29' , QUANTITY='HEAT TRANSFER COEFFICIENT', XYZ= 30.5,9.3,4 IOR=-3/
&DEVC ID='HT30' , QUANTITY='HEAT TRANSFER COEFFICIENT', XYZ= 31.5,9.3,4 IOR=-3/

Radiation
&DEVC ID='Rad1' , QUANTITY='RADIATIVE HEAT FLUX', XYZ= 2.5,9.3,4 IOR=-3/
&DEVC ID='Rad2' , QUANTITY='RADIATIVE HEAT FLUX', XYZ= 3.5,9.3,4 IOR=-3/
&DEVC ID='Rad3' , QUANTITY='RADIATIVE HEAT FLUX', XYZ= 4.5,9.3,4 IOR=-3/
&DEVC ID='Rad4' , QUANTITY='RADIATIVE HEAT FLUX', XYZ= 5.5,9.3,4 IOR=-3/
&DEVC ID='Rad5' , QUANTITY='RADIATIVE HEAT FLUX', XYZ= 6.5,9.3,4 IOR=-3/
&DEVC ID='Rad6' , QUANTITY='RADIATIVE HEAT FLUX', XYZ= 7.5,9.3,4 IOR=-3/
&DEVC ID='Rad7' , QUANTITY='RADIATIVE HEAT FLUX', XYZ= 8.5,9.3,4 IOR=-3/

```
&DEVC ID='Rad8' , QUANTITY='RADIATIVE HEAT FLUX', XYZ= 9.5,9.3,4 IOR=-3/
&DEVC ID='Rad9' , QUANTITY='RADIATIVE HEAT FLUX', XYZ= 10.5,9.3,4 IOR=-3/
&DEVC ID='Rad10' , QUANTITY='RADIATIVE HEAT FLUX', XYZ= 11.5,9.3,4 IOR=-3/
&DEVC ID='Rad11' , QUANTITY='RADIATIVE HEAT FLUX', XYZ= 12.5,9.3,4 IOR=-3/
&DEVC ID='Rad12' , QUANTITY='RADIATIVE HEAT FLUX', XYZ= 13.5,9.3,4 IOR=-3/
&DEVC ID='Rad13' , QUANTITY='RADIATIVE HEAT FLUX', XYZ= 14.5,9.3,4 IOR=-3/
&DEVC ID='Rad14' , QUANTITY='RADIATIVE HEAT FLUX', XYZ= 15.5,9.3,4 IOR=-3/
&DEVC ID='Rad15' , QUANTITY='RADIATIVE HEAT FLUX', XYZ= 16.5,9.3,4 IOR=-3/
&DEVC ID='Rad16' , QUANTITY='RADIATIVE HEAT FLUX', XYZ= 17.5,9.3,4 IOR=-3/
&DEVC ID='Rad17' , QUANTITY='RADIATIVE HEAT FLUX', XYZ= 18.5,9.3,4 IOR=-3/
&DEVC ID='Rad18' , QUANTITY='RADIATIVE HEAT FLUX', XYZ= 19.5,9.3,4 IOR=-3/
&DEVC ID='Rad19' , QUANTITY='RADIATIVE HEAT FLUX', XYZ= 20.5,9.3,4 IOR=-3/
&DEVC ID='Rad20' , QUANTITY='RADIATIVE HEAT FLUX', XYZ= 21.5,9.3,4 IOR=-3/
&DEVC ID='Rad21' , QUANTITY='RADIATIVE HEAT FLUX', XYZ= 22.5,9.3,4 IOR=-3/
&DEVC ID='Rad22' , QUANTITY='RADIATIVE HEAT FLUX',
 XYZ= 23.5,9.3,4 IOR=-3/
&DEVC ID='Rad23' , QUANTITY='RADIATIVE HEAT FLUX', XYZ= 24.5,9.3,4 IOR=-3/
&DEVC ID='Rad24' , QUANTITY='RADIATIVE HEAT FLUX', XYZ= 25.5,9.3,4 IOR=-3/
&DEVC ID='Rad25' , QUANTITY='RADIATIVE HEAT FLUX', XYZ= 26.5,9.3,4 IOR=-3/
&DEVC ID='Rad26' , QUANTITY='RADIATIVE HEAT FLUX', XYZ= 27.5,9.3,4 IOR=-3/
&DEVC ID='Rad27' , QUANTITY='RADIATIVE HEAT FLUX', XYZ= 28.5,9.3,4 IOR=-3/
&DEVC ID='Rad28' , QUANTITY='RADIATIVE HEAT FLUX', XYZ= 29.5,9.3,4 IOR=-3/
&DEVC ID='Rad29' , QUANTITY='RADIATIVE HEAT FLUX', XYZ= 30.5,9.3,4 IOR=-3/
&DEVC ID='Rad30' , QUANTITY='RADIATIVE HEAT FLUX', XYZ= 31.5,9.3,4 IOR=-3/

Convection
&DEVC ID='Conv1' , QUANTITY='CONVECTIVE HEAT FLUX', XYZ= 2.5,9.3,4 IOR=-3/
&DEVC ID='Conv2' , QUANTITY='CONVECTIVE HEAT FLUX', XYZ= 3.5,9.3,4 IOR=-3/
&DEVC ID='Conv3' , QUANTITY='CONVECTIVE HEAT FLUX', XYZ= 4.5,9.3,4 IOR=-3/
&DEVC ID='Conv4' , QUANTITY='CONVECTIVE HEAT FLUX', XYZ= 5.5,9.3,4 IOR=-3/
&DEVC ID='Conv5' , QUANTITY='CONVECTIVE HEAT FLUX', XYZ= 6.5,9.3,4 IOR=-3/
&DEVC ID='Conv6' , QUANTITY='CONVECTIVE HEAT FLUX', XYZ= 7.5,9.3,4 IOR=-3/
&DEVC ID='Conv7' , QUANTITY='CONVECTIVE HEAT FLUX', XYZ= 8.5,9.3,4 IOR=-3/
&DEVC ID='Conv8' , QUANTITY='CONVECTIVE HEAT FLUX', XYZ= 9.5,9.3,4 IOR=-3/
&DEVC ID='Conv9' , QUANTITY='CONVECTIVE HEAT FLUX', XYZ= 10.5,9.3,4 IOR=-3/
&DEVC ID='Conv10' , QUANTITY='CONVECTIVE HEAT FLUX', XYZ= 11.5,9.3,4 IOR=-3/
&DEVC ID='Conv11' , QUANTITY='CONVECTIVE HEAT FLUX', XYZ= 12.5,9.3,4 IOR=-3/
&DEVC ID='Conv12' , QUANTITY='CONVECTIVE HEAT FLUX', XYZ= 13.5,9.3,4 IOR=-3/
&DEVC ID='Conv13' , QUANTITY='CONVECTIVE HEAT FLUX', XYZ= 14.5,9.3,4 IOR=-3/
&DEVC ID='Conv14' , QUANTITY='CONVECTIVE HEAT FLUX', XYZ= 15.5,9.3,4 IOR=-3/
&DEVC ID='Conv15' , QUANTITY='CONVECTIVE HEAT FLUX', XYZ= 16.5,9.3,4 IOR=-3/
&DEVC ID='Conv16' , QUANTITY='CONVECTIVE HEAT FLUX', XYZ= 17.5,9.3,4 IOR=-3/
&DEVC ID='Conv17' , QUANTITY='CONVECTIVE HEAT FLUX', XYZ= 18.5,9.3,4 IOR=-3/
&DEVC ID='Conv18' , QUANTITY='CONVECTIVE HEAT FLUX', XYZ= 19.5,9.3,4 IOR=-3/
&DEVC ID='Conv19' , QUANTITY='CONVECTIVE HEAT FLUX', XYZ= 20.5,9.3,4 IOR=-3/
&DEVC ID='Conv20' , QUANTITY='CONVECTIVE HEAT FLUX', XYZ= 21.5,9.3,4 IOR=-3/
&DEVC ID='Conv21' , QUANTITY='CONVECTIVE HEAT FLUX', XYZ= 22.5,9.3,4 IOR=-3/
&DEVC ID='Conv22' , QUANTITY='CONVECTIVE HEAT FLUX', XYZ= 23.5,9.3,4 IOR=-3/
&DEVC ID='Conv23' , QUANTITY='CONVECTIVE HEAT FLUX', XYZ= 24.5,9.3,4 IOR=-3/
&DEVC ID='Conv24' , QUANTITY='CONVECTIVE HEAT FLUX', XYZ= 25.5,9.3,4 IOR=-3/
&DEVC ID='Conv25' , QUANTITY='CONVECTIVE HEAT FLUX', XYZ= 26.5,9.3,4 IOR=-3/
&DEVC ID='Conv26' , QUANTITY='CONVECTIVE HEAT FLUX', XYZ= 27.5,9.3,4 IOR=-3/
&DEVC ID='Conv27' , QUANTITY='CONVECTIVE HEAT FLUX', XYZ= 28.5,9.3,4 IOR=-3/
&DEVC ID='Conv28' , QUANTITY='CONVECTIVE HEAT FLUX', XYZ= 29.5,9.3,4 IOR=-3/
&DEVC ID='Conv29' , QUANTITY='CONVECTIVE HEAT FLUX', XYZ= 30.5,9.3,4 IOR=-3/
&DEVC ID='Conv30' , QUANTITY='CONVECTIVE HEAT FLUX', XYZ= 31.5,9.3,4 IOR=-3/

&TAIL/
```